# Moisture transport in coated wood

van Meel, P.A.

*Award date:*
2009

Technische Universiteit
Eindhoven
University of Technology

# Moisture transport in coated wood

P.A. van Meel

Oktober 15, 2009
N/TPM 2009-04

Supervisors:
dr.ir. S.J.F. Erich
prof.dr.ir. K. Kopinga

Department of Applied Physics
Transport in Permeable Media
Building N-laag
P.O. Box 513
5600 MB Eindhoven

**Abstract**

Moisture inside wood causes favorable conditions for decay. Application of a coating alters the moisture transport to prevent accumulation of moisture. The goal of the research presented in this thesis is to study the influence of a coating on the moisture transport in wood by NMR.

NMR allows to determine both wood moisture content and rate of water sorption during water absorption and desorption of coated and uncoated wood. In contrast to weighing, both quantities are measured dynamically and non destructively with high spatial and temporal resolution in relatively short experiments. In addition, NMR relaxometry distinguishes between moisture in lumina and moisture in cell walls which allows to accurately characterize sorption processes in wood. Samples were studied in a 4.7 T NMR scanner with a dynamic gradient of 752 mT/m and an echo time of 1700 $\mu$s which yielded a spatial resolution of 33 $\pm$ 3 $\mu$m.

To study the influence of a coating on the moisture transport in wood, several commonly used wood-coating combinations were studied. Dry samples were wetted and saturated samples were dried while monitored by NMR.

The open coating offers virtually no barrier for moisture transport. The alkyd coating offers a very strong barrier against moisture absorption and desorption. The acrylic coating offers a very low barrier for water absorption but a strong barrier against moisture desorption.

For all coatings, care must be taken to prevent moisture from entering the wood via for instance cracks. For the open and acrylic coating additional care must be taken to prevent accumulation of water on the coating. This is quickly absorbed but, for acrylic coated wood, is desorbed much slower.

This thesis shows that the sorption behavior of coated wood is dependent on the specific combination of wood and coating.

# Contents

Chapter 1

# Introduction

## 1.1 Wood and its degradation

Wood is a versatile material. It is readily available, easily worked and strong considering its weight. Wood is a renewable material; trees absorb carbon dioxide and use water and sunlight to produce a material used in for instance building and paper production, or to provide chemical feedstock. At the end of a product life cycle, the material constituents can be combusted or composted. In essence, timber use represents a classical example of a recycling material, mimicking natural cycles.

A major disadvantage of wood is its susceptibility to degradation due to environmental influences like temperature, radiation or damage from biological, mechanical or chemical attacks. Furthermore, all wood is sensitive to moisture, which not only causes swelling and shrinkage, but also favorable conditions for biological decay such as wood rot.

## 1.2 Protection of wood by coatings

Application of a coating provides protection of wood against weathering, besides adding the desired aesthetical properties like color and gloss. Apart from direct protection to photo irradiation, a coating decreases the weathering of a wood surface by influencing its moisture content. A coating reduces the rate of uptake by its barrier function against liquid water and water vapor diffusion. It also reduces the drying rates of wood. This raises the question of what the optimum moisture permeability of a coating would be. A coating with a low permeability might give a good protection against external moisture. But at the same time it possesses the risk of retaining moisture which has entered through a crack, for instance at corner joints of window frames. On the other hand, a very permeable coating might enable a rapid increase in moisture content, which gives rise to large dimensional changes resulting in cracking and loss of adhesion, or excessive stresses on joints. This means

that the optimum moisture permeability depends on the application area of the coated wood. The interest in coating permeability has gained interest with the introduction of waterborne paints, which generally exhibit a higher moisture affinity than solvent borne coatings.

## 1.3 Developments in coatings technology

The awareness of the environmental risks of several coating ingredients has grown over the years [1]. The European community and local governments force coating manufactures to produce coatings with a lower environmental impact. The currently most important environmental issues and legislatorial changes are discussed below.

The first is the strict legislation concerning the emission and usage of Volatile Organic Compounds (VOCs). Not only the environment is affected by these VOCs, but long term exposure to these chemicals can lead to mental disabilities. Since January of 2000, the Dutch government has changed the legislation concerning the use of VOCs, obligating professional painters to use products with low amounts of VOCs (less than 125 g of VOCs per liter of product) for indoor application [2, 3]. In 2004, the European committee issued the so called VOC Paints Directive which establishes limit values for the maximum VOC contents [4]. The products covered by this directive are decorative paints for use on buildings, their trims, fittings, structures associated to buildings and products for vehicle refinishing. The directive set up two sets of limit values for the maximum contents of VOCs. The first set of limit values applies since January 1, 2007. The second, and stricter, set of limit values applies from January 1, 2010. For vehicle refinishing products there is only one set of limit values for the VOC contents, which applies from January 1, 2007.

A new European Community Regulation on chemicals and their safe use also entered into force on June 1, 2007. It deals with the Registration, Evaluation, Authorization and Restriction of Chemical substances (REACH) [5]. The aim of REACH is to improve the protection of human health and environment through better and earlier identification of intrinsic properties of chemical substances. The central element of REACH is a completely new system of registration, evaluation, authorization and restriction for new and existing chemical substances, marketed in quantities of more than 1 tonne per enterprise per year. This new system has a major impact on the coating industry by increasing the cost of registration, but also on research and development to find suitable alternatives.

The change in legislation has driven coating manufactures to look for solutions, such as changing to other types of coatings. New technical developments have resulted in an increased production of waterborne coatings.

Obviously, the market demands that the properties of these reformulated coatings at least meet, or even surpass, their predecessors. Although waterborne systems have already been improved considerably, they still suffer from a variety of shortcomings, such as high surface tension resulting in bad flow and low gloss, faster biological degradation, less water repellency, and longer open times. However, waterborne coatings also have several advantages, next to reduced amount of VOCs, such as a reduced fire hazard and the fact that existing production and application equipment can still be used.

Nowadays, more than 95% of exterior wood coatings are applied in liquid form with either an organic solvent or water as the carrier for the other coating ingredients. A strong increase in the use of waterborne coatings is observed.

## 1.4 Measuring wood moisture content

The influence of coating systems on the moisture content of wood has been recognized for a long time. To study this influence, several approaches have been used. These include permeability measurements of free coating films or coated wood samples, moisture content monitoring in practice on panels or full scale wooden constructions [6] and computer simulations. Much effort is put into the understanding and modeling of drying processes of uncoated wood to shorten industrial kiln drying times using techniques such as weighing and x-ray tomography [7–10]. Weighing studies have shown that water absorption – a combined process of diffusion and capillary water uptake – is strongly influenced by a coating [11, 12]. However, weighing yields no spatial resolution – a low resolution can be achieved by tomography and subsequent weighing of each slice. Furthermore, prolonged experiments are required. Currently, the performance of a coating is graded following European norm EN927. However, these tests only asses the performance of a coating. None of the common techniques reveal the exact moisture behavior and underlying transport mechanisms and thus do not lead to fundamental understanding.

To fully understand the moisture transport in coated wood, it is necessary to measure the moisture content dynamically and quantitatively. It has been shown that Nuclear Magnetic Resonance (NMR) offers a powerful technique to do so [13–16]. NMR allows to measure the wood moisture content non-invasively as a function of position with high spatial and temporal resolution. In addition, information regarding the pore size distribution is also obtained with NMR measurements [17] allowing to discriminate water in cell walls from water in lumina and vessels [18–23].

The measurements presented in this thesis are performed using NMR at the Transport in Permeable Media (TPM) group at the Eindhoven University of Technology (TU/e). This group is specialized in transport processes in porous materials. The facilities enable measuring salt and water dynamics in building materials [24, 25] and high resolution in-depth profiling of curing processes in coatings [26]. The permeability of an alkyd coating was already found to depend on several factors like its degree and type of pigmentation and type of binder [27]. However, the substrate can also be expected to have a significant influence on the performance of coatings.

## 1.5 Aim of this thesis

The goal of the research presented in this thesis is to study the influence of a coating on the moisture transport in wood by NMR. In this exploratory study commonly used wood-coating combinations are investigated. This thesis is outlined as follows. Properties of wood and coatings are presented in chapter 2. Chapter 3 gives a theoretical introduction to nuclear magnetic resonance. Chapter 4 describes the samples and experimental setup including the NMR setup and settings. In chapter 5 the water uptake of four types of wood coated with different coatings is investigated. Chapter 6 discusses the drying of coated and uncoated saturated wood. The conclusions and recommendations are given in chapter 7.

Chapter 2

# Wood and coatings

Wide varieties of both wood and coatings exist. This chapter presents information regarding the used types of wood and coating. The first section of this chapter describes the anatomy of softwoods, hardwoods and a chemically modified wood. The behavior of moisture in wood is discussed subsequently. The third section gives the components of coatings and discusses the differences between acrylic and alkyd coatings, as well as the penetration of coatings into wood.

## 2.1 Wood anatomy

Wood is anisotropic and inhomogeneous. Figure 2.1 shows a section of a trunk in which three sections are defined: axial, radial and tangential. A tree grows in the radial direction by cellular fission of the cambium which forms sapwood on its interior and inner bark on its exterior. This means the cambium moves outward. At a certain age, generally after 10 to 20 years, the living cells in the sapwood die and harden turning into heartwood. The inner bark becomes outer bark. Sapwood and heartwood generally do not differ in strength; however, heartwood is much more durable. In a temperate climate, during springtime the cambium is most active and forms a layer of earlywood. The earlywood transports water and minerals from the roots to the leaves. The activity decreases when the crown is fully formed. The cambium then forms a thinner latewood layer of higher density and darker color which is visible as an annual ring. The cell walls are much thinner and the lumina much larger in earlywood than in latewood. The activity of the cambium stops roughly from autumn to spring.

Wood consists of three major components: cellulose is the skeleton (40 – 60% of the dry mass), hemicellulose the matrix (15 – 20%), and lignin (15 – 40%) the encrusting substance which binds the cells together and gives rigidity to the cell wall. In addition, heartwood in particular contains many low-molecular-weight organic compounds known as extractives. The content

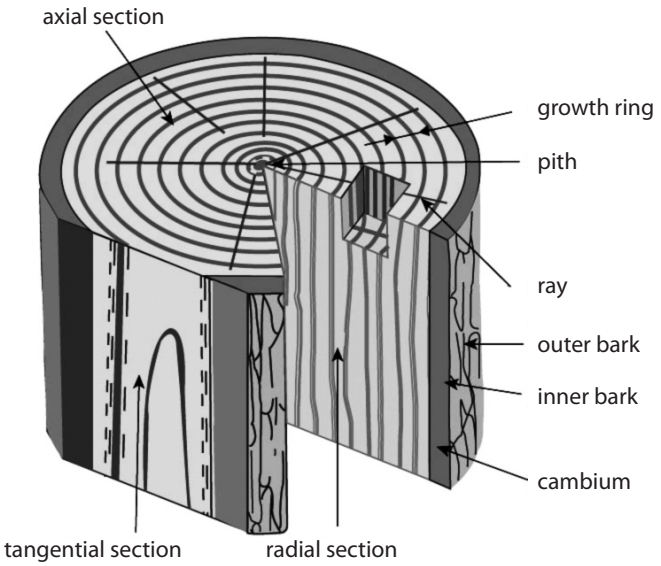


**Figure 2.1** *A schematic portion of a trunk. Three sections are defined: axial, radial and tangential. The pith, hardwood, sapwood, cambium and bark are indicated.*

of extractives can vary from near zero up to 25% by weight in temperate zone species and even much higher in some tropical hardwoods [28].

As mentioned, four types of wood were studied. One hardwood: dark red meranti; two softwoods: pine and spruce; and one chemically altered wood named Accoya.

### 2.1.1 Structure of softwoods

The bulk structure of softwood consists of longitudinal, i.e. axially oriented, cells called tracheids. Ray tracheids run along the radial direction. Tracheids are imperforate, long and narrow cells; the typical length is 3500 $\mu$m while the typical diameter is 35 $\mu$m. The ends are tapered along the radial surfaces for a considerable portion of their lengths where they are in contact with other tracheids. Fluid is exchanged between tracheids through so called pits. Most intertracheid pit pairs are along the tapered portions of the tracheids. Bordered pit pairs permit flow from longitudinal tracheids to ray tracheids. Typically, the ray volume for softwood is 7% on average and 17% for hardwoods. The longitudinal permeability of softwoods is much greater than the tangential permeability, due to the fact that there are fewer pitted cross walls to traverse per unit length in the longitudinal direction. Resin is transported in intercellular spaces called resin canals.

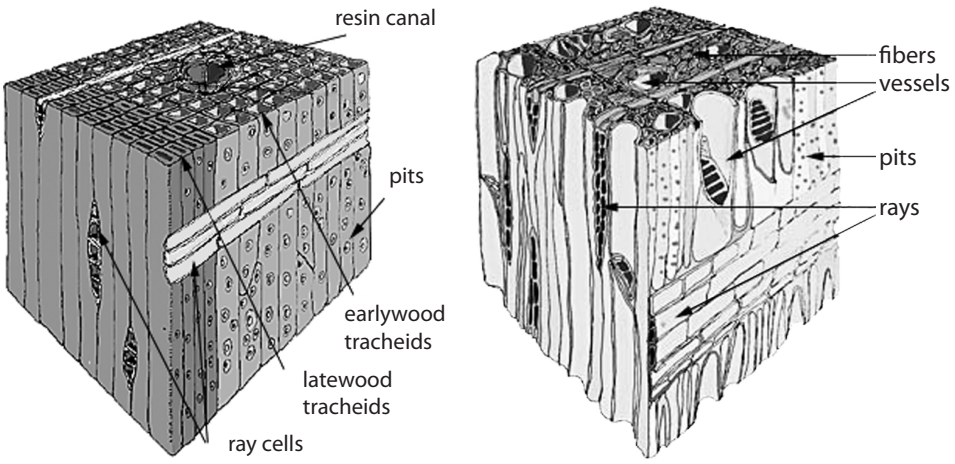


*(a) softwood* *(b) hardwood*

**Figure 2.2** *Schematic representation of softwood and hardwood.*

### 2.1.2 Structure of hardwoods

The hardwoods structure is more diverse and complex than that of softwoods. Hardwood is built up of vessels surrounded by fibers. Fibers are usually thin, relatively short, thick-walled, sparsely pitted and have a low permeability. Moisture is transported by vessel elements which are rather short compared to softwood tracheids and have a diameter of 50 – 100 $\mu$m for diffuse-porous wood types such as dark red meranti, and 50 – 400 $\mu$m for ring-porous wood types. The vessels are aligned end-to-end with perforation plates between them. The flow resistance of vessels is low so they behave as long, open capillaries. Vessels branch frequently and communicate through intervessel pits.

### 2.1.3 Pits

Most important conifers, in particular those belonging to the Pinaceae family such as pine and spruce, possess a bordered pit structure with pit membranes characterized by a centralized thickened disk, the torus, and a supporting membrane consisting of strands of cellulose microfibrils [29]. In green condition, most of the sapwood pit membranes are centrally located and quite permeable, see figure 2.3(a). When wood dries, water evaporates from, for instance, the upper pit cavity first. Next, water evaporates from the smaller openings in the pit membrane. This results in relatively high capillary forces which are capable of forcing the membrane toward the lumen still filled with water. This phenomenon is referred to as pit aspiration, see figure 2.3(c). Ev-

idence exists that, subsequently the torus deforms due to evaporation from even smaller openings in the torus yielding higher capillary forces [28]. If the pits are aspirated wood assumes a closed-cell structure and may become virtually impermeable.

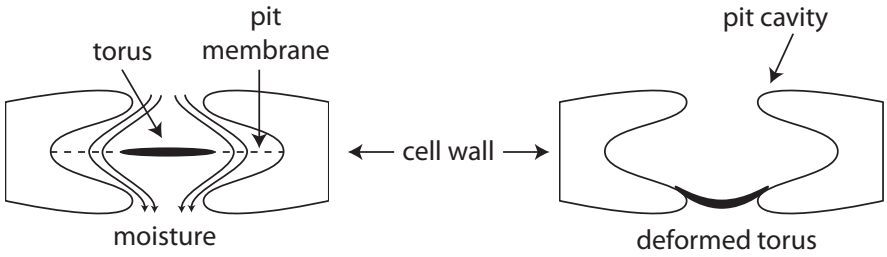


*(a) pit* *(b) aspirated pit*

**Figure 2.3** *A schematic representation of a pit, which translates to "Hofstippel" in Dutch. If a pit is aspirated, for instance by drying, it becomes highly impermeable.*

### 2.1.4 Acetylation

Chemical modification can increase the durability of fast growing and generally lower grade woods. One of the possible modifications is acetylation [31]. In the process of acetylation, acetyl groups form permanent covalent bonds with hydroxyl (OH) sites in wood cell walls, see figure 2.4. Acetic acid is produced as a by-product which is removed at the end of the reaction as well as unreacted acetic anhydride.

Acetylated wood provides an increase in dimensional stability under varying RH because the acetyl groups occupy space in the cell wall. Consequently, the acetylated wood is permanently in a swollen condition, the extent of which depends upon the level of modification. There is little residual swelling when the wood is soaked in water [32]. The reaction with wood can take place with anhydride in gas or liquid form. The latter is used in a production plant in Arnhem, The Netherlands where pine is acetylated to produce so called Accoya™ which is one of the wood types included in this research.

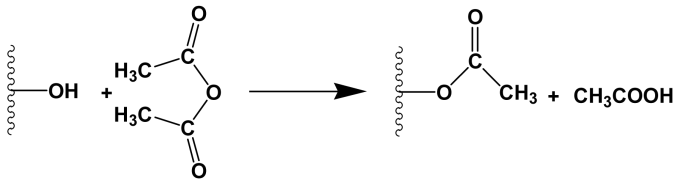


**Figure 2.4** *Reaction scheme for acetylation with acetic anhydride. Acetyl groups form permanent covalent bonds with hydroxyl (OH) sites in wood cell walls, taken from [30].*

## 2.2 Moisture in wood

Wood cells are complex structures, however, for moisture considerations the distinction between lumen and cell wall will suffice. Wood is a porous material and moisture in wood is present in two basic forms. The first is bound or hygroscopic water within the cell wall which is considered bound on and between cellulose fibers in the cell wall. The second is unbound or capillary water in the voids of the wood such as lumina and vessels. The amount of water in wood is expressed as a moisture content (MC) $\Theta_m$ which is defined as the mass of water in wood, as a percentage of the oven dry mass:

$$\theta = \frac{\text{weight of water in wood}}{\text{oven dry weight of wood}} \times 100\% = \frac{w_m - w_0}{w_0} \times 100\%, \qquad (2.2.1)$$

where $w_m$ is the moist mass. The oven dry mass $w_0$ is defined as the constant mass obtained after wood has dried in an air oven maintained at $102 \pm 3$ °C . Cell walls exchange moisture with air surrounding the wood. An equilibrium is attained between the bound water content and the relative humidity (RH) of the surrounding air. This MC is called the equilibrium moisture content (EMC). The RH is defined as:

$$\text{RH} = \frac{p}{p_0} \times 100\%, \qquad (2.2.2)$$

where $p$ is the partial vapor pressure in the air and $p_0$ is the saturated vapor pressure.

### 2.2.1 Fiber saturation point

The EMC increases with the RH until the cell walls become saturated when the RH approaches 100%. This point is called the fiber saturation point (FSP) which is reached in practice at 98% RH according to Siau [28]. For most wood types, the FSP corresponds to a MC of approximately 30%. Other factors influencing the EMC to a minor extent are drying history, temperature, mechanical stress and the extractive content. The relationship between EMC and RH at a given temperature is called the sorption isotherm. The EMC of wood decreases slightly with rising temperature, although the partial water vapor pressure increases very rapidly. Therefore, wood moisture content has a much stronger correlation with relative humidity than with absolute humidity.

Above the FSP, additional water is present in the unbound form in the lumina or voids of the wood. The maximum amount of unbound water is limited by the porosity of the wood. Unbound water is no cause for swelling or shrinkage since it is held only by relatively weak capillary forces. Many other physical properties of wood are strongly influenced by its MC. As

the bound water content increases the mechanical strength decreases and thermal and electrical conductivities increase. Large variations occur at the FSP which in fact provides possibilities to determine and define the FSP. An increase in moisture content will also result in a higher density since the mass of wood increases at a greater rate than its volume. This increase occurs at a greater rate above FSP because swelling has ceased.

### 2.2.2 Moisture sorption by wood

Figure 2.5 shows two adjacent cells with their cell walls and lumina. Picture (a) shows the case for fully saturated wood: the cell walls and lumina are filled with water. Picture (b) shows the first stage of desorption where the lumina are drying although the cell walls are still fully saturated. In picture (c) the lumina have dried completely but the cell walls are still saturated; this is the the fiber saturation point. When drying further, the bound water will start to desorb from the cell wall which is transported to the surface via vapor diffusion through the lumina and vessels – note that the permeability of cell walls is very low [28]. Since shrinkage and swelling are attributed to bound water this causes radial and tangential shrinkage. Any change in longitudinal direction is minor. Picture (e) shows the cells fully dehydrated as would be the case after oven-drying wood for several days at 103 °C. The process is largely reversible – going from (e) to (a) represents water absorption of wood – although hysteresis occurs. Cell walls can form internal hydrogen bonds during desorption, no longer allowing them to take up water. These bonds are broken during absorption but at a higher moisture content. Because of this, the EMC is generally higher during desorption than during adsorption. The ratio of the two is given by Siau [28] to be approximately 0.8. The sorption isotherms for the types of wood used in this study are given in appendix A. Above the FSP, the moisture density of bound water is largely independent of the total moisture content according to Araujo et al. [20]. However, the drying of cell wall and lumen is not always clearly separated, especially for low permeable woods, as shown by Almeida et al. [23] using NMR.

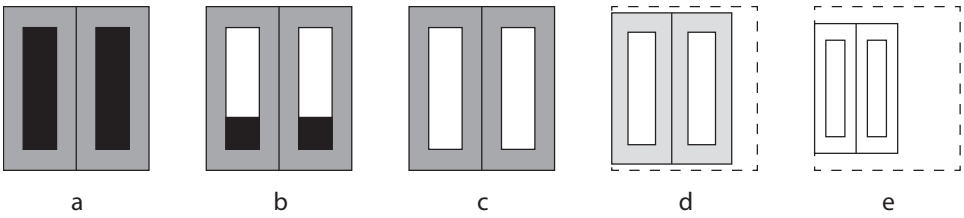


**Figure 2.5** *The drying process of wood represented schematically.*

### 2.2.3 Flow in wood

In all wood types, bound water is transported within a cell wall by diffusion. Moisture exchange between adjacent cell walls or with an RH outside the wood takes place via vapor diffusion through lumina which are connected by pits. Transport directly from cell wall to cell wall is negligible since the permeability of cell walls is very low.

Unbound moisture is transported differently in softwoods than in hardwoods because of their differences in structure [28]. Rays are a more important flow path in softwoods than in hardwoods. In pine, resin canals make a significant contribution to the flow. In spruce the permeability of rays is low and the ray tracheids contribute a small volumetric fraction resulting in low permeability. Latewood in softwood is generally more permeable than earlywood because of decreased pit aspiration during drying. Vessels are the most permeable axial flow path in hardwoods when they are not occluded, for instance by tyloses. The rays of hardwood generally contribute less to the overall flow than those of softwoods, despite the generally higher volumetric fraction of rays in hardwoods. For hardwoods there is little difference between radial and tangential permeability. Both in softwoods and in hardwoods, sapwood is nearly always more permeable than heartwood.

## 2.3 Coatings

A coating is a film which has protective, decorative and, or, other specific properties. Generally, the following components are found [33]:

**Binders or resins:** polymeric materials to bind together the other ingredients, to form a film and to protect against external influences like moisture. The binder determines most of the primary properties of the dried paint film such as adhesion, mechanical properties and resistance against various conditions.

**Carrier solvents:** water or organic solvents with the purpose to transfer the other ingredients to the substrate and to allow the formation of a film. Although the solvent is a transient ingredient, its quality and suitability have great influence on the coating's durability, binder solubility and miscibility, dispersion stability, application viscosity, drying time and film leveling. Historically, almost all coatings were solvent born. Other carriers, such as water, have been developed in attempts to reduce solvent content and therewith VOC emissions, as mentioned in section 1.3.

**Pigments and fillers or extenders:** materials that are mainly used to provide color but also opacity to protect wood against photo degra-

dation. Pigments also modify the mechanical, adhesion and barrier properties of the film.

**Additives:** substances added in small quantities (less than 5 wt%), to improve or modify certain properties of the coating material during its manufacturing, storage, transportation or application.

The binder of a coating is mostly classified with respect to the chemical composition of the polymer. The main binders in exterior wood coatings are nowadays based on acrylics and fatty-acid containing alkyd-polyesters, both of which are explained in more detail below.

### 2.3.1 Acrylic

The key attribute of acrylic coatings is their resistance to hydrolysis during extended exterior exposure, i.e. weathering. Solvent borne acrylic technology holds a strong position in the automotive coating industry and in the coating of general industrial plastics, although the usage of waterborne acrylics is increasing. The primary advantage of solvent borne acrylic technology is adhesion, quick drying, and durability. Waterborne acrylic coatings offer better VOC compliance, but suffer from adhesion limitations with a variety of plastic compositions (e.g. thermoplastic polyolefins and untreated polypropylene) and high cost.

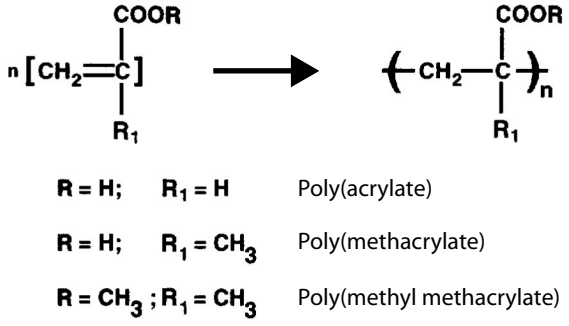


**Figure 2.6** *Typical types of acrylic resins, modified from [1].*

Acrylic paint is fast-drying and contains pigment suspended in an acrylic polymer emulsion. Acrylic resins are prepared through the polymerization of acrylic and methacrylic acids or their corresponding esters as shown in figure 2.6. Acrylic resins used in coatings are classified as being either thermoplastic or thermosetting depending upon their cure properties. Thermoplastic resins form hardened coatings simply through solvent evaporation. Thermoset resins form a cross linked structure through a chemical reaction with itself or various other types of resins. Coatings formed from thermosetting acrylic polymers offer improved hardness, toughness, and chemical resistance

over their thermoplastic counterparts. The film formation of acrylic dispersions consists of evaporation of water followed by coalescence and finally by interdiffusion of the polymers particles.

### 2.3.2 Alkyd

Alkyd resins are based on polymeric resins developed in the 1920's and were first produced commercially by General Electric. The term "alkyd" originates from "al", referring to alcohol, and "kyd", refereing to acid. Nowadays, the term alkyd refers to polyesters modified with fatty acids. Synthetic alkyd resins represent the resin group that has found the greatest utilization in the paint and coatings industry. Solvent borne and water reducible alkyd formulations dominate the general metal and maintenance coating markets although the market share of waterborne acrylics, epoxies, polyurethanes, and polyesters is increasing. Alkyd resins offer high gloss and are easily applied under variable environmental conditions.

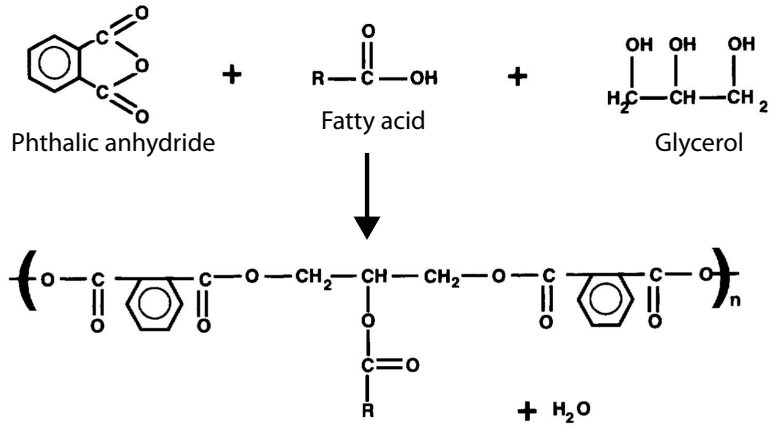


**Figure 2.7** *The structure of a typical alkyd resin, modified from [1].*

Alkyds are prepared via condensation polymerization of three types of monomers: polyalcohols, polybasic acids, and fatty acids or triglyceride oils to obtain fatty-acid containing polyesters, as shown in figure 2.7. The inclusion of the fatty acid confers a tendency to form a flexible coating. The film formation consists of evaporation of the solvent followed by oxidative cross linking.

### 2.3.3 Coating penetration

In this study, coatings are applied to wood, which is a porous material. Therefore, the penetration of a coating into wood is considered. The degree of coating penetration was measured by de Meijer [34] using microtomography. He found that the it was firstly determined by the ability of

the coating to flow into wood capillaries and secondly by coating transport from cell to cell through interconnecting pits. Mainly the type of binder but also pigmentation, solid matter content and drying speed influenced the penetration.

In softwoods the following different coating penetration routes were observed by de Meijer [34]: the flow into open ends of longitudinal early and latewood tracheids, the flow into ray cells and the transport from rays into longitudinal tracheids adjacent to rays. The possibility for the coating to follow the latter route was strongly influenced by the existing type of cross field pitting and to a lesser degree by the pigmentation of the paint. The penetration into ray tracheids was been found to be deeper for pine compared to spruce. The flow into open ends of longitudinal tracheids was strongly influenced by the grain angle of tracheids. Penetration into dark red meranti was mainly limited to vessels and rays. Tyloses can prevent the complete filling of vessels. The impact on penetration by the removal of extractives and by sanding of the surface appeared to be only of minor importance.

Chapter 3

# Basics of NMR

The first nuclear induction experiments were performed independently in 1945 by the groups of Bloch [35, 36] and Purcell [37] using continuous wave NMR. Five years later, Hahn [38] published his article about pulsed NMR spin echoes where the applied magnetic field is constant. Currently, the magnetic field is manipulated by applying time varying magnetic field gradients. Furthermore, in many NMR experiments liquids confined in porous materials were noticed to exhibit properties that are very different from those of the bulk fluid. The so called longitudinal and transverse relaxation time of bulk water are in the order of seconds, whereas for water in a porous material these times can be in the order of milli- or even microseconds. Many applications of NMR exist, such as Magnetic Resonance Imaging (MRI), spectroscopy and relaxometry. The most commonly used nucleus is that of hydrogen $^1$H.

This chapter first introduces the principles of NMR, starting from the resonance of spins, followed by the Bloch equations describing a spin system macroscopically. Subsequently, NMR pulse sequences and the use of field gradients to obtain spatial resolution are explained. The final section deals with NMR relaxation time distribution measurements.

## 3.1 Nuclear spin and magnetic moment

Unpaired electrons, protons and neutrons possess a spin of 1/2 which can be "up" or "down". Particles with spins having opposite signs (up or down) can pair up resulting in zero net spin. An example is helium: as the Pauli exclusion principle states, both proton spins and both neutron spins cannot occupy the same quantum state. Only nuclei with non-zero net spin can be manipulated by magnetic fields.

When a nucleus is placed in an external magnetic field $B_0$ the energy levels of the spin up and spin down states are separated. The energy difference is given by $E = h\gamma B_0$, where $h$ is Planck's constant and $\gamma$ is the gyromag-

netic ratio which is characteristic and unique for each isotope. Since the lower energy state, spin up, is preferable, a population difference arises. According to Boltzmann statistics, the difference between the number of spins in the up state $N_+$ and down state $N_-$ arising from the competition between temperature and energy difference is given by:

$$\frac{N_-}{N_+} = \mathrm{e}^{-\frac{E}{kT}} = \mathrm{e}^{-\frac{h\gamma B_0}{kT}}, \tag{3.1.1}$$

where $k$ is the Boltzmann constant and $T$ is the temperature in Kelvin.

A nucleus having non-zero net spin has a spin momentum $\vec{S}$. Combined with the nuclear charge this results in a magnetic moment $\vec{\mu}$. Similar to spin, $\vec{\mu}$ is also quantum mechanically bound to an up and down state. The two moments are related by the gyromagnetic ratio – for $^1$H or a single proton $\gamma/2\pi = 42.58$ MHz/T:

$$\vec{\mu} = \gamma \vec{S}. \tag{3.1.2}$$

From now on, a classical description will suffice to further describe the basics of NMR. Therefore, from this point onward $\vec{\mu}$ will represent the expectation value of the quantum mechanical magnetic moment: $\vec{\mu} \equiv < \vec{\mu} >$ [39]. The population difference given by the Boltzmann distribution results in a net magnetic moment in the direction of $\vec{B_0} = (0, 0, B_0)$. At room temperature and a field strength of 4.7 T, equation (3.1.1) equals 0.999794. This means that only a fraction of $2 \cdot 10^{-4}$ of the maximum magnetization is reached. In addition, this magnetic moment will experience a torque:

$$\vec{\tau} = \vec{\mu} \times \vec{B_0}. \tag{3.1.3}$$

Combining (3.1.2) and (3.1.3) and noting that $\frac{\partial \vec{S}}{\partial t} = \vec{\tau}$ gives:

$$\frac{d\vec{\mu}}{dt} = \gamma \vec{\mu} \times \vec{B_0}. \tag{3.1.4}$$

This means the magnetic moments will precess around the magnetic field. This precessional movement is called the Larmor precession.

## 3.2 Rotating frame

To describe the behavior of the precessing moments more conveniently, a rotating frame is introduced. In a frame rotating at frequency $\omega$ around the $z$-axis, the following equation holds for an arbitrary vector, $\vec{r}$, in the static or laboratory frame:

$$\frac{\partial \vec{r'}}{\partial t} = \frac{d\vec{r}}{dt} - (\vec{\omega} \times \vec{r}), \tag{3.2.1}$$

where $\vec{r'}$ is the vector in the rotating frame, $d/dt$ is the derivative in the static frame and $\partial/\partial t$ is the derivative in the rotating frame. This gives the equation of motion for the magnetic moment in a frame rotating at the Larmor frequency $\omega_0$:

$$\frac{\partial \vec{\mu'}}{\partial t} = \frac{d\vec{\mu}}{dt} - (\vec{\omega_0} \times \vec{\mu}). \tag{3.2.2}$$

Substituting equation (3.1.4) gives:

$$\frac{\partial \vec{\mu'}}{\partial t} = \vec{\mu} \times (\gamma \vec{B_0} + \vec{\omega_0}). \tag{3.2.3}$$

$\partial\vec{\mu'}/\partial t$ becomes zero for $\vec{\omega_0} = -\gamma\vec{B_0}$. So, the precessional motion around $\vec{B_0}$ is not seen in the frame rotating at a frequency of $\omega_0$, i.e. the magnetic moment $\vec{\mu'}$ is stationary in the rotating frame. Now, the frequency of rotation equals the frequency of precession in the laboratory frame. This frequency is called the Larmor frequency and depends linearly on $\gamma$ and $B_0$:

$$\omega_0 = \gamma B_0. \tag{3.2.4}$$

Applying a second magnetic field $\vec{B_1}$ which is fixed in the $xy$-plane of the rotating frame results in a precession around this field. In the static frame this is a spiraling motion called nutation over a sphere with radius $|\vec{\mu}|$. Similar to equation (3.1.4) and (3.2.4) the following now holds in the rotating frame:

$$\frac{\partial \vec{\mu'}}{\partial t} = \gamma \vec{\mu'} \times \vec{B_1'}, \tag{3.2.5}$$

$$\vec{\omega_1'} = -\gamma |\vec{B_1'}|. \tag{3.2.6}$$

To apply a constant field $\vec{B_1'}$ in the rotating frame, a field $\vec{B_1}$ is applied at the Larmor frequency in the stationary frame. This enables one to manipulate or "excite" the magnetic moments. Since the $B_1$-field is emitted at the Larmor frequency – which is generally in the Radio Frequency (RF) range – and the typical duration is in the order of several microseconds, it is often called an RF-pulse. The angle of rotation of $\vec{\mu'}$ in the rotating frame $\theta'$ with respect to $\vec{B_0}$ is determined by the duration $t_p$ and strength of the applied $B_1$-pulse:

$$\theta' = |\vec{\omega_1'}| t_p = \gamma |\vec{B_1'}| t_p. \tag{3.2.7}$$

After the $B_1$-field is switched off, the magnetic moment will realign with the main magnetic field $B_0$. This process is called relaxation. The next sections describe the practical usage of the possible manipulations. Since all of the above is microscopic, now a macroscopic description of a spin system in terms of magnetization is given since this directly relates to the measured NMR signal.

## 3.3 Magnetization

As mentioned, the population difference of the spin up and down states results in a non-zero net magnetic moment. In NMR experiments, one measures the net magnetization $\vec{M}$ being the vector sum over the magnetic moment vectors of all spins present in a sample:

$$\vec{M} = \sum_i \vec{\mu}_i. \tag{3.3.1}$$

In equilibrium, $\vec{M}$ is parallel to $\vec{B_0}$. After rotating $\vec{M}$ by applying a $\vec{B_1}$-field for a short time, $\vec{M}$ will restore to the main magnetic field by two relaxation mechanisms [40]. The first is longitudinal relaxation, or spin-lattice relaxation, which is the result of individual spins interacting with their molecular environment. For instance, molecular rotations and diffusion at frequencies close to the Larmor frequency are sources of time varying $B$-fields. This enhances the probability for spin-flips of nuclei, thereby resulting in spin-lattice relaxation. Longitudinal relaxation is characterized by a time $T_1$ which reflects the rate at which the parallel component of the magnetization $M_z$ restores to the $z$-axis.

The second is transverse relaxation, or spin-spin relaxation, which is the result of spins interacting with other spins. Transverse relaxation is characterized by a time $T_2$ reflecting the rate at which the transverse component of the magnetization $M_{xy}$ becomes zero. The manipulation of the magnetic moments and these two relaxation mechanisms are described macroscopically by the Bloch equations [35] in the rotating frame:

$$\frac{dM'_{x'}}{dt} = -\frac{M'_{x'}}{T_2}, \tag{3.3.2}$$

$$\frac{dM'_{y'}}{dt} = -\frac{M'_{y'}}{T_2}, \tag{3.3.3}$$

$$\frac{dM'_{z'}}{dt} = -\frac{M'_{z'} - M_0}{T_1}. \tag{3.3.4}$$

Combining (3.3.2) to (3.3.4) with (3.2.5) and (3.2.6), the following set of equations is obtained, describing the magnetization vector during NMR in the rotating frame of reference:

$$\frac{dM'_{x'}}{dt} = -\frac{M'_{x'}}{T_2} + \gamma(\vec{M'} \times \vec{B'_1})_{x'}, \tag{3.3.5}$$

$$\frac{dM'_{y'}}{dt} = -\frac{M'_{y'}}{T_2} + \gamma(\vec{M'} \times \vec{B'_1})_{y'}, \tag{3.3.6}$$

$$\frac{dM'_{z'}}{dt} = -\frac{M'_{z'} - M_0}{T_1} + \gamma(\vec{M'} \times \vec{B'_1})_{z'}. \tag{3.3.7}$$

In equilibrium, the magnetization is fully aligned along the main magnetic field: $\vec{M} = (0, 0, M_0)$. During NMR experiments, so called 90° and 180° pulses are applied. These pulses rotate the magnetization vector 90° or 180° in the rotating frame. When $\vec{B_1}$ is applied in the $-y$ direction, this results in $\vec{M'_{90}} = (M_0, 0, 0)$ and $\vec{M'_{180}} = (0, 0, -M_0)$ at $t = 0$, respectively. The solutions of the Bloch equations describe the magnetization after a 90° pulse at $t = 0$ as follows:

$$M'_{x'} = M'_0 \, \mathrm{e}^{-\frac{t}{T_2}}, \tag{3.3.8}$$

$$M'_{y'} = 0, \tag{3.3.9}$$

$$M'_{z'} = M'_0 \left(1 - \mathrm{e}^{-\frac{t}{T_1}}\right). \tag{3.3.10}$$

This tells us that, in the laboratory frame, a 90° pulse results in a magnetization vector within the $xy$-plane $\vec{M}_{xy}$ rotating around the $z$-axis at the Larmor frequency. $|\vec{M}_{xy}|$ decreases exponentially with a characteristic time $T_2$. The magnetization relaxes to the $z$-axis with a characteristic time $T_1$. It can be shown that $T_2 \leq T_1$ [40].

## 3.4 Free induction decay

The rotation angle of an RF-pulse is determined by its duration and strength as shown by equation (3.2.7). The pulse is emitted by a coil close to, or surrounding the sample. Since $\vec{M}_{xy}$ rotates in the $xy$-plane after a 90° pulse, it induces a voltage in the very same RF-coil as stated by Faraday's law. Directly after the 90° pulse at $t = 0$, all magnetic moments possess the same phase in the $xy$-plane, inducing maximum signal. For $t > 0$, the signal decays due to loss of phase coherence. The signal after a 90° pulse is called a free induction decay. The pulse sequence is depicted in figure 3.1.

Various sources for signal decay are present. Firstly, the total magnetic field experienced by a certain proton is perturbed by fluctuations of the position and orientation of other protons and molecules; the spin-spin relaxation. This randomly alters the precession frequency for each proton, resulting in dephasing of the magnetic moments and thus, decay of $M_{xy}$ which causes the previously mentioned $T_2$-decay. Secondly, due to static macroscopic field inhomogeneities either in the main magnetic field or caused by magnetic impurities or susceptibility variations inside the sample, $\omega_L$ also varies locally.

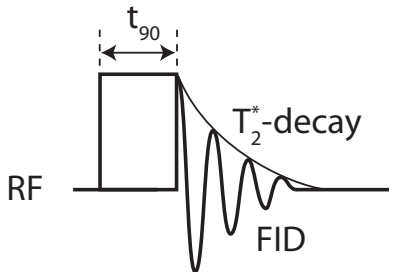


**Figure 3.1** *The Free Induction Decay (FID) pulse sequence. Both the 90° pulse and FID are shown. An exponential $T_2^*$-decay curve is shown.*

Again, this causes the magnetic moments to dephase which leads to decay of $\vec{M_{xy}}$. In the rotating frame, dephasing is perceived as moments slowly rotating backwards and forwards relative to the rotating frame. Together with the microscopic $T_2$ decay, the transverse decay is now governed by a macroscopic characteristic decay time $T_2^*$:

$$\frac{1}{T_2^*} = \frac{1}{T_2} + \frac{\gamma \Delta B}{2\pi}, \tag{3.4.1}$$

where $\Delta B$ incorporates all static macroscopic $B$-field inhomogeneities. Figure 3.1 shows the $T_2^*$-decay curve.

## 3.5 Obtaining spatial resolution

So far, only the total amount of $^1$H within a sample can be determined from the NMR signal intensity. To obtain one-dimensional spatial resolution in the $z$-direction, a magnetic field gradient is applied:

$$\vec{G} = (G_x, G_y, G_z) = \left( \frac{\partial B_z}{\partial x}, \frac{\partial B_z}{\partial y}, \frac{\partial B_z}{\partial z} \right). \tag{3.5.1}$$

The gradient is designed to be homogeneous in the volume of measurement. The gradient is applied during the signal acquisition and is therefore called the frequency encoding gradient. Consequently:

$$\omega_L = \gamma |\vec{B}| = \gamma (B_0 + \vec{r} \cdot \vec{G}), \tag{3.5.2}$$

meaning that the Larmor frequency now becomes dependent of position. By Fourier transformation of the induced signal, a spectrum depicting the amount of $^1$H as a function of frequency is obtained. Since the gradient strength and direction are known, this spectrum is easily transformed to a one-dimensional proton density profile, e.g. signal intensity versus position. In the absence of relaxation, the resolution $\Delta x$ is determined by the gradient

strength and acquisition time $t_w$ which is also called the window width. Theoretically, $\Delta x$ is given by:

$$\Delta x = \frac{2\pi}{\gamma |\vec{G}| t_w}. \tag{3.5.3}$$

When the relaxation time is very short, the best achievable resolution is no longer determined by the recording window but by $T_2^*$; the theoretical resolution is then given by equation (3.5.3) with $t_w$ replaced by $T_2^*$.

To enhance the resolution, the gradient strength $G$ or the recording window $t_w$ can be increased. When $t_w$ is increased, the inter-echo time $t_e$ also has to increase. However, due to $T_2$-decay this leads to a lower signal intensity and thus a lower Signal to Noise Ratio (SNR). In addition, the SNR is decreased when the resolution is enhanced, because the sample volume per spatial point decreases. The loss of SNR can be partly compensated for by averaging the signal. The following equation shows the dependence of the SNR to the number of averages $N_{avg}$ and the window width $t_w$:

$$SNR \propto \sqrt{\frac{N_{avg}}{t_w}}. \tag{3.5.4}$$

## 3.6 Spin echoes

The $T_2^*$-decay of a FID can be very fast, making it impossible to record the FID signal. The loss of signal due to dephasing caused by field inhomogeneities can be counteracted in so called spin echo experiments suggested by Hahn [38]. Figure 3.2 shows the magnetization vectors at different times during the spin echo sequence in the rotating frame. At $t < 0$, the magnetization vectors are in equilibrium (a). A 90° pulse is applied at $t = 0$ (b). After the 90° pulse an FID forms which decays, i.e. the magnetization vectors dephase (c). At $t = t_e/2$, a 180° pulse is applied (d); $t_e$ is the echo time and $t_{180} = 2t_{90}$ as a result of equation (3.2.7) for equal pulse strengths. This rotates all moments over 180° perpendicular to the $z$-axis. This is called a refocussing pulse since the accumulated phase of all moments is reversed. At $t = t_e$, the magnetization vectors refocus forming an echo (e). After the echo the spin dephase resulting in loss of signal (f). This means that the intensity of the spin echo is insensitive to field perturbations provided they are stationary during the echo time. The echo signal from stationary spins will experience $T_2$-decay only. Field variations fluctuating within $t_e$, for instance due to diffusion, are not completely refocused.

Figure 3.3 shows the Hahn Spin Echo (HSE) pulse sequence and definitions of various times. The letters (a) through (f) from figure 3.2 are indicated. Two axis are shown: the RF-axis and the gradient axis. In a spin echo

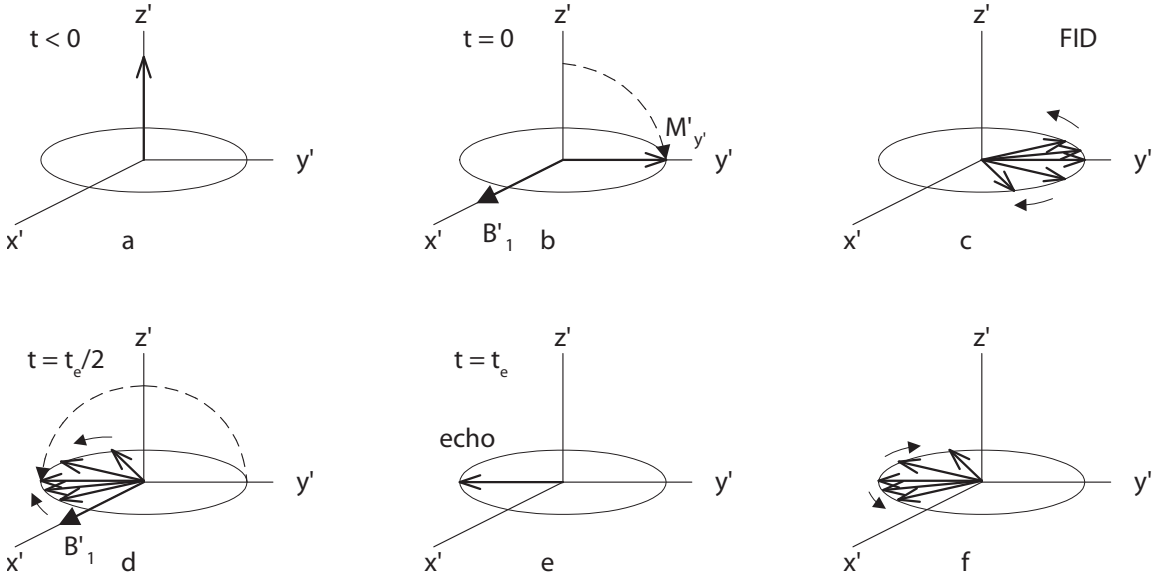


**Figure 3.2** *The magnetization vectors a different times during the spin echo sequence in the rotating frame.*

experiment, the frequency encoding gradient applied after the 180° pulse not only provides the afore mentioned spatial resolution; it also dominates the dephasing of the magnetic moments. To produce an echo, the gradient must also be applied after the 90° for a time $t_w/2$ to dephase $M_{xy}$. The first half of the frequency encoding gradient then rephases the moments which results in an echo at $t = t_e$.

## 3.7 Multi echo sequences

After recording an echo, one has to wait for the magnetization to fully relax to the $\vec{B_0}$-field before applying another 90° pulse; this waiting time is called the long delay. The longitudinal relaxation is governed by $T_1$ meaning the repetition time $t_r$, should at least be several times $T_1$. However, from the $T_2$-decay curve shown in figure 3.3 it is clear that, after the echo, the decay has not yet decreased to zero, i.e. a part of the magnetization is still present in the transverse plane. Applying another 180° pulse at $t = 3/2t_e$ will in fact again rephase the magnetization to produce another echo at $t = 2t_e$. This sequence can be extended to an arbitrary number of 180° pulses until the echo signal is below the detection threshold. This allows multiple echoes to be recorded within one pulse sequence without having to wait until $\vec{M_z}$ has fully relaxed.

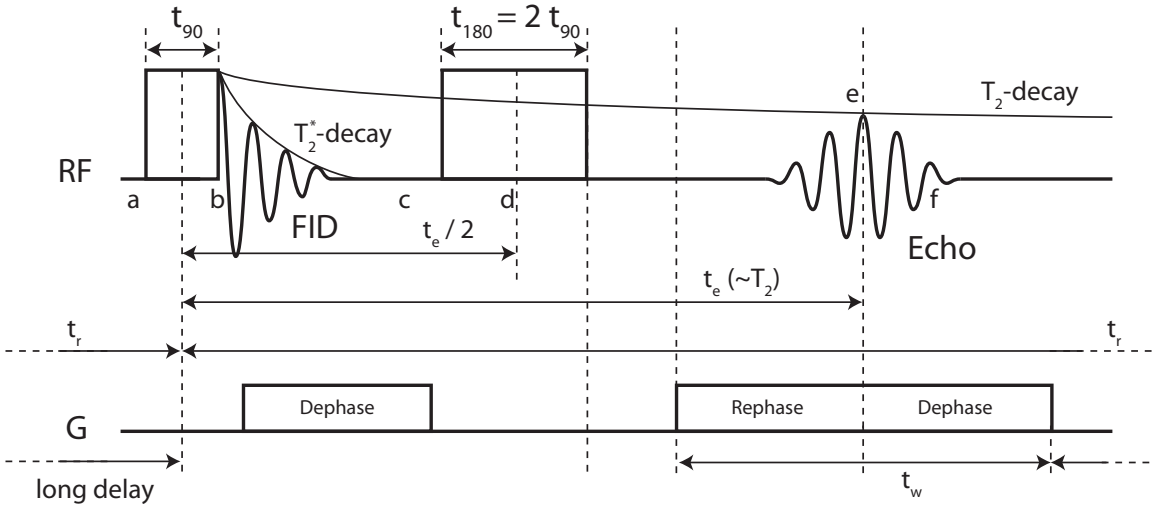


**Figure 3.3** *The Hahn Spin Echo (HSE) pulse sequence. The top axis shows the RF signals, i.e. 90° and 180° pulses, FID and echo. The bottom axis shows the one dimensional gradient at different times. Echo time $t_e$, window width $t_w$, repetition time $t_r$, and pulse durations $t_{90}$ and $t_{180}$ are indicated. An exponential $T_2$-decay curve is shown for the HSE and a $T_2^*$ curve for the FID.*

### 3.7.1 CPMG

Recording multiple echoes using the same gradient for all echoes after a single 90° pulse can be done using a Carr-Purcel-Meiboom-Gill (CPMG) sequence [41, 42] which is shown in figure 3.4. For a CPMG-sequence the axis of rotation of the 180° pulse is perpendicular to that of the 90° pulse which prevents the accumulation of phase errors. When the axes of rotation coincide for the even numbered 180° pulses and oppose for the odd ones, the sequence is sensitive to phase errors and is called a Carr-Purcell-Freeman-Hill (CPFH) sequence [43]. For $T_1 \gg T_2$, the signal intensity of subsequent echoes decays exponentially according to the Bloch equations:

$$S_{echo} = \rho \, \mathrm{e}^{-\frac{nt_e}{T_2}} \left(1 - \mathrm{e}^{-\frac{t_r}{T_1}}\right), \tag{3.7.1}$$

where $n$ is the number of the echo considered and $\rho$ is a material constant including the proton density. It is possible for a sample to exhibit more than one $T_2$-value. The signal intensity then decays multi-exponentially:

$$S_{echo} = \sum_i S_i \, \mathrm{e}^{\frac{-nt_e}{T_{2,i}}}. \tag{3.7.2}$$

The summation can be replaced by an integral for a continuous relaxation time distribution. Then, the resulting magnetization $M(t)$ yielding the NMR

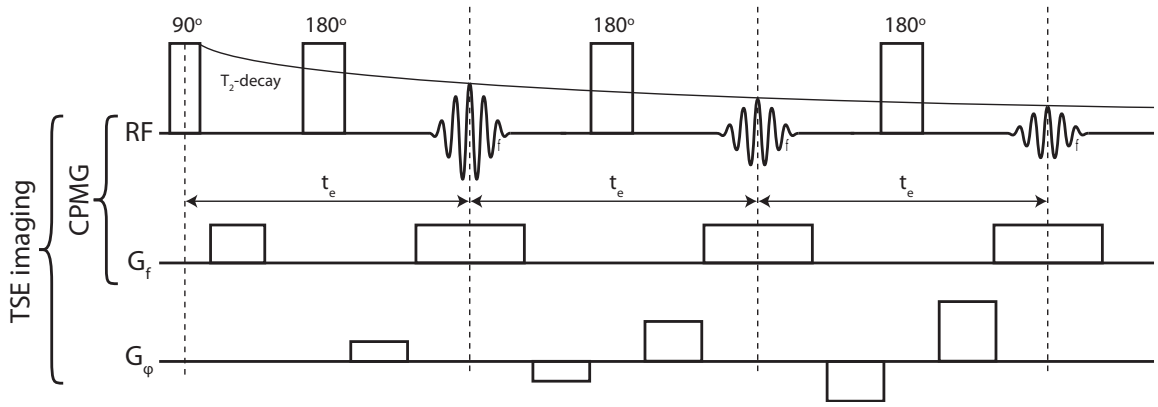


**Figure 3.4** *The pulse sequence diagram for the CPMG and turbo spin echo imaging sequences. The top axis shows the RF signals i.e. pulses and echoes. The middle and bottom axes show the frequency and phase encoding gradients respectively. The latter applies only to TSE imaging.*

signal for a multi-exponential decay is related to the Laplace transform of the probability distribution $P(T_2)$ of the relaxation times :

$$M(t) = \int_0^\infty P(T_2) \mathrm{e}^{-\frac{t}{T_2}} d(T_2). \tag{3.7.3}$$

The inverse transform yields the $T_2$-distribution. However, the transform from $M(t)$ to $P(T_2)$ is numerically instable and far from trivial but can be performed by means of a mathematical routine called CONTIN [44]. Under certain conditions, the relaxation time distribution can give the pore size distribution of a sample as will be explained in section 3.8.

### 3.7.2 Turbo spin echo imaging

Thus far, all sequences produce one-dimensional proton density profiles. Imaging (MRI) requires at least two-dimensional spatial resolution. This is achieved by application of a second gradient, called a phase encoding gradient $G_\phi$. This gradient is applied between the 90° pulse and the frequency encoding gradient $G_f$, see figure 3.4. $G_f$ and $G_\phi$ are applied perpendicular in the $xy$-plane. $G_\phi$ imposes a specific phase angle upon the transverse magnetization vectors. As a result of equation (3.5.2), this phase angle depends on the position in the sample and the duration of $G_\phi$. To reconstruct an image from the data, a two dimensional Fourier transform is applied. This resolves both phase and frequency information. Three-fold spatially resolved measurements are possible using a second phase encoding gradient. These advanced pulse sequences are more conveniently described in the so called $\vec{k}$-space [45]. Each image pixel requires one phase encoding gradient

step. For high resolution images this leads to a drastic increase in acquisition time. As mentioned above, it is possible to record more than one echo per sequence. A CPMG sequence used to record a small number of echoes – approximately 4 to 16 echoes – with varying gradients to obtain an image is generally called a Turbo Spin Echo (TSE) imaging sequence. For samples with a sufficiently long $T_2$, this sequence strongly decreases the measuring time, although averaging is necessary to maintain an acceptable SNR.

## 3.8 Relaxation time distributions

The NMR signal relaxation behavior of a fluid inside a porous material is influenced by interactions with the pore wall. The relaxation time is shorter than that of free water and the decay is often multi-exponential. This is caused by the interaction of moving water due to Brownian motion – characterized by the self diffusion coefficient $D$ – inside a pore with the pore wall. This section first presents the Brownstein and Tarr model which describes relaxation effects inside pores [46, 47]. Secondly, moisture in wood is considered since wood is a porous material comprising different pore sizes in addition to moisture contained in cell walls.

### 3.8.1 Pore size distribution

NMR measures an electronic signal proportional to the total nuclear magnetization of the sample $M(\vec{r}, t)$ at position $\vec{r}$ and time $t$ which is the result of the magnetic moment density $\rho(\vec{r}, t)$:

$$M(t) = \int_V \rho(\vec{r}, t) d\tau. \tag{3.8.1}$$

During an NMR experiment, the water molecules and thereby the magnetic moments move within the pore due to Brownian motion. The model reported by Brownstein and Tarr describes the magnetization of a spin system in a porous material. The model uses the bulk diffusivity of water, instead of assuming altered properties of water, to explain the shortening of relaxation effects in pores.

Brownstein and Tarr assume that the total transverse magnetization can decay due to volume-like sinks $\kappa$ and surface-like sinks $\nu$. The physical nature of these sinks is not discussed, but they hypothesize magnetic impurities such as macromolecules and water that is bound to the pore wall. The governing equations for such a system are:

$$\vec{\nabla} \cdot (\mathcal{D} \cdot \vec{\nabla}\rho - \kappa\rho) = \frac{\partial \rho}{\partial t}, \tag{3.8.2}$$

$$(\vec{n} \cdot \mathcal{D} \cdot \vec{\nabla}\rho + \nu\rho)|_s = 0, \tag{3.8.3}$$

$$\rho(\vec{r}, 0) = \frac{M(0)}{V}. \tag{3.8.4}$$

Equation (3.8.2) is a diffusion equation allowing for volume-like sinks where $\mathcal{D}$ denotes the self-diffusion tensor. Equation (3.8.3) is the boundary condition containing a sink at the pore surface. The initial condition, equation (3.8.4), assumes a uniform magnetization density $M(0)$ at $t = 0$. The solution of this problem can be expressed as a sum of normal modes. These consist of constants $A_i$, orthogonal spatial eigenfunctions $F_i$ and eigenvalues $T_i$ manifested by a multi-exponential decay. Equations (3.8.2) to (3.8.4) are actually indifferent to the relaxation type; $T_i$ is $T_{1,i}$ for spin-lattice relaxation or $T_{2,i}$ for spin-spin relaxation. Since measuring times for $T_2$ are in general shorter than those for $T_1$, from now on $T_2$-decay is considered. The sum of normal modes looks as follows:

$$\rho(\vec{r}, t) = \sum_i A_i F_i(\vec{r}) \mathrm{e}^{-\frac{t}{T_{2,i}}}. \tag{3.8.5}$$

The observed quantity is a sum of the exponential eigenfunctions:

$$M(t) = M_{xy}(0) \sum_i I_n \ \mathrm{e}^{-\frac{t}{T_{2,i}}}, \tag{3.8.6}$$

where $I_n$ is the $n$th relative intensity. The solution contains a number of eigenvalues $T_{2,i}$ which can be ordered such that:

$$T_{2,0} > T_{2,1} \geq T_{2,2} \geq T_{2,3} \geq \ldots \geq 0, \tag{3.8.7}$$

in which $i$ refers to the so called mode.

Brownstein and Tarr solved the differential equations and boundary conditions for simple geometries under several assumptions. The volume-like sinks are assumed to be absent, $\kappa = 0$. The self-diffusion tensor is taken to be homogeneous and isotropic, $\mathcal{D} = D\mathcal{I}$. $D$ is taken constant and equal to that for bulk water. From the solutions of their equations, they showed that a dimensionless sink strength parameter – $\nu r/D$, where $r$ is the typical pore size – divides the relaxation behavior into three distinct regions:

- $\nu r/D \ll 1$
  The fast diffusion region. The lowest mode completely dominates the behavior, $I_0 \to 1$ and $T_2 = T_{2,0}$.

- $1 \ll \nu r/D \ll 10$
  The intermediate diffusion region. The lowest mode still dominates, but the higher modes contribute a few percent.

- $10 \ll \nu r/D$
  The slow diffusion region. The higher modes contribute a few tens of percents.

For a system containing $N$ different pore sizes, equation (3.8.6) generalizes to:

$$M(t) = M_{xy}(0) \sum_{j=1}^{N} \sum_{i} I_{i,j} \, \mathrm{e}^{-\frac{t}{T_{2,i,j}}}, \tag{3.8.8}$$

where $j$ is one of the total number of pore sizes $N$.

In the fast diffusion region, all eigenvalues can be related directly to a specific pore size, since the lowest mode is completely dominant. In other words, $I_{i,j} \to 0$ for $i > 0$ and each $T_{2,0,j}$ represents exactly one pore size. In the intermediate or slow diffusion region, the measured $T_{i,j}$ values can still be related to pore sizes. However, a single pore size is then represented by more than one relaxation time. In the fast diffusion region, where $I_{0,j} \to 1$, equation (3.8.8) can be simplified to:

$$M(t) = M_{xy}(0) \sum_{j=1}^{N} I_{0,j} \, \mathrm{e}^{-\frac{t}{T_{2,0,j}}}. \tag{3.8.9}$$

This is a multi-exponential decay which can be measured by means of a CPMG sequence as shown by equation (3.7.2) which yields a relaxation time distribution via the inverse transform of equation (3.7.3). Brownstein and Tarr showed that, in the fast diffusion region for a single pore, the lowest mode is given by $T_{2,0} = V/\nu S$, where $V$ is the pore volume and $S$ is the active surface area. In case of a spherical pore this mode can be rewritten as:

$$T_{2,0} = \frac{V}{S\nu} = \frac{r}{3\nu}, \tag{3.8.10}$$

with which the pore-size distribution can be estimated from the distribution of relaxation times when the surface sink strength $\nu$ is known or the other way around when the pore size distribution is known. It is possible to measure $\nu$, also called the surface relaxivity, by NMR [17].

### 3.8.2 Bound and unbound moisture in wood

As explained in section 2.2, moisture in wood exists in two basic forms, unbound and bound. Unbound moisture, present the voids of wood such as lumina and vessels, behaves as a fluid inside a porous material. This means, the Brownstein and Tarr model can be used to obtain information regarding the pore size or relaxivity distribution from a relaxation time distribution measured by NMR. Moisture in the cell walls has a shorter relaxation time compared to that of unbound water because it is bound on and between cellulose fibers. However, the relaxation times cannot be linked to pore sizes since bound water cannot be treated as bulk water.

Chapter 4

# Materials and methods

The experiments can be divided into water uptake or absorption measurements and drying or desorption measurements. This chapter first presents the combinations of woods and coatings which were studied. Next, the sample holder design is explained. Subsequently, the NMR settings used for both wetting and drying measurements are given. Finally, the calibration from signal intensity to moisture content is given.

## 4.1 Coated wood samples

Four types of wood were studied. One hardwood, dark red meranti heartwood (*Shorea Sapupira*); two softwoods, pine (*Pinus radiata*) and spruce (Norway *Picea abies*); and one acetylated wood named Accoya. Appendix A shows the sorption isotherms of each. Meranti and spruce were chosen because of their frequent application in building. Note that the name meranti is a generic term for wood from several species. Three coating types were used in this study which were sprayed in two or four layers: an open and an acrylic coating which were both waterborne and an alkyd coating which was solvent born. The open coating is a non-film forming alkyd emulsion. The acrylic and alkyd coatings were both film forming. Samples were studied uncoated and with coating thicknesses of 100 $\mu$m and 200 $\mu$m for both the alkyd and acrylic coating and applied masses of 50 g m$^{-2}$ and 150 g m$^{-2}$ for the open coating. To study the influence of surface treatment, the wood surface was either planed of sanded before coating application.

All combinations of sanded wood, coating and coating thickness which were measured are shown in table 4.1; • indicates an absorption experiment and ∘ a desorption experiment. Absorption experiments were performed on all wood types with all coatings applied with a thickness of 100 $\mu$m or 50 g m$^{-2}$ to study the influence of wood type and coating type on water uptake. For meranti, a coating thickness of 200 $\mu$m or a mass of 150 g m$^{-2}$ were also included to study the influence of coating thickness. Absorption

and desorption experiments were performed on all uncoated wood samples to study the moisture transport in each wood type. Meranti samples with 100 $\mu$m or 50 g m$^{-2}$ of all coating types were dried to study the coating boundary properties during desorption. The other wood types were dried with 100 $\mu$m or of acrylic coating applied, to study the performance of the acrylic coating on these wood types.

**Table 4.1** *Performed measurements on sanded samples: • indicates a wetting experiment; ∘ a drying experiment.*

| Coating | Mass | Thickness | Wood | | | |
|---|---|---|---|---|---|---|
| | (g m$^{-2}$) | ($\mu$m) | meranti | pine | Accoya | spruce |
| Open | 50 | | • ∘ | • | • | • |
| | 150 | | • | | | • |
| Alkyd | | 100 | • ∘ | • | • | • |
| | | 200 | • | | | |
| Acrylic | | 100 | • ∘ | • ∘ | • ∘ | • ∘ |
| | | 200 | • | | | |
| None | 0 | | • ∘ | • ∘ | • ∘ | • ∘ |

## 4.2 Samples and sample holders

Round samples were used with a diameter of 20.00 mm and a height of 10.00 mm, as shown schematically in figure 4.1. The coating is applied on the tangential plane for meranti, Accoya and pine and on the radial plane for spruce. The samples were machined from coated wooden boards by milling at high spindle speeds. The $B_0$ field and frequency encoding gradient are aligned along the positive $z$-direction, also see section 4.5. The sample holders were designed to seal the sides of the sample, only allowing moisture to enter or leave the wood through the coating. The sample holders were made of Teflon to prevent interference with the NMR signal.

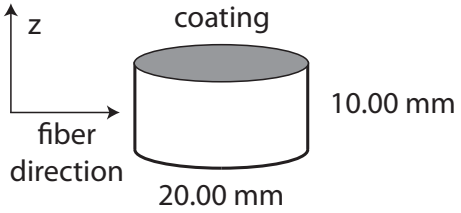


**Figure 4.1** *Schematic representation of a sample.*

## 4.3 Absorption experiments

To study the water uptake of a sample, a sample holder with an inner diameter of 20.00 mm was used. The wood sample is placed on top of a reference holder. The reference is used to correct for variations in the NMR signal intensity (SI) to allow for absolute measurements; in this case calculation of the MC from the SI which is described in detail in section 4.6. The edge of the coating is sealed with vaseline to prevent moisture from entering the sample via the sides, see figure 4.2(a). Because vaseline contains hydrogen, it can be measured by NMR. The vaseline-coating interface was used in the alignment of the sample at the start of a measurement with no water present. Water was placed on the sample and the system was monitored in the NMR scanner for approximately 24 hours.

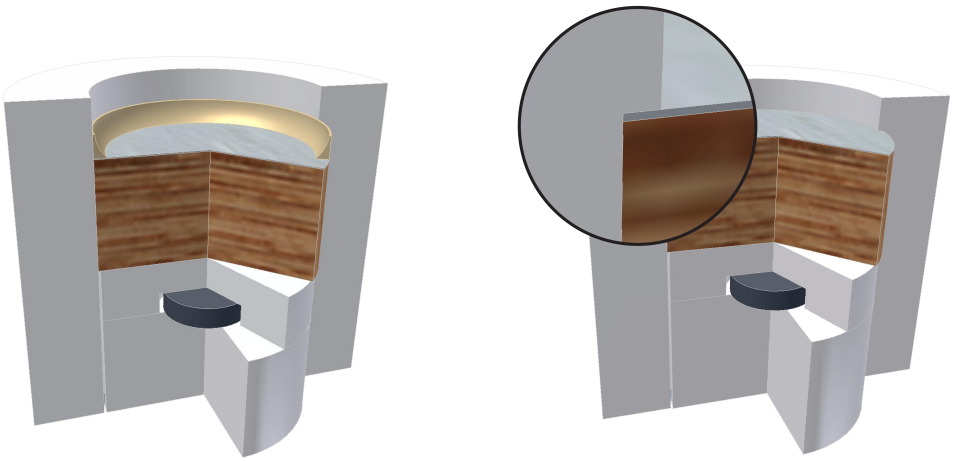

*(a) Wetting* *(b) Drying*

**Figure 4.2** *Schematic representation of the wetting and drying sample holders.*

## 4.4 Desorption experiments

The sample holder for the drying measurements had an inner diameter of 19.95 mm. By placing it in an oven at 103 °C the Teflon expands, after which the wood sample equilibrated at 33% RH could be inserted. Subsequent cooling of the holder and water uptake of the sample by submersion in water ensure a tight seal of the sides of the sample. The inset in figure 4.2(b) shows the upper part of the holder, which has a diameter of 19.00 mm ensuring that the sides of the sample remain sealed as the sample shrinks during drying – mainly in the tangential and radial direction as explained in section 2.2.2. The samples were dried outside the NMR setup in a climate chamber in which the RH was kept constant at approximately 2%. The samples were measured once a day to allow simultaneous monitoring of multiple samples.

## 4.5 NMR settings

A main magnetic field of 4.7 T was used, resulting in a Larmor frequency of approximately 200 MHz for $^1$H, see equation (3.2.4). Three pulse sequences where used. A HSE sequence, $90^\circ_x - \tau - 180^\circ_y - \tau - echo - \tau$ with $t_e = 2\tau$, was used to obtain one dimensional hydrogen density profiles. The signal intensity is calibrated allowing transformation to moisture content, see section 4.6. Every point on a profile thus reflects the average MC of a round slice of the sample, perpendicular to the $z$-axis as defined in figure 4.1. A CPMG sequence recording 1000 echoes, $90^\circ_x - \tau - [180^\circ_y - \tau - echo - \tau]_n$, was used to measure the $T_2$-relaxation yielding spatially resolved relaxation time distributions. TSE imaging was used to obtain qualitative images in the $xz$-plane to check whether the experiment was in fact one dimensional.

The parameters of the HSE and CPMG sequences are displayed in table 4.2. The scanner uses dynamic $x, y$ and $z$-gradients with a maximum field strength for the latter of 752 mT/m. The theoretical resolution $\Delta x_t$ is given by equation (3.5.3). For both the HSE and the CPMG sequence, the frequency encoding gradient is applied in the $z$-direction, i.e. parallel to $B_0$. The $x$ and $y$-gradients were used to align $\vec{G}$ exactly perpendicular to the sample surface to optimize the resolution. For the HSE measurements this resulted in a slice thickness of 33 $\pm$ 3 $\mu$m. This was tested by measuring a stack of coverslips with sticky type applied in between. $N_{avg}$ is the number of signal averages and $t_{acq}$ is the acquisition time for one profile. A long delay of 3 s was used in all measurements with $t_{90} = 65$ $\mu$s and $t_{180} = 120$ $\mu$s.

**Table 4.2** *Measurement parameters for the HSE and CPMG pulse sequences.*

| | $t_e$ ($\mu$s) | $G_z$ (mT/m) | $\Delta x_t$ ($\mu$m) | $N_{avg}$ | $t_{acq}$ (min) |
|---|---|---|---|---|---|
| HSE | 1700 | 752 | 31 | 128 | 6.4 |
| CPMG | 1200 | 300 | 78 | 128 | 8.8 |

## 4.6 Measuring wood moisture content by NMR

The signal intensity of the HSE sequence (SI) was calibrated to obtain the wood moisture content. To this purpose, samples of all four wood types were equilibrated at 22%, 53%, 75%, 93% and 100% RH over saturated salt solutions. One of each was fully saturated by immersion in water. The average SI, wet mass and oven dry mass of each sample were measured. The EMC of each sample was calculated from the masses and is plotted against

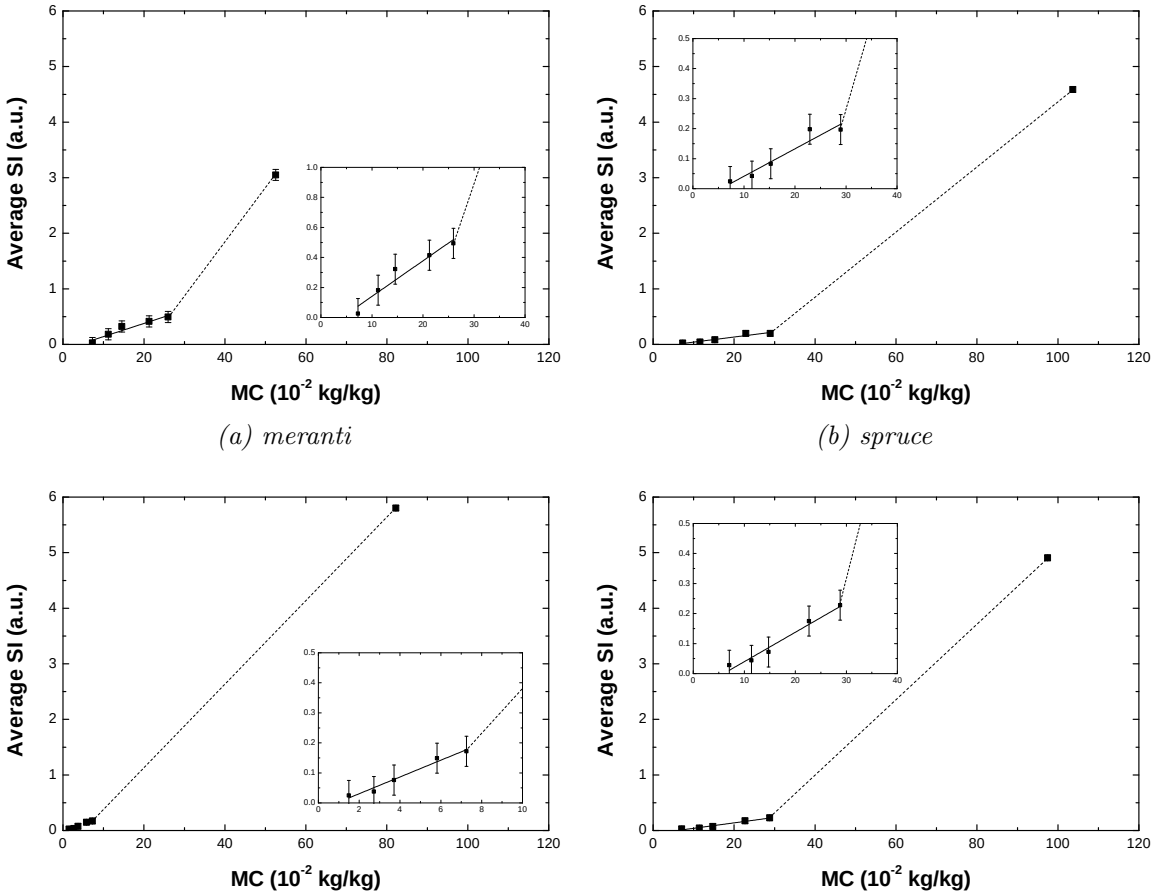


**Figure 4.3** *Average HSE signal intensity of each wood type for samples equilibrated at 22%, 53%, 75%, 93% and 100% RH and at saturation. The insets show a magnification of the data for the samples equilibrated at an RH. Note the larger vertical scale of the inset in figure (a) and the smaller horizontal scale in the inset in figure (c). For MCs above the FSP, the SI is assumed to increase linearly with the MC.*

the corresponding average SI in figure 4.3. The errors are indicated in the insets of the plots. The MC is given as a percentage of the oven dry weight which corresponds to $10^{-2}$ kg/kg, see equation (2.2.1).

A change in slope of the SI is observed at the FSP which is caused by a difference in relaxation time for bound and unbound water. As explained in section 3.8, the distribution of relaxation times measured by NMR allows to distinguish between bound and unbound water. Relaxation time distributions were calculated by the CONTIN routine [44] from measurements on meranti, see figure 4.4. The horizontal axes show the relaxation time. The shortest relaxation time that can be measured equals the echo time of the CPMG sequence, $t_e = 1200$ $\mu$s. Note that the signal from solid wood

decays to zero in tens of microseconds and is therefore not measured [18]. The vertical axes show the the intensity of the distribution. The distribution shown in figure 4.4(a) was measured on a sample equilibrated at 100% RH. A single peak is observed at low relaxation times. Since this sample only contains water in its cell walls, this peak is attributed to bound water. A relaxation time distribution measured on a fully saturated sample, see figure 4.4(b), shows additional peaks at higher relaxation times which result from unbound water, present in the lumina and vessels. The peak in figure 4.4(b) corresponding to bound water is significantly broader than that in figure 4.4(a). This most likely results from the regularization applied by the CONTIN routine. This is supported by the fact that the surface area of a peak, which is comparable for both peaks, indicates the intensity of a relaxation time contribution rather than the height of the peak. Because of the difference in relaxation times, the signal from bound water has decayed more than the signal from unbound water at the first moment of acquisition. FID measurements which record the signal only 100 $\mu$s after excitation, as opposed to 1700 $\mu$s for a HSE, confirm this; the change in slope is significantly smaller for the FID SI plotted against MC, which is shown appendix B. Since the NMR SI is directly related to the hydrogen density, the SI is assumed to increase linearly with the MC for MCs above the FSP. For each wood type, the two slopes are fitted linearly. These fits are used to convert the HSE SI to MC.

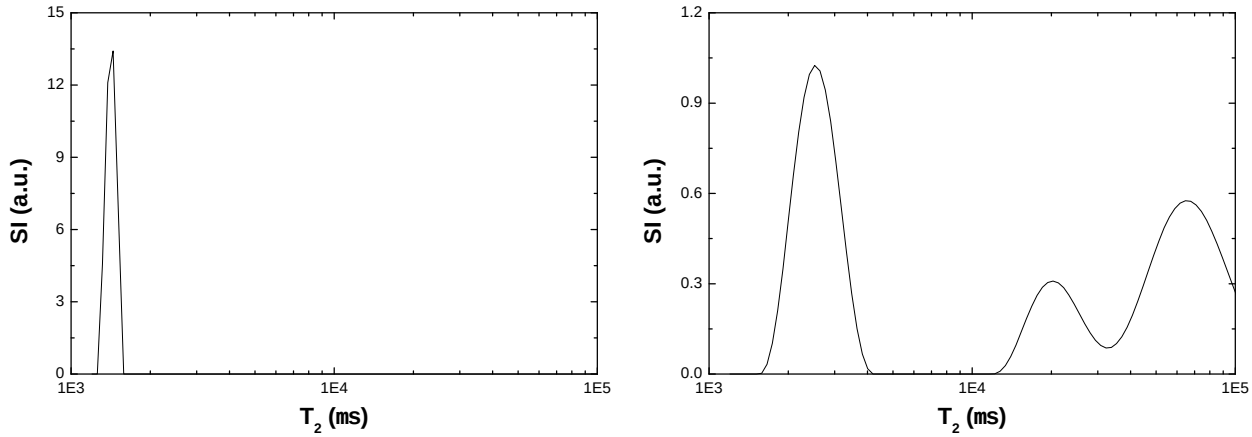


*(a) 100% RH* *(b) saturated*

**Figure 4.4** *Relaxation time distributions for a meranti sample equilibrated at 100% RH and for a fully saturated sample.*

Note that the diffusion regime can be estimated from the relaxation time distributions. Substituting the condition for the fast diffusion region $\nu r/D \ll 1$ in equation (3.8.10), gives $r^2/(3DT_2) \ll 1$ as a condition for the fast diffusion regime. The value of this parameter is given in table 4.3 for the types of moisture present in wood using pore sizes from literature. Since

bound water cannot be treated as bulk water as explained in section 3.8.2, relaxation times from bound water cannot be linked to a pore size even though the criterion would be met when assuming a pore size of 1 $\mu$m. For unbound water, the criterion is not met. Bound water is in the intermediate diffusion region which means that a single pore size is represented by more than one relaxation time. As a result, equation (3.8.8) can no longer be simplified to equation (3.8.9) since $I_{i,j} \nrightarrow 0$ for $i > 0$. However, the first higher mode of the relaxation time $T_{2,1,j}$ is an order of magnitude smaller than the lowest mode $T_{2,0,j}$ so an estimate of the pore sizes can still be obtained from the relaxation times of unbound water.

**Table 4.3** *Calculated diffusion regimes for the different types of moisture in wood.*

| | Relaxation time ($\mu$s) | Pore size ($\mu$m) | $r^2/(3DT_2)$ |
|---|---|---|---|
| cell wall | $1 \cdot 10^3$ | – | – |
| softwood lumina | $2 \cdot 10^4$ | 35 | 8 |
| hardwood vessels | $8 \cdot 10^4$ | 50 – 100 | 4 – 16 |

The maximum MC of spruce, Accoya and pine is higher than that of meranti although the FSP of all wood types occurs at approximately 27% MC except for Accoya. The relatively low MC of saturated meranti is partially caused by the differences between hard- and softwoods but also by the fact that meranti has a higher density. This results in a lower MC according to equation (2.2.1). To illustrate this, table 4.4 shows the average density, the measured FSP and the relative mass change of water uptake, for samples equilibrated at 100% RH and saturated ones. Meranti increases the most in mass at 100% RH but the least when fully saturated. Accoya is shown to take up a relatively small amount of water at 100% RH which results in a low FSP at 7% MC. This is due to the acetylation which reduces water uptake of the cell walls, as explained in section 2.1.4. This effect has been shown using NMR by Thygesen [48]. Note that the measured FSPs are approximately $3 \cdot 10^{-2}$ kg/kg below those reported in literature [49]. The most likely cause is that the temperature in the humidity chamber in which the samples were equilibrated, was below the standard test temperature. This resulted in a lower absolute humidity because of which the samples absorbed to little moisture.

**Table 4.4** *Average density at a MC of approximately 10%, FSP and relative mass change for the samples equilibrated at 100% RH and the fully saturated samples. The error is* $1 \cdot 10^{-2}$ *kg/kg for the FSPs and* $1 \cdot 10^{-2}$ *g/g for the mass measurements.*

| | $< \rho >$ | FSP | $\Delta m/m_0$ | $\Delta m/m_0$ |
|---|---|---|---|---|
| | (kg/m$^3$) | ($10^{-2}$ kg/kg) | 100% RH | saturated |
| Meranti | 710 | 25 | 0.26 | 0.53 |
| Spruce | 472 | 27 | 0.31 | 1.04 |
| Accoya | 475 | 7.1 | 0.07 | 0.82 |
| pine | 451 | 29 | 0.29 | 0.97 |

Chapter 5

# Water absorption by coated wood

This chapter presents the results of the wetting experiments in which the influence of a coating on the water absorption by wood is studied. The first section presents the water uptake experiments on coated meranti. The second section compares the water uptake of the softwoods pine and Accoya. The final section presents water uptake experiments on spruce.

## 5.1 Coatings on meranti

This section presents moisture profiles for uncoated and coated meranti. From these profiles the average MC directly behind the coating is determined as a function of time. Next, the influence of a coating on the rate of water uptake is quantified by determining the diffusion coefficient. Finally, this section discusses the behavior of the coating.

### 5.1.1 Moisture profiles during wetting

Hydrogen density profiles reflecting the moisture content were obtained by means of a HSE sequence as explained in section 4.5. Profiles of the wetting of uncoated and coated meranti are shown in figure 5.1. The time between each profile is given by $\Delta$t; the duration of the experiment by t. These profiles were obtained by interpolating and averaging a total number of approximately 68 profiles, measured every 21 min. All profiles presented in this chapter are obtained similarly unless specified otherwise. The top of the sample is located at position $x = 0$. All samples were equilibrated at 22% RH corresponding to an initial MC of about 7%. The error in the MC profiles is approximately $1 \cdot 10^{-2}$ kg/kg; the irregularities of the profiles are a result of wood inhomogeneities. The horizontal dashed line indicates the FSP as determined in section 4.6.

Water uptake profiles of uncoated meranti are given in figure 5.1(a). These show that the MC remains below the FSP. Only directly below the

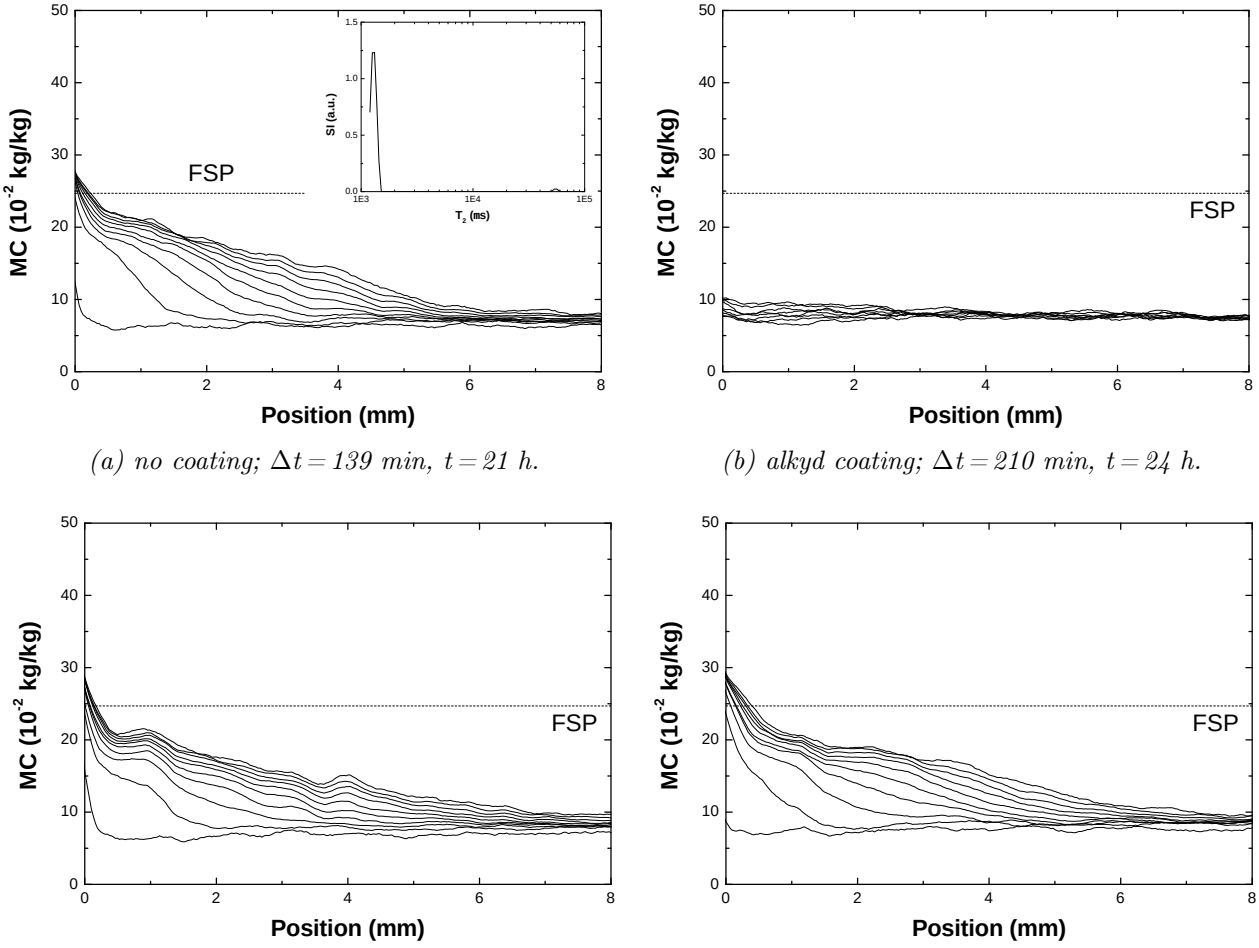


*(a) no coating; $\Delta t = 139$ min, $t = 21$ h.*

*(b) alkyd coating; $\Delta t = 210$ min, $t = 24$ h.*

*(c) open coating; $\Delta t = 140$ min, $t = 21$ h.*

*(d) acrylic coating; $\Delta t = 140$ min, $t = 21$ h.*

**Figure 5.1** *Moisture Content (MC) profiles of water absorption of meranti with 100 $\mu$m or 50 g m$^{-2}$ of a coating applied. The top of the sample is located at $x = 0$. The horizontal dashed lines indicates the FSP as determined in section 4.6. The inset in figure (a) shows the relaxation time distribution of uncoated meranti after 21 hours.*

surface of the sample the MC exceeds the FSP, because of direct contact of lumina with water at the surface. This is confirmed by the relaxation time distribution at the end of the experiment which is shown in the inset of figure 5.1(a). The contribution at short relaxation times represents bound water and is relatively large compared to the minute contributions observed at higher relaxation times. Figure 5.1(b) shows the water uptake of an alkyd coated sample. Very little water ingress is observed in comparison to the uncoated sample. This indicates that the alkyd coating forms an effective barrier against moisture. Profiles of open coated meranti are shown in figure 5.1(c), those of acrylic coated meranti in figure 5.1(d). The profiles in figures (a), (c) and (d) display similar behavior. The similarities between uncoated

and open and acrylic coated samples are confirmed by mass measurements. The relative mass change after 24 hours of water uptake is displayed in table 5.1.

**Table 5.1** *Relative mass change of uncoated and coated meranti samples. The error in the mass change is* $0.1 \cdot 10^{-2}$ *g/g.*

| Coating | Mass ($g\ m^{-2}$) | Thickness ($\mu$m) | $\Delta m/m_0$ ($10^{-2}$ g/g) |
|---|---|---|---|
| None | | | 4.1 |
| Open | 50 | | 3.8 |
| | 150 | | 3.1 |
| Alkyd | | 100 | 0.6 |
| | | 200 | 0.3 |
| Acrylic | | 100 | 4.0 |
| | | 200 | 4.3 |

It has to be remarked that after 24 hours the samples are not fully saturated. However, the profiles suggest that already after approximately 24 hours a steady state is reached near the surface. This is confirmed by an experiment which ran for 6 days; the MC near the surface remained constant after one day. Firstly, this means that NMR offers a possibility to assess the absorption behavior of wood in considerably shorter experiments than other techniques which may require days or even hundreds of days [9–12]. Secondly, NMR allows to determine the MC of a sample while water is still present on the sample. When weighing, the water has to be removed from the surface which introduces an additional error. The steady state is considered in more detail in the next section.

### 5.1.2 Final water uptake

The average MC from the wood-coating interface to a depth of 1 mm is determined and plotted against time in figure 5.2. At $t = 0$ the MC is approximately 7% reflecting the initial MC of the samples. The figure confirms that the water uptake by the alkyd coated samples is low and that a thicker alkyd coating results in less uptake. For the other samples, the increase of the MC directly behind the surface decreases with time to become nearly constant after 24 hours. The final average MC is above the FSP because of filling of lumina in direct contact with the sample surface, as already mentioned above.

The average MC reaches a constant final value near the surface which the entire sample will reach later times. A similar constant value for the

planed or sanded, uncoated, open and acrylic coated samples was found. The interface between coating and wood is not always clearly identifiable. This results in a spread of the final values. These results show the coating to be of no influence on the amount of water uptake. The rate of water uptake is studied next.

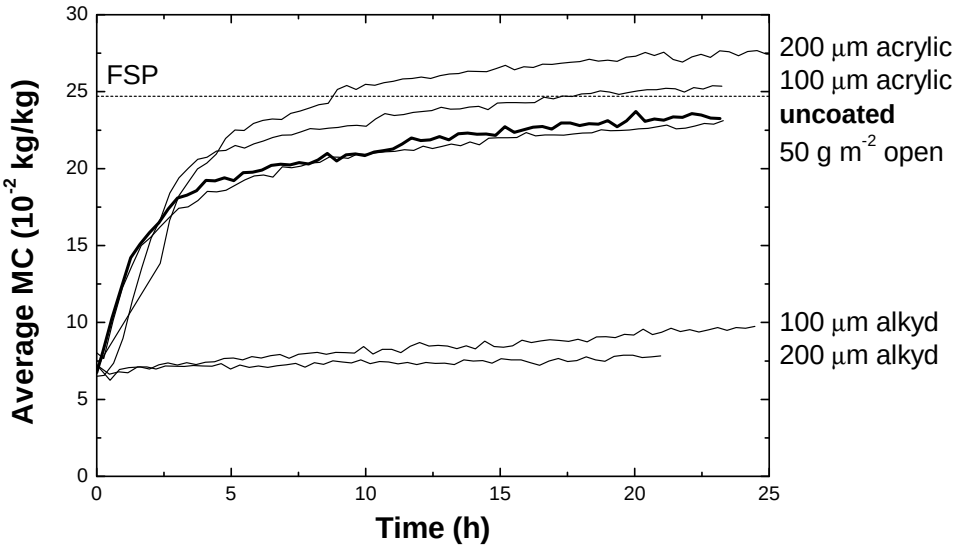


**Figure 5.2** *Average MC of a 1 mm thick slice directly behind the meranti-coating interface, plotted against time. Coating thicknesses of 100 µm and 200 µm and 50 g m$^{-2}$ are shown. The horizontal dashed line indicates the FSP. The bold curve represents the average MC of an uncoated sample.*

### 5.1.3 Rate of water uptake

The rate of water uptake is quantified by the effective diffusivity which can be determined directly from moisture profiles such as those given in figures 5.1(a), 5.1(c) and 5.1(d). Since the MC is below the FSP, moisture transport takes place via vapor transport through the lumina, see section 2.2.3. This transport process is dominated by diffusion which, in the case of one-dimensional moisture transport, can be described to a good approximation by a non-linear diffusion equation [50]:

$$\frac{\partial \theta}{\partial t} = \frac{\partial}{\partial x}\left(D_{eff}\frac{\partial \theta}{\partial x}\right), \tag{5.1.1}$$

where $\theta$ is the MC, $x$ the position, $t$ the time and $D_{eff}$ the effective diffusivity of the system. The diffusivity can depend on the MC as is the case for certain porous materials as shown by Pel et al. [51] using NMR. Weighing measurements by de Meijer and Militz [12] and X-ray computed tomography measurements by Danvind and Ekevad [52] showed that the local diffusivity

of spruce was dependent on the MC. The moisture transport during water absorption can be described by equation (5.1.1) with the initial and boundary conditions:

$$\theta = \theta_0 \quad \text{for} \quad x > 0,\ t = 0, \tag{5.1.2}$$

$$\theta = \theta_{cap} \quad \text{at} \quad x = 0,\ t > 0, \tag{5.1.3}$$

where $\theta_0$ is the initial uniform moisture content of 7% and $\theta_{cap}$ is the maximum moisture content under atmospheric conditions, which in this case equals the FSP. When the well-known Boltzmann transformation [53]:

$$\lambda = \frac{x}{\sqrt{t}}, \tag{5.1.4}$$

is applied, the non-linear diffusion equation (5.1.1) reduces to an ordinary differential equation:

$$2\frac{d}{d\lambda}\left(D_{eff}\frac{d\theta}{d\lambda}\right) + \lambda\frac{d\theta}{d\lambda} = 0, \tag{5.1.5}$$

with boundary conditions [54]:

$$\theta = \theta_0 \quad \text{for} \quad \lambda \to \infty, \tag{5.1.6}$$

$$\theta = \theta_{cap} \quad \text{at} \quad \lambda = 0. \tag{5.1.7}$$

Figure 5.3 shows the moisture profiles of open coated meranti, shown in figure 5.1(c), after Boltzmann transformation. All transformed profiles overlap, except for the first few since for these profiles the boundary condition (5.1.7) is not met. This confirms that the moisture transport is diffusion dominated and that the profiles at different times are related by a simple $\sqrt{t}$ scaling.

If $D_{eff}$ is assumed to be constant, equation (5.1.5) with boundary conditions (5.1.6) and (5.1.7) has only one solution given by an error function:

$$\theta = C_1 + C_2 \ \text{erfc}\left(\frac{\lambda}{\sqrt{4D_{eff}}}\right), \tag{5.1.8}$$

in which $C_1$ and $C_2$ are constants. Profiles of 3 uncoated, 2 open coated and 6 acrylic (2 sanded and 4 planed) coated samples were Boltzmann transformed and fitted. The data is fitted well by equation (5.1.8) which means the assumption that $D_{eff}$ can be treated as a constant is a suitable for these experiments. In addition, fitting the transformed profiles yields $D_{eff}$. The resulting values for the effective diffusivity are given in table 5.2. All values of $D_{eff}$ are equal within the error margin. In fact, the values correspond to the transverse (tangential and radial) diffusion coefficient of meranti of approximately $1 \cdot 10^{-10}$ m$^2$ s$^{-1}$ [28]. This means that the open and acrylic coating have no influence on the rate of water uptake of meranti.

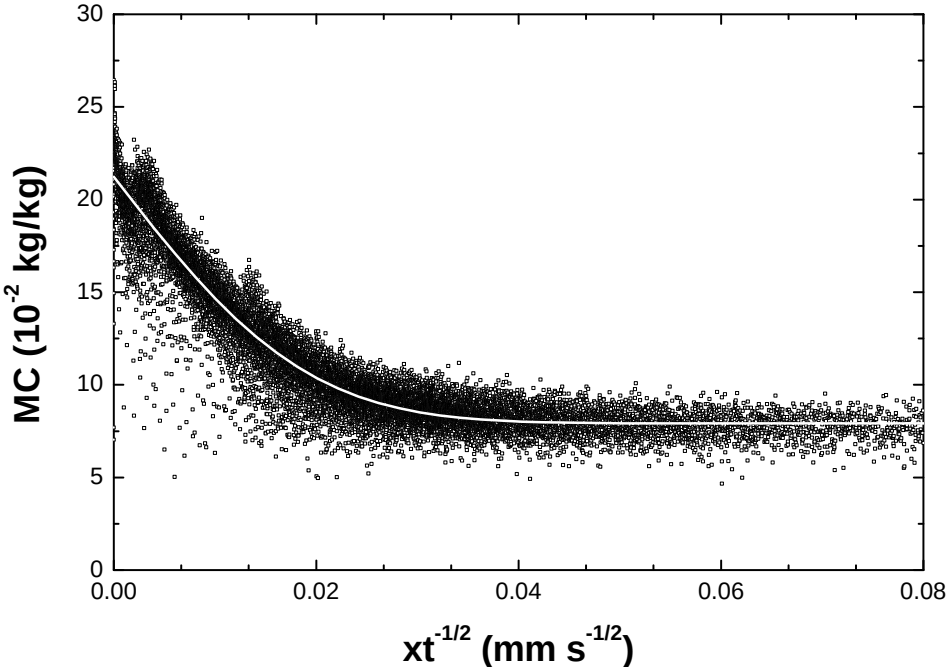


**Figure 5.3** *Profiles of open coated meranti shown in figure 5.1(c) after Boltzmann transformation. The solid line is the fitted error function* (5.1.8) *from which* $D_{eff}$ *is obtained.*

**Table 5.2** *Diffusion constant for coated and uncoated meranti as found from the Boltzmann transformed profiles. The error in* $D_{eff}$ *is* $3.0 \cdot 10^{-11}$ $m^2$ $s^{-1}$.

| Coating | Mass ($g\ m^{-2}$) | Thickness ($\mu$m) | $D_{eff}$ ($10^{-11}$ $m^2$ $s^{-1}$) |
|---|---|---|---|
| None | | | 8.3 |
| Open | 50 | | 11 |
| | 150 | | 8.3 |
| Acrylic | | 100 | 9.5 |
| | | 200 | 8.4 |

### 5.1.4 Performance of the coatings

The open and acrylic coating have been found to be of no influence on the rate and amount of water uptake of meranti over a period of 24 hours. In order to explain this, the water uptake of the coating itself is studied. The resolution of 33 $\pm$ 3 $\mu$m allows to distinguish the alkyd and acrylic coating from the wood – the open coating does not form a film, making it indistinguishable from the wood surface. Two to five slices, depending on the coating thickness, were measured inside the alkyd and acrylic coating. The SI of these slices

is averaged by integrating the profiles between the wood-coating interface and the coating-water interface. The average SI in the coating is plotted against time in figure 5.4. Note that the vertical axis does not represent MC since the calibration can only be used within wood. However, the SI is a measure for the amount of moisture present in the coating. The interface between coating and wood cannot always be clearly identified. This causes the irregularities in the average SI. It also results in an uncertainty in the final values which explains the difference in average SI after approximately 24 hours of both acrylic coatings.

Alkyd coatings of both 100 $\mu$m and 200 $\mu$m thick are shown absorb nearly no water. This could explain why the alkyd coating forms an effective barrier against moisture. On the other hand, the acrylic coating absorbs relatively large amounts of water because of which it does not form an effective barrier against moisture absorption. This explains why the values for the effective diffusivity of coated meranti, presented in table 5.2, are all comparable to that of uncoated meranti. This means, the absorption is fully limited by the wood itself; the open and acrylic coating have no influence on the absorption.

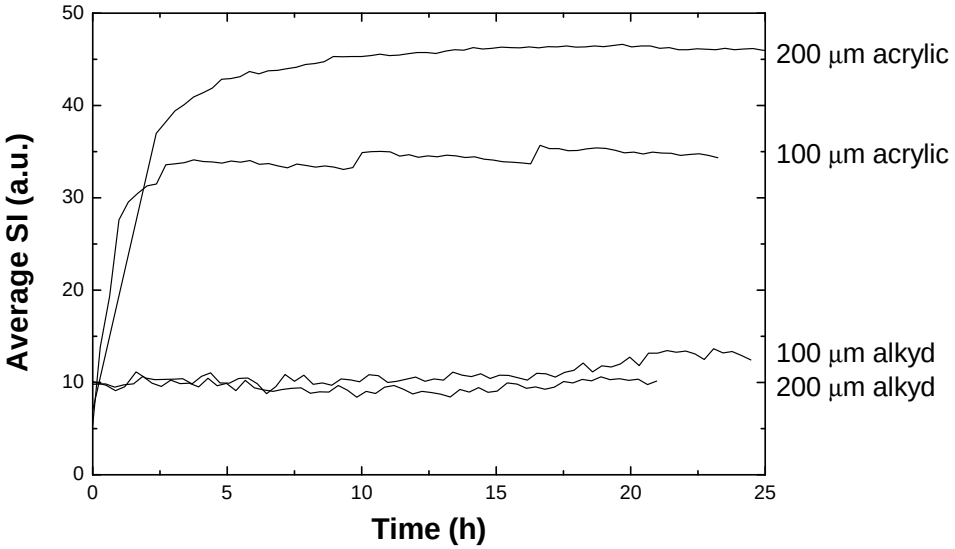


**Figure 5.4** *Average SI measured in the coating. Lines for coating thicknesses of 100 $\mu$m and 200 $\mu$m are shown.*

### 5.1.5 Summary

NMR was shown to be suitable to study the water absorption of coated and uncoated wood samples. Relatively short experiments suffice to determine the amount and rate of water uptake with high accuracy, while the water placed on the surface does not have to be removed.

It was shown that the alkyd coating absorbs very little water. Therefore, it forms an effective barrier against moisture thus offering a good protection

of meranti against moisture. For the open and acrylic coating the final amount and rate of water uptake were shown to be internally limited, i.e. by meranti. This is expected behavior for the open coating since it does not form a film. Although the acrylic coating does form a film, it absorbs water at such rates that it has no influence on the water absorption of meranti. This means that both the open and acrylic coating offer no protection for meranti against external moisture. Coating thickness and surface treatment (planing or sanding) show no significant influence on the water uptake.

## 5.2 Coatings on pine and Accoya

This section presents the results of the measurements on coated and uncoated pine and Accoya. As explained in section 2.1.4, Accoya is acetylated pine. Moisture profiles are shown for coated and uncoated samples. To study how the coatings influence the water uptake, a relaxation time analysis is presented subsequently.

### 5.2.1 Uncoated pine and Accoya

Profiles of the water uptake of uncoated pine and Accoya obtained by NMR are given in figure 5.5. The time between each profile is given by $\Delta$t; the duration of the experiment by t. The top of the sample is located at position $x = 0$. The error in the MC profiles is approximately $1 \cdot 10^{-2}$ kg/kg; the irregularities of the profiles are a result of wood inhomogeneities. In pine, and thus also in Accoya, the difference in late- and earlywood is larger than for meranti. Because of this, annual rings are more apparent in the moisture profiles; especially since the samples are made of tangential boards. Annual rings are observed between 3 and 5 mm in figure 5.5(a) and at approximately 0 mm and 7 mm in figure 5.5(b).

The homogeneously increasing profiles indicate capillary water uptake immediately from the beginning of the experiment. As opposed to meranti, pine and Accoya contain relatively large and high permeable rays. These run in the radial direction which is parallel to the $z$-axis as shown in figure 4.1. The rays quickly absorb water by capillary suction. This is confirmed by relaxation time distributions determined after a short time of water uptake, shown by the dashed curves in figure 5.6. These show both bound and unbound contributions. Because the rays, and possibly also lumina, contain water before the cell walls are saturated, bound an unbound water are not in equilibrium at the beginning of the experiment. Therefore, the calibration cannot be used so the vertical axes of the profiles show signal intensity instead of MC.

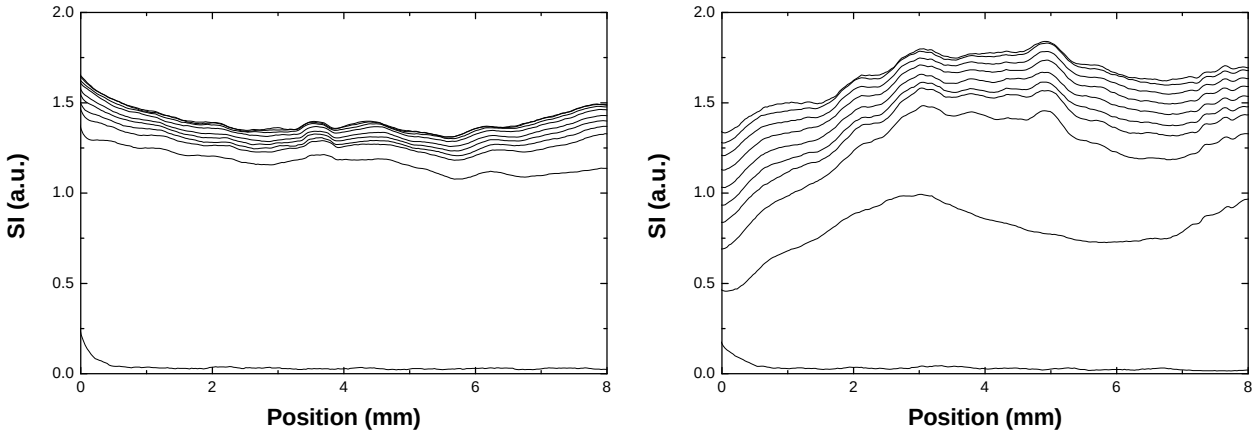


*(a) uncoated pine; $\Delta t = 143$ min, $t = 21$ h.* *(b) uncoated Accoya; $\Delta t = 125$ min, $t = 19$ h.*

**Figure 5.5** *Moisture content profiles of uncoated pine and Accoya. The top of the sample is located at position $x = 0$. Note that the vertical axis shows SI since the calibration cannot be used because of fast capillary water uptake by rays at the beginning of the experiment.*

Relaxation time distributions were obtained when equilibrium was reached. These are shown by the solid profiles in figure 5.6. For Accoya, a significant shift of the bound water contribution towards a higher relaxation time is observed. Because a shift is not observed for pine although pine swells more than Accoya, the relaxation time does not increase because bound water is less bound as a result of swelling. This is confirmed by the relaxation time distributions of the calibration samples shown in appendix C.

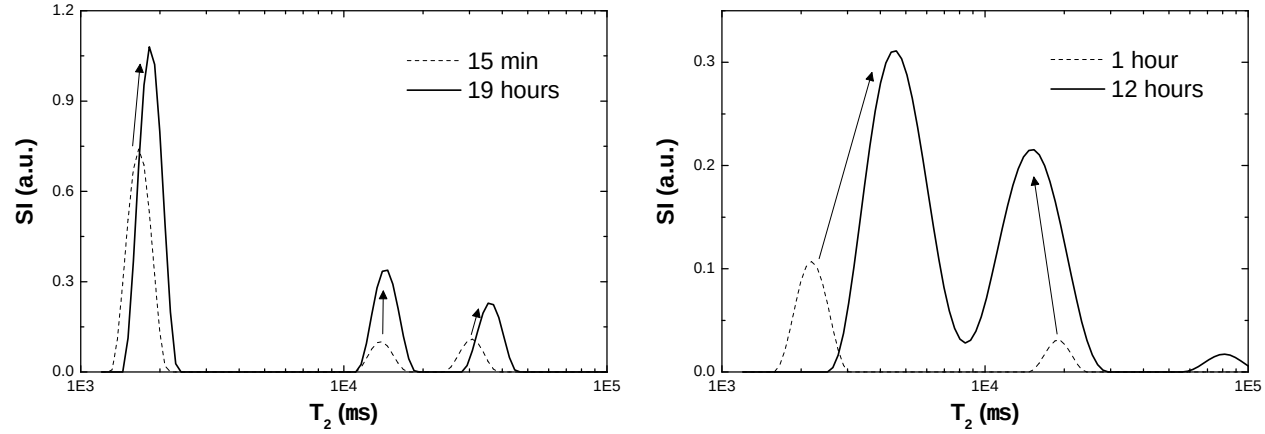


*(a) uncoated pine.* *(b) uncoated Accoya.*

**Figure 5.6** *Relaxation time distributions for uncoated pine and Accoya after a short time of water uptake, shown by the dashed curves and after equilibrium has been reached, shown by the solid curves.*

A possible cause of the shift is the acetylation. In Accoya, most bound water sites are occupied by acetyl groups. Upon water absorption, the few remaining sites are occupied first. This could lower the interactions of additional moisture with the cell wall because of which the relaxation time of bound water increases with increasing MC. This behavior reappears in section 5.2.4 where the water uptake of the coated samples is studied.

### 5.2.2 The influence of a coating

The alkyd coating shows similar behavior as on meranti; moisture absorption was fully inhibited for both wood types. As opposed to meranti, the open

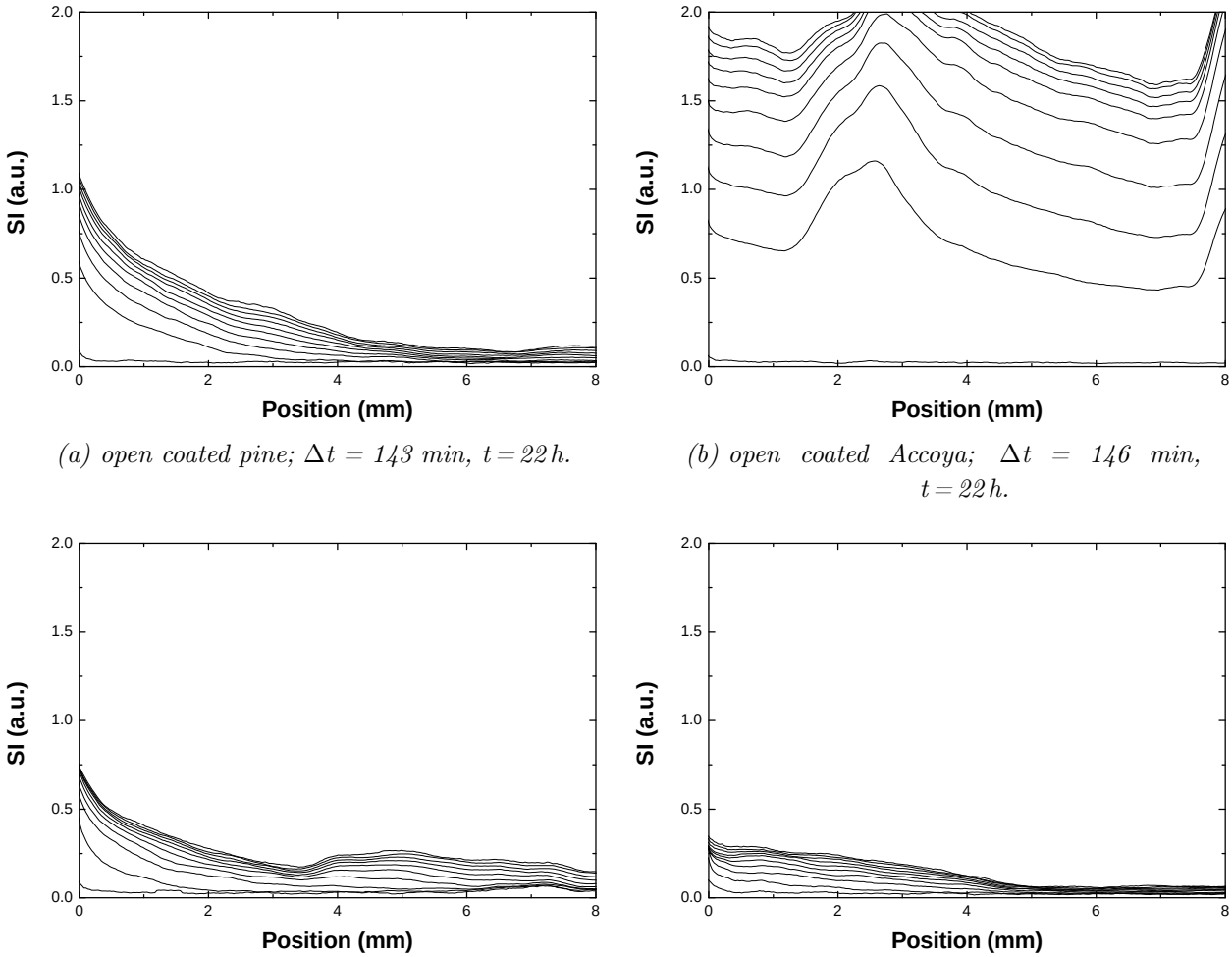


*(a) open coated pine; $\Delta t$ = 143 min, $t = 22\,h$.*

*(b) open coated Accoya; $\Delta t$ = 146 min, $t = 22\,h$.*

*(c) acrylic coated pine; $\Delta t$ = 135 min, $t = 20\,h$.*

*(d) acrylic coated Accoya; $\Delta t$ = 135 min, $t = 20\,h$.*

**Figure 5.7** *Moisture content profiles of coated pine and Accoya. The top of the sample is located at position $x = 0$. The horizontal dashed lines indicate the FSP, see table 4.4.*

coating limits the water uptake of pine as shown by the profiles in figure 5.7(a). The profiles for the water uptake of acrylic coated pine shown in figure 5.7(c) display comparable behavior. The difference between the profiles beyond a depth of 3 mm is caused by annual rings which are observed at approximately 4 mm in figure 5.7(a) and 3 mm and 7.5 mm in figure 5.7(c). Unlike pine, a clear difference is seen for the open an acrylic coating on Accoya. The acrylic coating dramatically reduces the water uptake of Accoya as can be seen in figure 5.7(d). However, the open coating is shown to have no significant influence on the water uptake in figure 5.7(b). Regarding the MC to a depth of approximately 3 mm, the water uptake is not influenced by inhomogeneities.

### 5.2.3 Final water uptake

The profiles in figures 5.5 and 5.7 indicate that, after approximately 24 hours, a steady state is reached near the surface. Hence, the average MC of a 1 mm thick slice directly behind the wood surface is determined and plotted against time in figure 5.8. At $t = 0$ the MC is approximately 9% for pine and 5% for Accoya reflecting the initial MC of the samples. Note that the first profile is obtained before water is placed on the sample so for that profile the calibration can still be used. Times at which bound and unbound water are not in equilibrium, thus not representing the average MC, are shown by dashed curves in figure 5.8. The curves are given for the full length of the experiment to show that equilibrium is obtained after approximately 20 hours. From then on, the solid parts of the curves accurately represent the MC. This steady state MC will be discussed below in more detail.

A MC of approximately 48% is observed for uncoated pine and 25% for uncoated Accoya. This is in accordance with a lowering of the FSP (see table 4.4) of 29 - 7 = 22% as a result of acetylation. Both the open and acrylic coating are shown to equally reduce the water uptake of pine. However, on Accoya the open coating has no influence on the uptake. The difference in final MC of uncoated and open coated Accoya is caused by the annual ring observed at the top of the uncoated sample in figure 5.5(b). A large reduction in water uptake is observed for acrylic coated Accoya. The MC in fact remains below the FSP which has already been lowered by acetylation, which results in very little water uptake.

### 5.2.4 Performance of the coatings

To determine how the coatings reduce the water uptake, a relaxation time analysis is performed to asses the state of the water absorbed by the wood. Relaxation time distributions for coated and uncoated pine and Accoya at the end of the water uptake are plotted in figure 5.9.

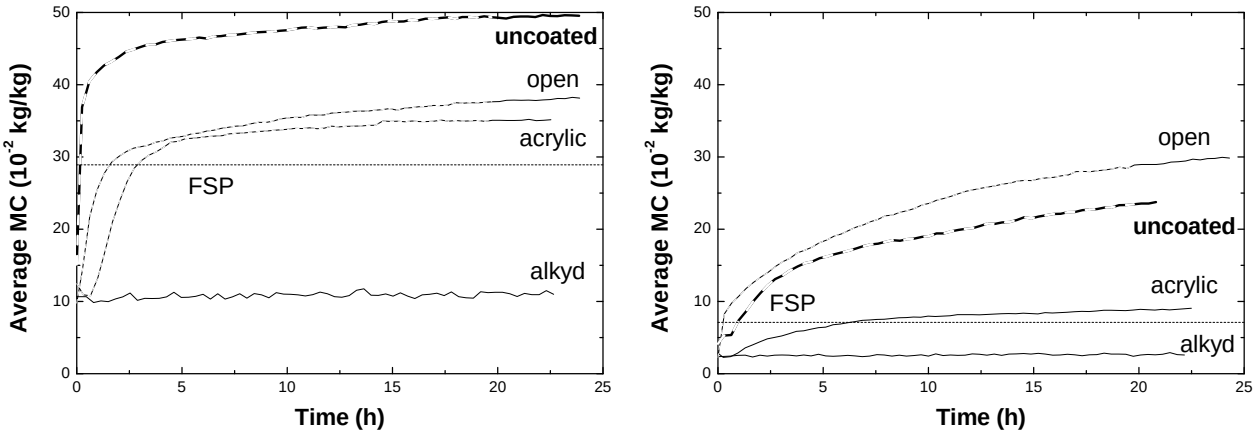


*(a) pine.* *(b) Accoya.*

**Figure 5.8** *Average MC of a 1 mm thick slice directly behind the wood-coating interface, plotted against time. Curves are shown for a coating thickness of 100 µm or a mass of 50 g m$^{-2}$. The horizontal dashed lines indicate the FSP. At times where the calibration cannot be used, the curves are dashed.*

The distributions of pine, given in figure 5.9(a), show that the open coating reduces the unbound water uptake. Also the contribution of bound water decreases. The shift of the bound water contribution is insignificant. The acrylic coating completely prevents the uptake of unbound water and further reduces the absorption of bound water.

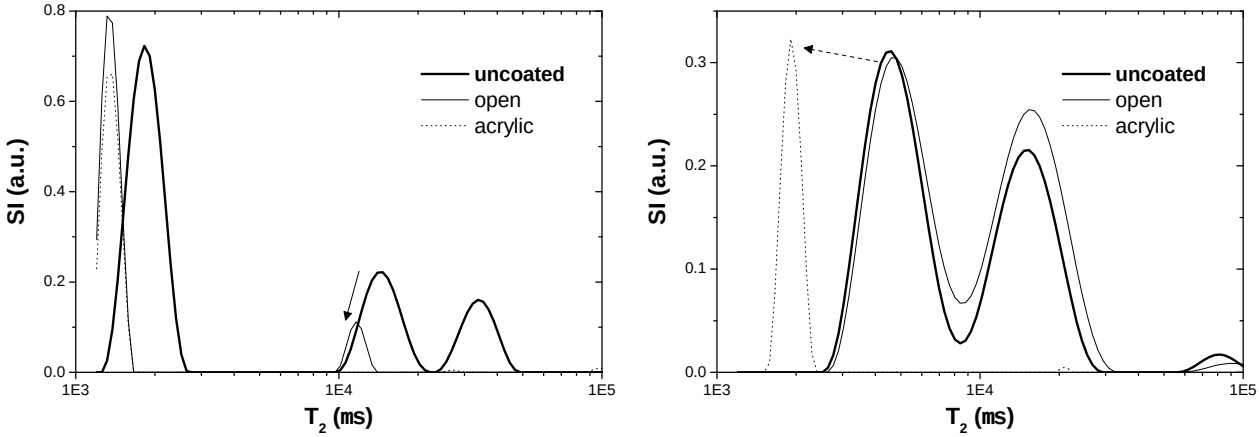


*(a) pine.* *(b) Accoya.*

**Figure 5.9** *Relaxation time distributions for coated and uncoated pine and Accoya samples after a time of approximately 24 hours.*

From the relaxation time distributions of uncoated Accoya in figure 5.6(b), the contribution at low relaxation times is shown to correspond to bound water whereas the contribution at high a relaxation times is attributed to unbound water. The distribution for open coated Accoya shows an increased contribution of unbound water as a result of density differences between the various samples. For acrylic coated Accoya, only a bound water contribution is observed at a relaxation time comparable to that at the beginning of water uptake of uncoated Accoya, see figure 5.6(b). This means the acrylic coating prevents the uptake of unbound water and reduces the uptake of bound water. The latter results in a lower relaxation time for the bound contribution. Because the acrylic coating prevents the uptake of unbound water, the calibration can be used throughout the experiment; the corresponding curve in figure 5.7(d) is shown solid.

### 5.2.5 Summary

Because of the fast capillary water uptake of rays in pine and Accoya, the calibration cannot be used until bound and unbound water are in equilibrium. This was the case after approximately 24 hours at which point the MC was determined accurately by NMR. The ability to distinguish bound water from unbound water by NMR offered an explanation of the observations.

Despite the acrylic coating becoming fully wet, it reduces the water uptake of pine and Accoya by approximately 40 to 50%, whereas on meranti this coating was of no influence. The same holds for the open coating on pine. The absorption is reduced because all coatings effectively seal the relatively large rays thereby strongly reducing the capillary water uptake. This greatly reduces the moisture content of the wood. Only the open coating on Accoya showed no influence. Presumably, one or more of the large rays were not sealed. The alkyd coating also strongly reduces the bound water uptake of pine and Accoya.

## 5.3 Coatings on spruce

Moisture profiles of the water uptake of coated and uncoated spruce were also obtained by NMR. The average moisture content of a 1 mm thick slice directly beneath the surface is shown in figure 5.10. Similar to pine and Accoya, uncoated spruce and 50 g $m^{-2}$ open coated spruce absorb both bound and unbound water at the start of the experiment, as a consequence of which the calibration cannot be used. This region is indicated by the dashed sections of the curves. As for the other wood types, alkyd coated spruce absorbs very little water.

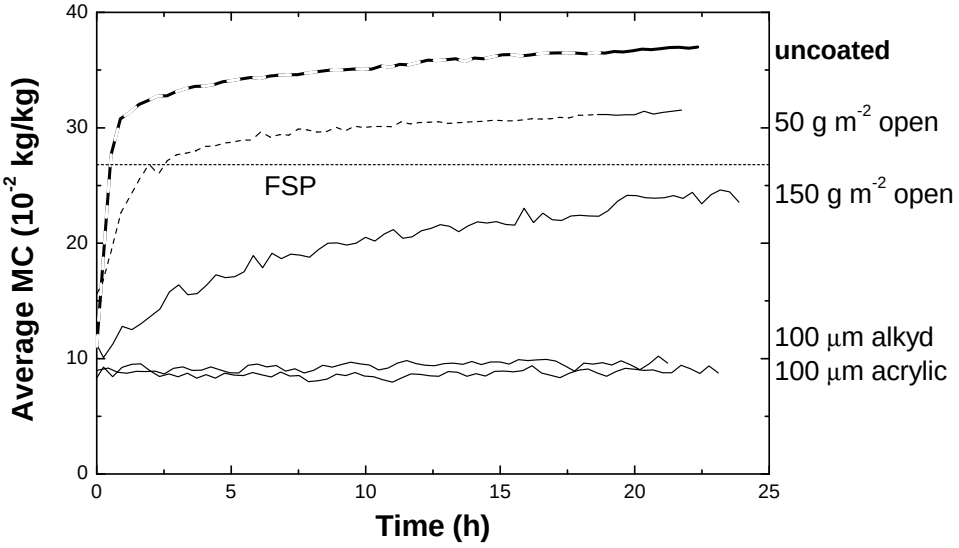


**Figure 5.10** *Average MC of a 1 mm thick slice directly behind the spruce-coating interface, plotted against time. The horizontal dashed line indicates the FSP. Coating thicknesses of 100 µm or 50 g m$^{-2}$ and 150 g m$^{-2}$ are shown.*

The open coating is found to decrease the absorption depending on the amount of coating applied. The state of the absorbed water, bound or unbound, is determined for the uncoated and open coated samples on the basis of relaxation time distributions shown in figure 5.11. The open coating reduces the amount of unbound water uptake. Small contributions at higher relaxation times are present for 50 g m$^{-2}$ open coated spruce accounting for the final MC being above the FSP. 150 g m$^{-2}$ of open coating inhibits the uptake of unbound water and further reduces the bound water uptake. Note that the intensity of a relaxation time contribution is indicated by the surface area of a peak, not by its height, as is explained in section 4.6.

The acrylic coating strongly reduces the moisture absorption as shown in figure 5.10, although the acrylic coating was observed to absorb water. This behavior of the acrylic coating largely differs from its behavior on meranti, pine and Accoya. The reduction in bound water uptake of spruce caused by the acrylic coating might be a result of wood drying prior to coating application. Because of this, the pits interconnecting the lumina are aspirated as explained in section 2.1.3. Upon contact with water, the pits reopen allowing water absorption, as seen for uncoated spruce. However, application of the acrylic coating fixates the aspirated pits at the surface of the wood. Despite the absorption of water by the acrylic coating, water no longer flows or condensates in lumina beneath the sealed pits. Moisture can only enter the wood by evaporation from the coating in a pit and subsequent vapor transport through the lumina. This strongly reduces the water uptake.

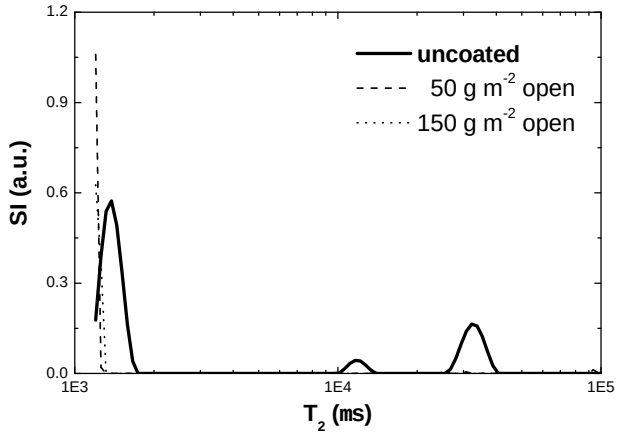


**Figure 5.11** *Relaxation time distributions for uncoated and open coated spruce samples after a time of approximately 24 hours.*

Another possible cause for the reduction of water uptake is given by de Meijer and Militz [11]. By weighing spruce samples, they found that an acrylic coating strongly reduces the water absorption of spruce. Using micro tomography, they found that an acrylic coating penetrates only the first two cell layers of spruce whereas in pine a coating was observed to penetrate much deeper, up to 1000 $\mu$m [34]. This could be caused by fixation of the aspirated pits present in spruce by a coating as we suggested before. Alternatively, de Meijer suggests that because the pits of spruce are relatively small – 2 to 5 $\mu$m, compared to 10 to 25 $\mu$m for those of pine – the pits of spruce are more easily clogged with agglomerates of pigment particles. However, from impregnation studies, the permeability of spruce is known to be strongly reduced by drying [55, 56], largely as a result of the aspiration of bordered pits. Therefore, the low water uptake of acrylic coated spruce is also most likely a result of pit aspiration caused by drying of the wood.

The open coating only fixates part of the aspirated pits, the extent of which depends on the amount of coating applied, since the open coating contains less binder material.

## Summary

The steady state MC of spruce during water absorption is determined accurately by NMR within 24 hours. Both the alkyd and acrylic coating were found to greatly reduce the water absorption. The alkyd coating does not absorb water. Although the acrylic coating does, no water is absorbed by acrylic coated spruce. A possible explanation is that the acrylic coating fixates aspirated pits. The open coating reduces the water absorption to lesser extent since it only fixates part of the aspirated pits, the extent of which depends on the amount of coating applied.

## 5.4 Conclusions

### 5.4.1 NMR measurement technique

NMR was shown to be a suitable technique to determine the wood moisture content of coated and uncoated wood samples during water absorption. In contrast to weighing techniques, NMR allows to determine the MC dynamically, i.e. when the wood is not in equilibrium with the boundary conditions posed by water or a relative humidity. This means that NMR allows to monitor the water absorption process; both the amount and rate of water uptake are determined with high accuracy in relatively short experiments. Additionally, the accuracy is increased with respect to weighing measurements because NMR measurements are performed while the water remains on top of the sample. Also, NMR distinguishes between bound and unbound water which allows to accurately characterize the absorption process. Because of the fast initial capillary water uptake of pine and Accoya, the steady state calibration explained in section 4.6 cannot be used at the start of the experiments because bound and unbound water are not yet in equilibrium. However, the MC of all four wood species can be determined accurately after approximately 24 hours.

### 5.4.2 Coatings on wood

The behavior of the coatings can be summarized as follows:

- The **open** coating has no influence on the water absorption when applied on meranti, pine and Accoya because this coating is not a film forming system. Tripling the applied mass has no influence on the water uptake of meranti. The influence of applied coating mass was not studied for pine and Accoya but is expected to have no influence. The open coating reduces the absorption of spruce by clogging a part of the pits near the surface, the extent of which depends on the amount of coating applied.
- The **alkyd** coating inhibits moisture absorption of the woods studied and is expected to also strongly reduce the absorption of other wood types. This is most likely explained by the fact that the alkyd coating absorbs very little water and seals rays. The alkyd coating thus forms an effective barrier against moisture, offering a good protection against external moisture.

- The **acrylic** coating absorbs a large amount of water. As a consequence, the wood type is of great influence on the moisture absorption:

  **Meranti** For acrylic coated meranti, the final amount and rate of water uptake are equal to uncoated meranti. This means that the acrylic coating offers no protection for meranti against external water. The coating thickness showed no significant influence on the water uptake.

  **Pine and Accoya** The acrylic coating reduces the unbound water uptake of pine and Accoya by approximately 40 to 50% by sealing the relatively large rays, inhibiting fast capillary water uptake. Especially on Accoya, this resulted in a low final moisture content. The influence of coating thickness was not studied.

  **Spruce** The acrylic coating almost completely inhibits water absorption of spruce. This is most likely the result of fixation of aspirated pits near the surface by coating constituents. The influence of coating thickness was not studied.

The wood surface treatment (planing or sanding) prior to coating application showed no significant influence on the water uptake.

Summarizing, the moisture absorption for MCs below the FSP is limited either by the wood, i.e. internally (I), or by the coating, i.e. externally (E). An overview of the limiting factor for all measured wood-coating combinations is given in table 5.3.

**Table 5.3** *Limiting factor, (I) internal or (E) external, of the moisture absorption for MCs below the FSP for the studied wood-coating combinations.*

| | uncoated | open | alkyd | acrylic |
|---|---|---|---|---|
| meranti | I | I | E | I |
| pine | I | I | E | E |
| Accoya | I | I | E | E |
| spruce | I | E | E | E |

Chapter 6

# Water desorption from coated wood

This chapter presents the results of the drying experiments. The first section presents moisture profiles of drying wood samples. Typical drying behavior for each wood type is described. Next, the speed of drying is quantified by calculating the moisture flux. An elevated MC near the surface of acrylic coated meranti was found. To find the origin of this increase in MC, the direction of moisture transport and the state of this moisture, i.e. bound or unbound, are determined by means of a relaxation time analysis.

## 6.1 Moisture profiles during desorption

Coated and uncoated samples were saturated by submersion in water. Moisture content profiles were obtained every 24 hours by NMR while drying the samples, see section 4.4. Interpolated and averaged profiles are presented in figure 6.1 of open coated and alkyd coated meranti, uncoated and acrylic coated Accoya and uncoated and acrylic coated spruce. Note that profiles were obtained for more wood-coating combinations, as given in table 4.1. The time between each profile is given by $\Delta$t; the duration of the experiment by t. The top of the sample is located at position $x = 0$. The FSPs found in section 4.6 are indicated by the horizontal dashed lines. The profiles show MCs larger than the FSP which indicates that the samples contain both bound and unbound water as expected after submersion. The calibration can be used during drying because bound and unbound water remain in equilibrium. The first profile of each sample is inhomogeneous except for uncoated spruce. This is partially caused by annual rings but it also indicates that the samples were not yet homogeneously saturated, although they were immersed in water for over 6 weeks. This is caused by the Teflon holder which seals the tangential and radial sides of the samples. Because of this, water transport only takes place in the low permeable transverse direction. Annual rings are observed in the measurements on Accoya at approximately 6 mm in figure 6.1(c) and 5 mm in figure 6.1(d).

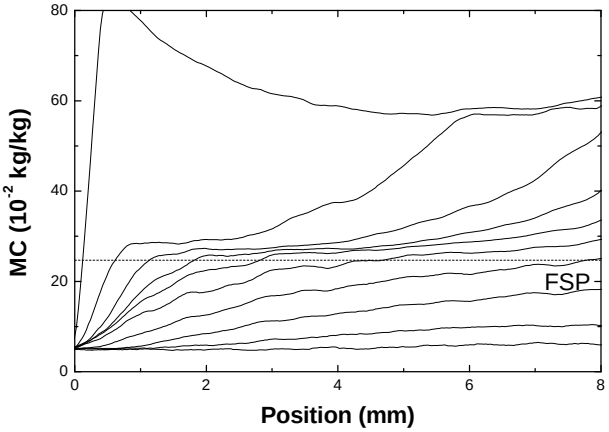


*(a) 50 g $m^{-2}$ open coated meranti; $\Delta t = 17$ h, $t = 6.3$ days.*

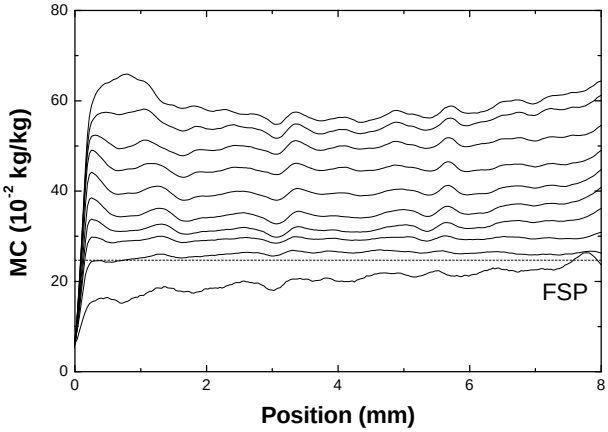


*(b) 100 $\mu$m alkyd coated meranti; $\Delta t = 98$ h, $t = 37$ days .*

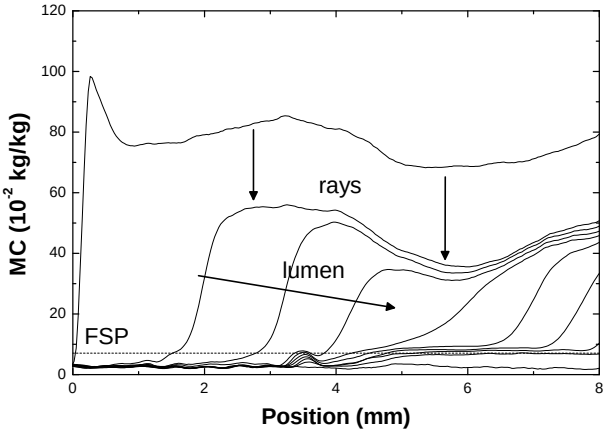


*(c) uncoated Accoya; $\Delta t = 19$ h, $t = 7.1$ days.*

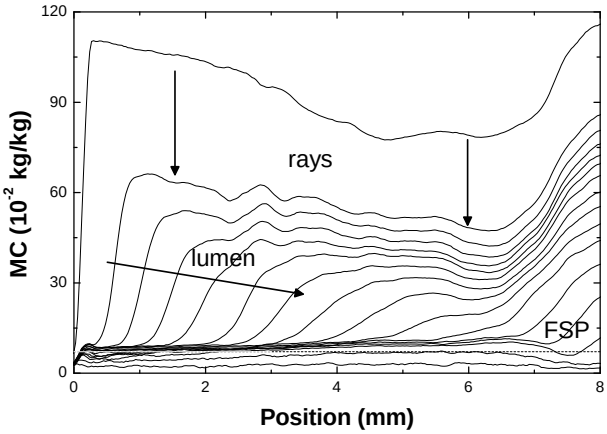


*(d) 100 $\mu$m acrylic coated Accoya; $\Delta t = 24$ h, $t = 31$ days.*

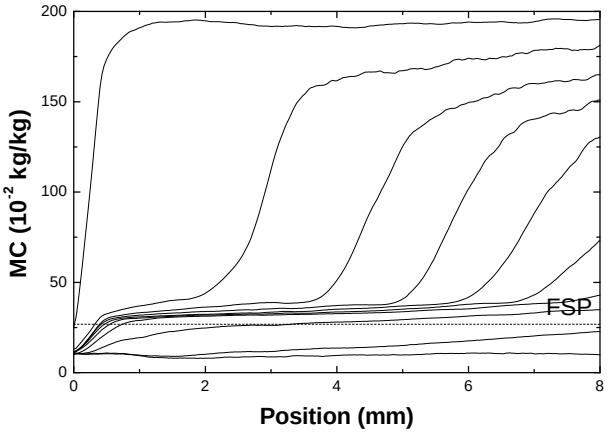


*(e) uncoated spruce; $\Delta t = 24$ h, $t = 9$ days.*

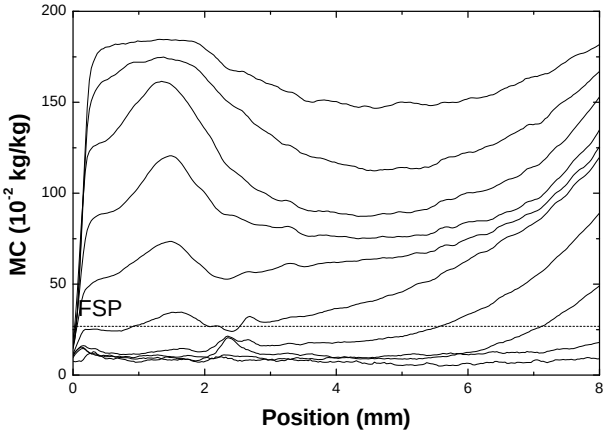


*(f) 100 $\mu$m acrylic coated spruce; $\Delta t = 58$ h, $t = 22$ days.*

**Figure 6.1** *Moisture content profiles of open coated and alkyd coated meranti, uncoated and acrylic coated Accoya, and uncoated and acrylic coated spruce. The top of the sample is located at $x = 0$. The horizontal dashed lines indicate the FSP.*

From the profiles, typical drying behavior for the studied wood-coating combinations can be observed. All samples showed two distinct drying stages. For MCs below the FSP, moisture is transported similarly for all wood types, namely by moisture diffusion out of the cell walls and subsequent vapor diffusion through the lumina. For MCs above the FSP, the drying behavior differs per combination of wood and coating.

A drying front is observed to move into uncoated, open and acrylic coated meranti. The profiles of open coated meranti are shown in figure 6.1(a) as a representative example. The profiles of acrylic coated meranti are treated in more detail in section 6.3. The width of the front is of the same order of magnitude as the sample thickness. Such a front is not observed in alkyd coated meranti, see figure 6.1(b). While the MC is above the FSP, the MC decreases homogeneously throughout the sample. In pine and Accoya, fast drying of the rays initially causes the MC to decrease homogeneously. Next, a sharp front moves into the samples while the MC continues to decrease homogeneously, only much slower as can be seen in figure 6.1(d). Comparing uncoated and acrylic coated pine and Accoya, shows that the acrylic coating lowers the speed of the front but leaves the typical drying behavior unchanged. Uncoated spruce shows a sharp front to move into to wood during drying. However, the MC of acrylic coated spruce decreases almost homogeneously, see figure 6.1(f). Summarizing, the behavior of the MC can be characterized according to three categories:

- **Sharp front:** the width of the front is significantly smaller than the thickness of the sample.
- **No front:** the moisture profiles decrease homogeneously.
- **Wide front:** the width of the front is comparable to the thickness of the sample.

A combination is also possible, as observed for Accoya, where a sharp front moves in along with a homogeneous decrease. To obtain a better understanding of the different drying processes, the drying rate is quantified.

## 6.2 Rate of water desorption

To quantify the rate of water desorption, the moisture flux $J(x,t)$ as a function of time is calculated from the profiles. The moisture flux out of the sample, i.e. to the left in the profiles, is defined as positive; the rate of change of $\theta$ is negative. The resulting mass balance:

$$\frac{\partial \theta(x,t)}{\partial t} = \frac{\partial J(x,t)}{\partial x}, \tag{6.2.1}$$

is integrated from the bottom of the sample at $x = L$ to a position $x$:

$$J_x(t) - J_L(t) = \int_L^x \frac{\partial\theta(x,t)}{\partial t}\partial x. \tag{6.2.2}$$

The bottom of the sample is sealed so $J_L(t) = 0$. The time derivative is taken outside the integral since $\theta$ is independent of time for each individual profile. This yields the flux $J_x(t)$ at position $x$ as a function of time:

$$J_x(t) = \frac{\partial}{\partial t}\int_L^x \theta\partial x. \tag{6.2.3}$$

Since $\theta$ is expressed in kg/kg, the unit of $J_x(t)$ is m $s^{-1}$. The total moisture flux is obtained by integrating equation (6.2.3) from $x = L$ to the surface of the sample at $x = 0$. The calculated fluxes for meranti are shown on a logarithmic scale in figure 6.2(a); those for pine, Accoya and spruce are shown in figure 6.2(b). Note that a sharp increase of the flux is observed for some measurements, such as for 100 $\mu$m acrylic coated meranti around 20 days. These peaks are most likely caused by cracking of the wood and coating due to shrinkage of the wood. This brings the interior of the wood into contact with dry air giving rise to a sudden increase of the flux.

Each curve in figures 6.2(a) and 6.2(b) can be characterized according to one of the three categories described in the previous section. The flux can be i. nearly constant as a result of no front moving into the sample, or ii. initially high and decreasing as a result of a sharp front moving into the sample, or iii. continuously decreasing as a result of a wide front. An overview is given in table 6.1. The table also indicates whether the transport is internally (I) or externally (E) limited. Each type of behavior including the limitation is explained below in more detail.

**Table 6.1** *Correspondence between the type of front behavior and the type of flux behavior. The desorption can be internally (I) or externally (E) limited.*

| Front | Flux | Limit |
|---|---|---|
| none | nearly constant | E |
| sharp | high to low | I |
| wide | continuously decreasing | I/E |

### 6.2.1 No drying front

A nearly constant flux is the result of homogeneously decreasing MC profiles. Such profiles indicate that moisture is redistributed inside the sample because

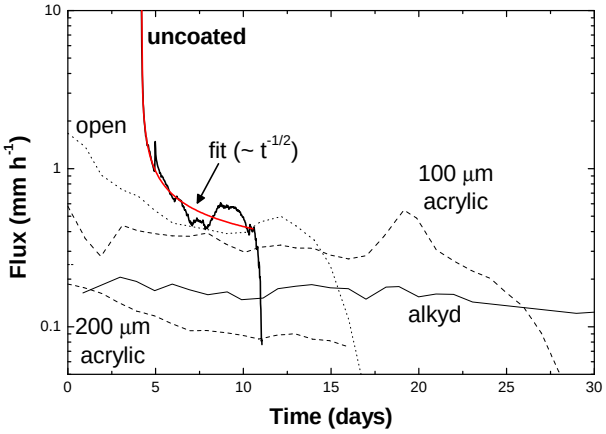


*(a) fluxes for meranti.*

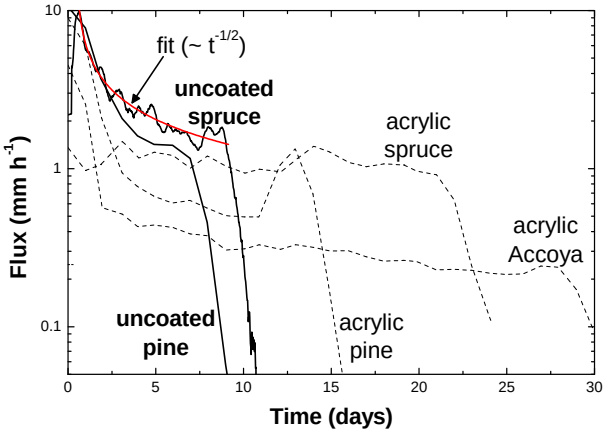


*(b) fluxes for pine, Accoya and spruce.*

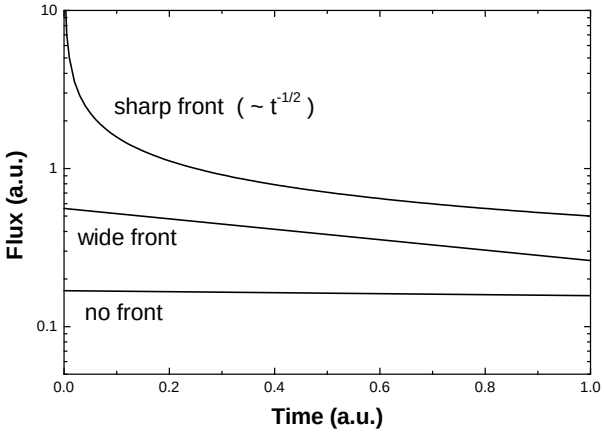


*(c) modeled fluxes.*

**Figure 6.2** *Calculated fluxes for the drying of meranti (a) and pine, Accoya and spruce (b). The fluxes of uncoated meranti and uncoated spruce have been fitted by equation* (6.2.9)*. Three types of behavior of the flux and the corresponding front behavior are shown schematically in figure (c).*

of which no front is formed during drying. This means that the desorption at the surface is slower than the internal transport. The desorption is said to be externally limited (E) as already indicated in table 6.1.

This behavior of the profiles and the flux is observed for alkyd coated meranti and acrylic coated spruce. Due to the redistribution of moisture inside the wood, the coatings remains in contact with unbound water. The alkyd coating absorbs very little water so very little moisture is transported to the coating surface where it can evaporate. The resulting low desorption flux for alkyd coated meranti is in accordance with its low absorption, see section 5.1.4.

For acrylic coated spruce, the desorption is limited by clogging of the pits at the surface as explained in section 5.3. During desorption the substances of the coating present in the pits remain in contact with unbound water. Unlike the alkyd coating, the acrylic coating will absorb this unbound water which subsequently evaporates at the coating surface, although at a much lower rate than uncoated spruce. Note that almost no absorption was observed because the duration of the absorption experiments was only 24 hours in contrast to several weeks for desorption.

### 6.2.2 Sharp drying front

An initially high flux of which the rate of change decreases over time, is the result of a sharp drying front moving into the sample. This can be explained by a simple model. We assume that the saturated vapor pressure $p_{sat}$ at the front is always in equilibrium with the unbound water. Consequently, $p_{sat}$ is constant throughout the drying process. Additionally, we assume that the MC of the undried part of the wood $\theta_{sat}$ is constant. The vapor transport to the surface then determines the evaporation rate. This desorption process is thus internally limited (I). A stepwise front forms which starts to move into the wood at $t = t_0$.

As the front advances, cell walls at the surface start to dry because there the vapor pressure equals the low external vapor pressure. The area where both unbound and bound water have dried will be called the dry shell which widens during drying. According to a model of Salin [57], this dry shell determines the drying speed of wood. This model was based on measurements by Rosenkilde et al. [14–16] and Wiberg et al. [7] in which both found a dry shell to form at the surface. Rosenkilde et al. used high resolution NMR to study the drying of uncoated wood surfaces. Wiberg et al. [7] used x-ray tomography. However, because of their limited field of view of approximately 500 $\mu$m and limited resolution, respectively, they did not observe the sharp front moving into the wood which we suggest to be the determining factor.

At the surface of the wood, the moisture content $\theta_0$ equals the MC of the external air. $\theta_0'$ is the MC behind the dry shell which for uncoated wood equals the FSP. $\theta_{sat}$ is the constant MC of the undried part of the wood, see figure 6.3. Since the flux transporting vapor away from the front determines the evaporation at the front, the position of the front $f$ is related to the flux $J$ by mass conservation:

$$J = \frac{df}{dt}. \tag{6.2.4}$$

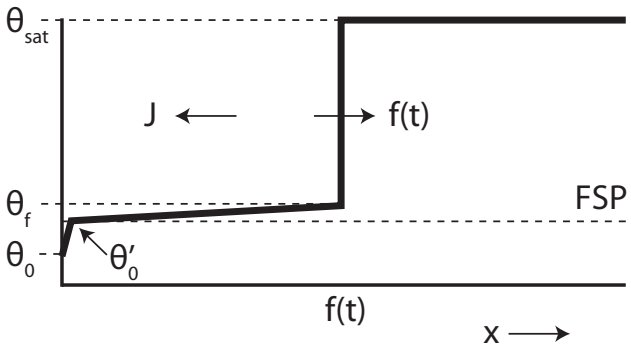


**Figure 6.3** *Schematic representation of a stepwise drying front moving into wood. The bold curve indicates the MC.*

The MC at the low side of the front $\theta_f$ consists of vapor in addition to bound water and is given by:

$$\theta_f = \left(\frac{p_{sat} V_M}{RT}\right) + \theta'_0, \tag{6.2.5}$$

where $p_{sat}$ is the saturated vapor pressure inside the lumina, $V_M$ is the molar volume of water, $R$ is the gas constant and $T$ is the temperature. $p_{sat}$ depends on the lumen diameter and can be calculated using the Kelvin and Clausius-Clapeyron equations. The gradient in moisture content drives a moisture flux from the front to the wood surface:

$$J = D\frac{d}{dx}(\theta_f - \theta'_0). \tag{6.2.6}$$

Furthermore, we assume that the moisture flux is constant in the region where the front has passed. This assumption is valid between the front and the dry shell since there are no sinks or sources for moisture. However, the cell walls drying in the dry shell contribute slightly to the flux. In addition, the MC is assumed to adapt itself immediately to changes of the front position, resulting in a quasi-steady state approach for the MC. With these assumptions, the MC decreases linearly from the front to the surface. The position of the front at $t = t_0$ is denoted by $f_0$. Equation (6.2.6) can now be rewritten as:

$$J = D\frac{\theta_f - \theta'_0}{f(t) - f_0}. \tag{6.2.7}$$

When equations (6.2.4) and (6.2.7) are combined, the following expression for the front position is obtained:

$$f(t) = f_0 + \sqrt{2D(\theta_f - \theta'_0)(t - t_0)}. \tag{6.2.8}$$

Substituting this in equation (6.2.7) yields:

$$J = \sqrt{\frac{D(\theta_f - \theta_0')}{2(t - t_0)}}, \tag{6.2.9}$$

so the flux decreases proportional to $t^{-1/2}$. This is schematically shown in figure 6.2(c). This can be understood by noting that the path length for vapor increases as the front advances. As a consequence, the flux and because of that the evaporation rate decrease. The curves representing the fluxes of the uncoated woods behave as described by equation (6.2.9). This is demonstrated by fitting the data of uncoated meranti and spruce by equation (6.2.9) in figure 6.2.

When a coating is applied, $\theta_0'$ represents the MC at the wood-coating interface. $\theta_0$ still equals the MC of the external air but now at the coating surface. Acrylic coated Accoya shows a lower flux than uncoated Accoya although the general behavior is similar. This can be explained by stating that the acrylic coating raises $\theta_0'$. According to equation (6.2.7) this results in a lower flux. However, despite the quite sharp front in the profiles, the fluxes do not decrease exactly proportional to $t^{-1/2}$ because the MC also decreases homogeneously. This can be seen clearly in the profiles of acrylic coated Accoya in figure 6.1(d). The initially high fluxes are caused by fast drying of the rays but after that, the acrylic coating reduces the rate of desorption by increasing the MC at the wood-coating interface.

### 6.2.3 Wide drying front

The acrylic coating absorbs large amounts of water as shown in section 5.1.4. This can be represented in the sharp front model by a large increase of $\theta_0'$. This reduces the flux to such an extent that the moisture partially redistributes because of which the front becomes wider. However, a front is still present so the flux continuously decreases because the path length for vapor still increases as the front advances. This means that the moisture transport is at the boundary between internally and externally limited, as already indicated in table 6.1. This behavior is observed in open and, to greater extent, in acrylic coated meranti which means that these coatings lower the desorption of meranti by increasing the MC at the wood-coating interface.

The flux for a coating thickness of 200 $\mu$m on meranti is lower than that for 100 $\mu$m coated meranti so, in addition, the acrylic coating also forms a barrier against moisture transport. Note that in section 5.1 the acrylic coating was found to have no influence on the water uptake of meranti. The difference between uptake and drying occurs because the coating remains in contact with water during absorption whereas during desorption, the coating is in contact with vapor. In other words, this coating influences the moisture

transport by its impact on the moisture content at the surface and by a change in effective diffusivity.

The increase of surface MC has been suggested by de Meijer and Militz [11, 12] in order to explain the outcome of their drying experiments on acrylic coated spruce. However, the results presented in section 6.2.1 suggest clogging of pits to be the cause of the reduced desorption of spruce, which is in accordance with the results found for the water absorption of spruce in section 5.3.

### 6.2.4 Summary

For MCs below the FSP, all studied wood-coating combinations desorb by diffusion of moisture out of the cell wall into the lumen and subsequent vapor diffusion through lumina towards the surface. This transport is internally limited.

For MCs above the FSP, the studied coatings lower the desorption by different mechanisms. The desorption can be i. internally limited (I), or ii. at the boundary of internally and externally limited (I/E), or iii. externally limited (E):

**I** If the transport is internally limited, the only influence of the coating on the desorption behavior is a small reduction of the flux by a slight increase of the MC at the wood surface. The drying behavior remains unchanged: a front moves into the wood and moisture leaves the wood by vapor transport through the lumina and coating.

**I/E** If the transport is at the boundary between internally and externally limited, the coating increases the wood MC at the wood surface. This reduces the flux to such an extent that the drying behavior changes: the front widens. In addition, the coating can form a low barrier against moisture transport. In this case, moisture desorbs via vapor diffusion through the lumina. Alternatively, when a sharp front is accompanied by a homogeneous decrease of the MC, moisture desorbs both via vapor diffusion and water flow through lumina and rays.

**E** If the transport is externally limited, the MC is homogeneous throughout the wood. Moisture redistributes inside the wood as a result of which the coating remains in contact with unbound water. The flux is therefore fully determined by the constant and relatively low rate of water transport through the coating.

The limitations for all studied wood-coating combinations are given in table 6.2 by I, E or I/E. For wood-coating combinations which were not measured, the expected behavior is given, based on the typical behavior of the wood

types and coatings observed in the performed measurements. Expected behavior is given in italics; [*I*] and [*E*]. The alkyd coating is expected to also limit the desorption of the other wood types which were studied. The open coating forms no barrier against moisture transport so it is not expected to influence the desorption of pine or Accoya. When applied on spruce, the open coating clogs the pits as is discussed in section 5.3 and 6.2.1. Therefore, the open coating is expected to lower the rate of desorption of spruce.

**Table 6.2** *Desorption behavior for MCs above the FSP of the studied wood-coating combinations: i. internally limited (I), or ii. at the boundary of internally and externally limited (I/E), or iii. externally limited (E). Expected behavior is given in italics, [*I*] and [*E*].*

| | uncoated | open | alkyd | acrylic |
|---|---|---|---|---|
| meranti | I | I | E | I/E |
| pine | I | [*I*] | [*E*] | I/E |
| Accoya | I | [*I*] | [*E*] | I/E |
| spruce | I | [*E*] | [*E*] | E |

## 6.3 Moisture peak below the meranti-acrylic interface

As explained above, a wide front moves into acrylic coated meranti during drying. The acrylic coating decreases the desorption rate from meranti by increasing the MC at the wood surface. To study the increase of the MC in more detail, moisture profiles of the drying of initially saturated meranti with 100 $\mu$m of acrylic coating, were obtained by NMR every 23 minutes. Interpolated and averaged profiles are shown in figure 6.4(a) for a period of 104 hours. A magnification of the profiles is shown in figure 6.4(b).

The desorption flux is driven by a gradient in the moisture density according to equation (6.2.3). However, for MCs above the FSP, the profiles show an increase of the MC up to a depth of approximately 0.7 mm throughout the drying process. The profiles show that $\theta_0'$ has in fact increased to such an extent that the moisture gradient becomes negative close to the surface. However, moisture can only leave the wood through the coated surface since the bottom and sides of the sample are sealed. This means that moisture moves against the moisture gradient, which suggests that an additional driving force exists near the surface.

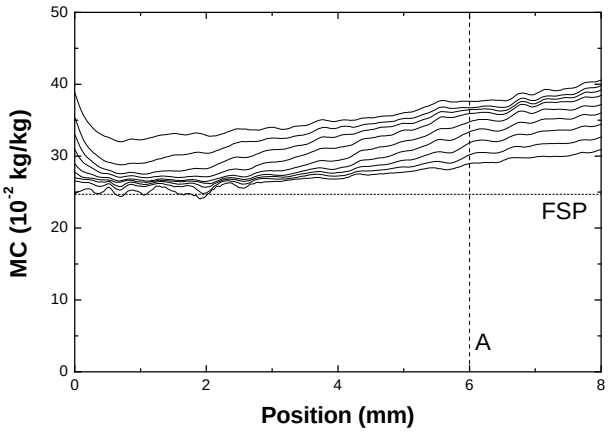


*(a) 100 $\mu$m of acrylic coating; $\Delta t = 12$ hours, $t = 4$ days.*

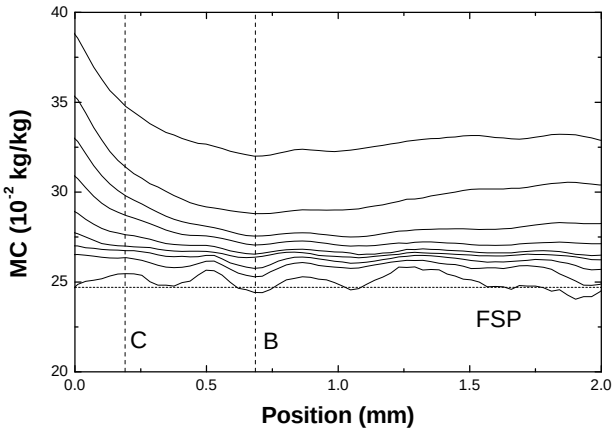


*(b) magnification of the increased MC.*

**Figure 6.4** *Moisture content profiles of 100 $\mu$m acrylic coated meranti. A magnification of the data is shown in figure (b). The top of the sample is located at $x = 0$. The horizontal dashed lines indicate the FSP. A, B and C denote the positions at which the moisture flux is determined in section 6.3.1.*

### 6.3.1 Direction of moisture transport

To determine whether the moisture actually moves against the density gradient towards the top of the sample, or that it redistributes within the sample, the flux is calculated using equation (6.2.3), at positions A, B, C and D which are characterized in table 6.3 and indicated in figure 6.4. The resulting fluxes are shown in figure 6.5. The fluxes are positive and continuously decreasing at all positions and times with:

$$J_A(t) < J_B(t) < J_C(t) < J_D(t). \tag{6.3.1}$$

This shows that the moisture is in fact moving towards the increased MC near the surface. Similar behavior was found for 200 $\mu$m acrylic coated meranti, although with lower fluxes in accordance with the results presented

**Table 6.3** *Positions at which the flux is calculated. The positions are indicated in figure 6.4.*

| | |
|---|---|
| A | far from the surface |
| B | at the lowest MC behind the surface |
| C | on the slope of the increased MC |
| D | above the surface of the sample |

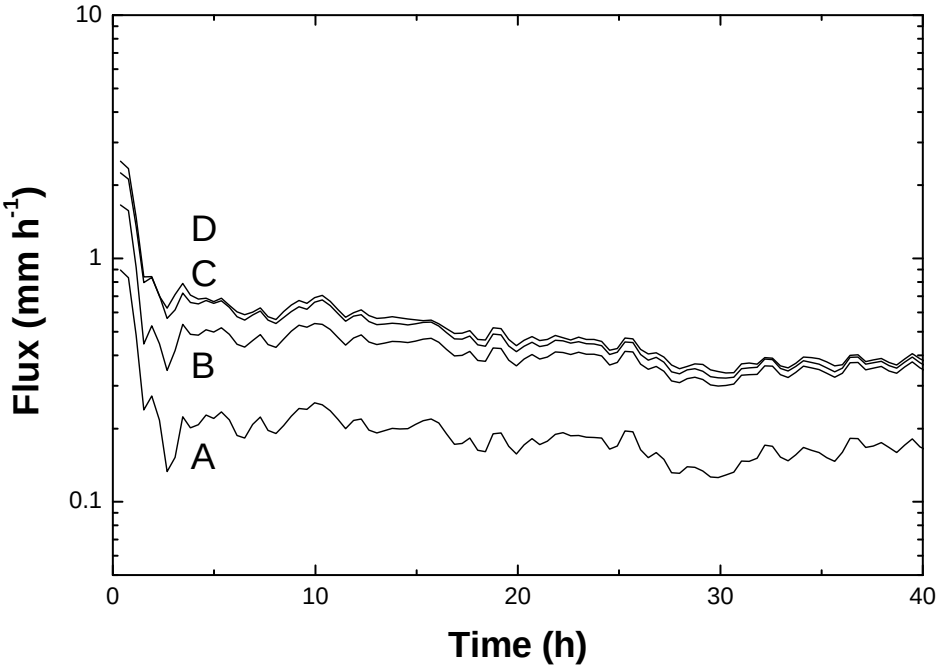


**Figure 6.5** *The flux calculated from the profiles in figure 6.4 at the indicated positions A, B, C and D.*

in section 6.2. The peak is not a result of density variations, such as for instance annual rings, because the irregularities in the profiles show that density variations in meranti are small compared to the peak. The peak is also unlikely to be a result of inhomogeneous saturation during sample preparation because in that case the peak would disappear prior to drying of lumina deeper within the wood. This is confirmed by two dimensional images obtained by NMR which show the drying was one dimensional, i.e. no moisture gradients were present in the $x$ or $y$-direction. Therefore, we suggest that an additional driving force exists from a depth of approximately 0.7 mm to the wood-coating interface.

### 6.3.2 Bound or unbound water

A relaxation time analysis has been performed to determine whether the additional driving force affects bound or unbound water. Logarithmic relaxation time distributions as a function of drying time at positions A, B and C are shown in figure 6.6. In all three distributions, the largest contribution is that at a low relaxation time which represents bound water. Its intensity is nearly constant which indicates that the cell walls do not dry significantly. The low relaxation time of this contribution at positions B and C decreases slightly indicating minor shrinkage of the cell walls. The contributions at higher relaxation times show that the lumina and vessels have completely

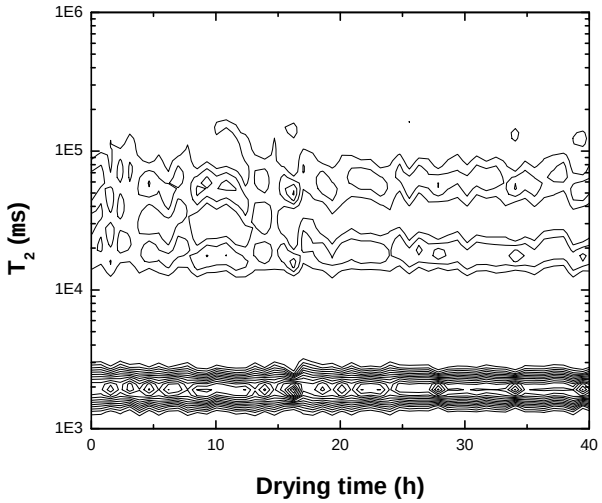


*(a) Position A; far from the surface.*

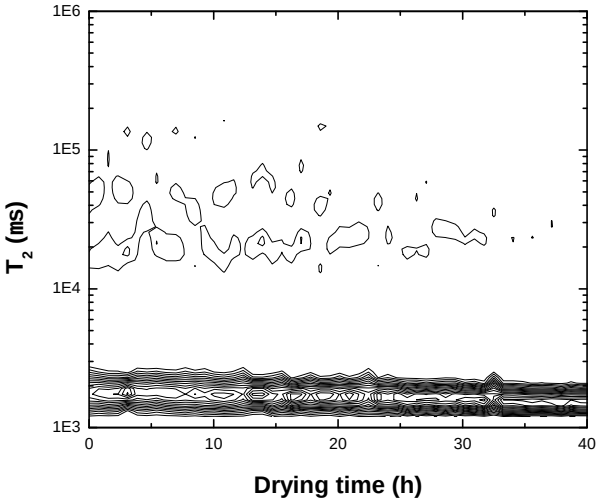


*(b) Position B; at the lowest MC near the surface.*

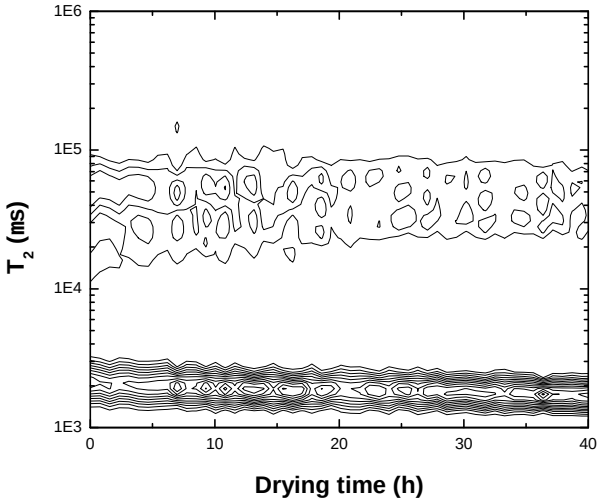


*(c) Position C; on the slope of the increase in MC.*

**Figure 6.6** *The $T_2$-distributions of the sample with an acrylic coating of 100 $\mu$m at positions 0,1 and 2 plotted as a function of drying time.*

dried after approximately 40 hours at position B which corresponds to a depth of approximately 0.7 mm. However, unbound water is still present both deeper within the sample at position A, as well as near the surface at position C. This means that the increased MC consists of unbound water. So lumina and vessels at a depth of 0.7 mm contain less water than lumina and vessels near the surface, although the latter are expected to dry first, as is the case for uncoated meranti.

The additional driving force, responsible for the increased amount of unbound water beneath the surface, might be generated by hydrophilic ex-

tractives present in meranti. These are dissolved in water which permeates the wood during application of the waterborne acrylic coating. Additionally, hydrophilic coating additives can be transported into the wood. During drying of the coating, the water evaporates, transporting extractives from the wood towards the surface which collect in lumina and vessels near the surface. As the coated wood dries, the hydrophilic extractives and additives increase the moisture content of lumina and vessels near the surface. This hypothesis is substantiated by the fact that a peak is not observed for alkyd coated meranti. The alkyd coating is solvent borne and solute ingress after coating application does not dissolve the hydrophilic wood extractives.

The other wood-coating combinations mentioned in table 4.1 did not show a significant increase in moisture content near the coated surface during drying. This corresponds to the fact that pine, Accoya and spruce contain less extractives than meranti. The open coating is also waterborne so an increased MC could also occur on open coated meranti. However, this was not observed because of the relatively fast drying, since only one profile a day was measured on these samples. A peak was observed on acrylic coated Accoya although to small to study in detail. Also note that the internal moisture transport in Accoya is considerably faster that in meranti. Because of this, extractives and hydrophilic coating additives could be redistributed more homogeneously throughout the wood, instead of being accumulated in lumina near the surface.

## 6.4 Conclusions

NMR was shown to be a suitable technique to determine the wood moisture content of coated and uncoated wood samples during water desorption for both MCs above and below the FSP. In contrast to weighing techniques, NMR allows to determine the MC dynamically, i.e. when the wood is not in equilibrium with the surrounding air. This means that NMR allows to monitor the water desorption process – both the amount and rate of water desorption are determined with high accuracy – which reveals the underlying processes.

A coating influences the desorption of coated wood by different mechanisms. The open coating increases the MC at the wood surface slightly which lowers the moisture density gradient within the wood. This in turn results in a decreased moisture flux. The acrylic coating increases the the MC at the surface to greater extent in addition to forming a barrier against moisture transport resulting in a lower flux. The alkyd coating gave the lowest desorption flux of all three coatings studied. This means that it forms the strongest barrier against moisture transport which indicates its moisture permeability is very low.

In addition, application of an acrylic coating on meranti results in an increased moisture content from the wood surface to a depth of approximately 0.7 mm. This increase is not a result of sample preparation or wood inhomogeneities; it persists throughout the drying process and affects unbound water. A possible cause is the presence of hydrophilic extractives and additives in meranti and the acrylic coating respectively, which accumulate in lumina and vessels near the surface because of water evaporation after coating application.

Chapter 7

# Conclusions and recommendations

## 7.1 Nuclear Magnetic Resonance on wood

NMR allows to determine both wood moisture content and rate of water sorption during water absorption and desorption of coated and uncoated wood. In contrast to weighing, both quantities are measured dynamically and non destructively with high spatial and temporal resolution in relatively short experiments. The accuracy of absorption experiments performed by NMR is higher when compared to weighing because the first can be performed while water remains on top of the sample. The NMR signal intensity was calibrated which allowed to accurately determine the MC of the four wood species studied. In addition, NMR relaxometry distinguishes between bound and unbound water which allows to accurately characterize sorption processes in wood.

The 4.7 T NMR setup used in this study is suitable to study the water sorption of coated and uncoated wood samples measuring 20 mm in diameter and 10 mm in height. The $x$ and $y$-gradients were used to align the main dynamic $z$-gradient of 752 mT/m perpendicular to the sample surface to optimize the resolution. The echo time of 1700 $\mu$s excludes solid wood from being measured because of its short relaxation time. However, this echo time is sufficiently short to measure all moisture in wood with a spatial resolution of $33 \pm 3$ $\mu$m in a field of view of approximately 30 mm. Moisture profiles were obtained roughly every half an hour, which was more than adequate to study adsorption processes. Measuring once every 24 hours was sufficient for moisture desorption experiments with the exception of relatively fast initial processes. Software was adapted to allow easy processing of the profiles and relaxation time distribution data.

## 7.2 Coating barrier properties

Moisture inside wood causes favorable conditions for decay. Application of a coating alters the moisture transport into and out of wood in an effort to prevent accumulation of moisture. To study the influence of a coating on the moisture transport in wood, several commonly used wood-coating combinations were studied. Samples were equilibrated at 22% RH or saturated by immersion in water. Water was placed on the dry samples and the absorption was monitored by NMR for 24 hours. The saturated samples were dried in a climate chamber, kept at constant low RH, and monitored by NMR until they were dry.

From the results, different transport mechanisms which control the moisture transport were identified. When the coating has a significant influence on the moisture transport, the transport is said to be externally (E) limited; in case of limitation by the wood, it is said to be internally (I) limited. The sorption measurements showed that only for certain wood-coating combinations, the absorption (a) behavior differs from the desorption (d) behavior which is shown in table 7.1. These differences and the behavior of each coating are explained in more detail below.

**Table 7.1** *Differences in absorption (a) and desorption (d) behavior of the studied wood-coating combinations: i. internally limited (I), or ii. at the boundary of internally and externally limited (I/E), or iii. externally limited (E).*

| | uncoated | open | alkyd | acrylic |
|---|---|---|---|---|
| meranti | I | I | E | a: I, d: I/E |
| pine | I | I | E | a: E, d: I/E |
| Accoya | I | I | E | a: E, d: I/E |
| spruce | I | E | E | E |

### 7.2.1 Alkyd coating

The alkyd coating strongly reduces the rate of absorption and desorption. In both cases, the coating remains in contact with water. This means that the alkyd coating forms a strong barrier against water. It is expected that this coating also forms a strong barrier against a relative humidity. This behavior might be caused by the low water absorption of this coating. As a result, the alkyd coating offers a good protection against external moisture. The strongly reduced desorption could have a positive effect for moisture contents below the fiber saturation point. Because the coating could prevent wood from completely drying, its mechanical strength remains intact.

### 7.2.2 Open coating

The influence of the open coating of the moisture transport highly depends on the wood type. The open coating has no influence on the absorption of meranti, pine and Accoya because the coating is not film forming. The desorption of meranti was reduced slightly. For the same reason, a minor reduction of the desorption is expected for open coated pine and Accoya. However, when applied on spruce, a reduction of the absorption was observed and a reduction of the desorption is expected – since both were reduced even more by the acrylic coating an explanation is given below. This means that the open coating could offer a moderate protection for spruce.

### 7.2.3 Acrylic coated wood

The acrylic coating absorbs large amounts of water and the type of wood has a strong influence on the sorption behavior.

**Meranti** The effective moisture diffusivity of the wood-coating system of acrylic (and open) coated meranti is equal to that of uncoated meranti. This means that the acrylic coating has no influence on the water uptake of meranti.

However, the acrylic coating strongly reduces the moisture desorption from meranti. This is a result of two mechanisms; firstly, the coating increases the moisture content at the wood-coating interface. This lowers the moisture vapor gradient which is the driving force for the the desorption flux which is consequently lower. Secondly, the coating forms a barrier against moisture transport similar to the alkyd coating only much lower.

The unaffected absorption and reduced desorption can cause moisture to accumulation in wood which leads to favorable conditions for decay. In fact, increasing the coating thickness from 100 $\mu$m to 200 $\mu$m further reduces the desorption whereas the absorption remains comparable to uncoated meranti. So increasing the acrylic coating thickness could actually stimulate moisture accumulation in meranti.

**Pine and Accoya** The acrylic coating adequately seals rays and lumina of pine and Accoya. As a result, moisture is only transported into and out of the wood by vapor diffusion through the lumina and rays. This results in a reduction of the water uptake of 40 to 50%. The acrylic coating forms a lower barrier for moisture transport than the alkyd coating but could also prevent wood from completely drying which preserves the mechanical strength of the wood.

**Spruce** The acrylic coating strongly reduces both moisture absorption and desorption of spruce. Application of a coating could fixate the aspirated pits present in dried spruce. Alternatively, application of a coating could clog pits near the surface. The pits of spruce are smaller than those of for instance pine, 2 – 5 $\mu$m and 10 – 25 $\mu$m respectively, because of which the pits of spruce are more easily clogged. However, from impregnation studies, the permeability of spruce is known to be strongly reduced by drying as a result of aspiration of the bordered pits. Therefore, the latter is most likely the cause of the low water uptake of acrylic coated spruce because, despite the absorption of water by the acrylic coating, moisture can only enter acrylic coated spruce by vapor transport through the lumina.

The open coating only fixates part of the aspirated pits, the extent of which depends on the amount of coating applied, since the open coating contains less binder material.

### 7.2.4 Moisture peak below the wood-coating interface

During drying of acrylic coated meranti, the moisture content from the surface to a depth of approximately 0.7 mm is higher than the moisture content at greater depths. However, wood closest to the surface is expected to dry first. A possible cause are hydrophilic extractives present in meranti and/or hydrophilic additives in the acrylic coating. These are dissolved in water which permeates the wood during application of the waterborne acrylic coating. As the coating dries, water evaporates and transports the extractives and/or additives towards the surface where they collect in lumina and vessels. This increases the moisture content of lumina and vessels near the surface during drying.

The increased moisture content can cause very localized dimensional changes in the wood. In turn, this can lead to stresses in the coating film which might result in cracking of rigid coatings, such as the studied alkyd coating. In addition, high moisture contents at the wood surface could create favorable conditions for the growth of blue-stains and molds.

A peak was not observed in pine, Accoya and spruce. Not only do these woods contain less extractives than meranti but their internal moisture transport is considerably faster. Because of this, extractives and hydrophilic coating additives redistribute more homogeneously throughout the wood, instead of accumulating in lumina near the surface.

## 7.3 Performance of the coatings

The performance of each wood-coating combination on the moisture transport in wood, as expected on the basis of their typical behavior in the measurements, is given in table 7.2. The performance ranges from very good (++) to bad (−−). For absorption (A), ++ means the absorption is strongly reduced whereas −− means the influence on the absorption was very low. For desorption (D), ++ means moisture leaves the wood very easily whereas −− means moisture desorbs very slowly. However, for desorption a strong barrier can be both positive and negative as mentioned in paragraph 7.2.1. This is the case for the alkyd coating which offers a very strong barrier against both moisture absorption and desorption. The open coating offers virtually no barrier for moisture transport so its performance for water absorption is bad, that for desorption is good. The performance of the acrylic coating is bad for absorption on meranti, good for both absorption and desorption on pine and Accoya and very good for the absorption of spruce. Its barrier function is expected to be strong against RH which would result in a better performance on all wood types.

For all coatings, care must be taken to prevent moisture from entering the wood via for instance cracks. For the open and acrylic coating additional care must be taken to prevent accumulation of water on the coating. This is quickly absorbed but, especially for acrylic coated wood, desorbed slower.

**Table 7.2** *++: very good, +: good, -:medium, −−:bad.*

| | open | | alkyd | | acrylic | |
|---|---|---|---|---|---|---|
| | A | D | A | D | A | D |
| meranti | −− | + | ++ | −− | −− | + |
| pine | − | + | ++ | −− | + | + |
| Accoya | − | + | ++ | −− | + | + |
| spruce | + | +/− | ++ | −− | ++ | − |

### Concluding remarks

This thesis has shown that the moisture permeability of a coating is dependent on the specific combination of wood and coating. These cannot be treated separately because the coatings influence the moisture sorption of wood in different manners. The alkyd coating absorbs very little water and is therefore expected to have a low permeability. The acrylic coating absorbs much water and increases the surface moisture content. As a consequence, the performance of these coatings should be assessed in a manner suitable

for the coating. Nowadays, the performance of coatings is graded in a similar fashion using European norm EN927. Although this allows for objective comparison of the performance of coatings, inherent differences between the coatings are not taken into consideration which might lead to false test results. This is for instance the case for meranti at moisture contents above the fiber saturation point; the alkyd coating remains in contact with water whereas the acrylic coating is in contact with water vapor.

## 7.4 Recommendations

### 7.4.1 Materials and methods

**Wood and coating** Both the carrier solvent and the resin are expected to affect the moisture transport through a coating. In a waterborne coating, the resin is emulsified in water; a solvent borne coating is a molecular solution. Because of this, a solvent borne coating is expected to form a denser film and coating constituents are expected to penetrate deeper into the wood. For the latter, the suction of wood is also of influence. So, in order to study the performance of a certain resin, it should be applied both as a waterborne and as a solvent borne coating. Vise versa, to study the carrier, a single resin should be used. Also the degree of pigmentation is worth varying since this also influences the moisture transport properties of a coating.

More samples of the different wood type should be studied to determine exactly which wood properties, such as permeability and suction, are responsible for certain effects For instance, water uptake experiments on a larger variety of meranti samples with acrylic coatings with varying amounts of additives could verify the performance of the acrylic coating and the cause for the moisture peak.

**Sample holder** Despite immersion for over 6 weeks, the wooden samples, especially those of meranti, were still inhomogeneously saturated. Saturating a sample before placing it in the holder swells the wood making it impossible insert the sample into the holder. In addition, the holder also limits the radial and tangential swelling during water uptake both in absorption experiments as well as during submersion. The influence hereof is assumed to be insignificant but remains unknown. Shrinkage and swelling as well as the sensitivity of NMR to all hydrogen containing compounds, prohibit sealing the sample by resins. A sample holder allowing to saturate the sample before placing it into the holder as well as sealing the sample sides during an experiment would be very useful.

### 7.4.2 Coating barrier properties

**Relative humidity** The desorption measurements showed that the open and acrylic coating limit vapor transport despite their limited barrier function against water absorption. This can be studied in absorption experiments with an RH instead of water. If the RH is cycled – switching the RH between high and low at a set interval – the difference between vapor absorption and desorption can be studied. This is of importance since a faster absorption leads to moisture accumulation. Additionally, the wood is expected to be influenced only up to a certain depth. This can be made visible with NMR.

A vapor absorption experiment was conducted on uncoated meranti showing a reduced rate of uptake compared to wetting by water. This indicates vapor absorption studies on coated samples will require prolonged experiments. However, many samples can be studied simultaneously – similar to the performed desorption experiments – by wetting the samples in a climate chamber outside the setup and measuring each, once a day.

**Modeling** A start was made on a wood drying model. This showed that the two stage drying behavior of wood can be simulated by a two pore system. Large pores represent the lumina which dry first; the small pores represent the cell walls. Two mechanisms by which a coating lowers the desorption from wood were suggested; forming a barrier against moisture transport or increasing the moisture content at the wood-coating interface. These can be implemented to study their individual effect on desorption.

### 7.4.3 Coating water absorption

The water absorption of a coating is expected to strongly influence the moisture transport through a coating and, consequently, the sorption behavior of coated wood. In addition, hydrophilic additives in the acrylic coating are likely the cause for the large water absorption of this coating. These additives are known to wash out by rain. This could lower the water absorption and thus improve the barrier function. This could also affect the increased moisture content beneath the surface of acrylic coated meranti. These notions suggests the water sorption behavior of a separate coating film should be studied. High resolution NMR setups present at the TPM group in Eindhoven are proven to be highly suitable to study these processes [27, 58].

# Acknowledgements

Although the title page of this thesis caries my name, this project would not have been the succes it is without the help of many people. Therefore I thank:

Bart Erich, my two-days-a-week-supervisor. However, others mostly saw us as partners in crime. In particular the sight of both of us behind an arbitrary number of computers made most people leave the room with a sigh. Paul and Bart are processing data, one holding the mouse, the other the keyboard: click this and that, load here, export there, import, transpose, regrid and plot. This all takes about 10 seconds with four hands... Over the past year I found that Bart is best described as a wave function which actually is a superposition of simple Bart states in the infinite (only for Bart states) dimensional continuous Holland space of which the major subsets are (in decreasing order): Delft, b-vleugel, de 'Salon' and Breda. Although everybody knows Bart is present in the b-vleugel on Thursdays and Fridays, people generally have only seen him passing by at a certain time during the day. This means that although nobody ever really seems to know what his exact location is, everybody always knows his exact speed (.9 or above). Yet, this seemingly adverse feature could be put to good use for instance when teaching young students the Heisenberg uncertainty principle. However, this means it can be quite difficult to get a hold of Bart as a graduate student in need of some supervision (this can be the students own will or that of others). A solution is presented in the form of a modern quantum tunneling device with which it is almost always possible to communicate with a number of the ever fast moving Bart states (the exact number of states available for communication is negatively related to their mutual interaction). There is only one flaw left in this device: the Bart states seem to lose their coherence to this device at unpredictable intervals during the day.

Truth be told, Bart always found time to help me when I really needed it (sometimes I found this time for him, sorry Nico). His enthusiasm made me try to surprise him with new cool results every single week. Bart frequently challenged me, with or without letting me know it and the discussions afterwards taught me a lot, not only about physics but also about for instance the politics involved in big projects. Thanks Bart!

Klaas Kopinga for accommodating me in the TPM group. His intelligence covers many areas – moisture transport, running the faculty as dean, noisy airplanes and currently also coated wood – but when talking about NMR hard- and software (double super-heterodyne receivers with image reject double balanced mixers) his true passion is revealed, whoeiiii!

Jan de Jong for his enthusiastic participation in this project from day one. His vast knowledge from practice always allowed me to check the plausibility of hypotheses. Our discussions were very Dutch: direct but always honest, which led to quite a few new insights for the both of us.

Henk Huinink for his ever increasing interest in this project. The afternoons discussing and structuring my data were of great importance for the final results.

Olaf Adan for our conversations surpassing physics which gave direction to my project and perhaps the start of my career.

Special thanks go to Gerrit Kroesen for virtually attending my graduation presentation in spite of being ill.

Leo Pel, although not directly involved in my project, was always available to discuss whatever matter. His style of communication may seem blunt or even rude to some; my replies, given in a similar fashion, often resulted in discussions which scared others. But I found that his honesty and directness mostly led to useful and purified insights.

Hans Dalderop for his help with all sorts of practical problems. His idea to seal sample sides using heated vaseline was invaluable for the realization of all results in chapter 5.

Jef Noijen for his infinite knowledge about electronics and his enviable ability to have fun with everyone. Although my project did not involve any zelfbouwkastjes, Jef got me through some backbreaking problems with the 4.7.

Ria Groenendijk for the administrative support and in particular for printing my report and distributing it amongst my graduation committee during my holiday.

Waldemar Homan and Wolfgang Gard for sharing their knowledge regarding wood.

Nick van Gils for letting me know what it feels like to see one of your own kids graduate. I also have to thank Nick on behalf of Bart for graduating because since that moment Bart had to deal with only half the noise pesky graduate students tend to make. This dramatically lowered Bart's blood pressure. I have to thank Nick for all the fun we had in the TPM group in particular when one of us was stuck with our projects. The relaxation (induced by pranks) was always good to clear the mind. That is, *our* minds,

most other group members might feel otherwise. A special thanks goes to Nick's ears for always being there and allowing me to vent my frustrations by the occasional "flepper". This role was gratefully taken over by Erik after Nick's graduation although Erik's ears are placed significantly higher.

My roommates: Gijs van der Heijden was always ready to help, albeit with small questions or major issues. Vica for her warm smile which, although our room was always cold according to her, brightened up most days. Kahif for scrutinizing my thesis and finding all small omissions everybody else always misses until printed. His contagious smile and our shared love for cookies (stroopwafels) made working weekends a lot more fun.

The other promovendi and students in the TPM and BMT group for the great and relaxed atmosphere. It was a true pleasure working in the b-vleugel of N-laag!

All computers I used for not crashing, at least not to often. I especially wish a long and reliable life to the n-mri. Also the best of luck to the next user of my keyboard (any questions about it should be directed to either Gijs or Nick). I hold no responsibility for any keys or keyboards which might not have survived their bashing by Bart, myself or the both of us together.

To conclude, I thank my parents and sisters for their never ending support during my entire study. They always encouraged me to develop myself, whether it was by studying or by partaking in other activities. And Marieke. When I met her, about half way through my graduation, my productivity dropped considerably (mainly during the morning). Nevertheless, she gave and still gives me a lot of energy. I thank her for all the love with which she supported me during my graduation and I hope I get to enjoy much more of it for a long time still to come.

# References


[1] K.D. Weiss. Paint and coatings: a mature industry in transition. *Progress in Polymer Science*, 22:203–245, 1997. (pages 4, 14 and 15).

[2] J.F. Hoogervorst. Wijziging arbeidsomstandighedenregeling betreffende werkzaamheden met vluchtige organische stoffen. *Staatscourant*, 2001. (page 4).

[3] M. Rutte. Wijziging arbeidsomstandighedenregeling. *Staatscourant*, 2004. (page 4).

[4] European Commission. Voc paints directive (2004/42/ec). `http://ec.europa.eu/environment/air/pollutants/paints_directive.htm`, 2004. (page 4).

[5] European Commission. Registration, evaluation and authorization of chemicals (ec 1907/2006). `http://ec.europa.eu/environment/chemicals/reach/reach_intro.htm`, 2006. (page 4).

[6] M. de Meijer. *Interactions between wood and coatings with low organic solvent content*. PhD thesis, University of Wageningen, 1999. (page 5).

[7] P. Wiberg, S.M.B Sehlstedt-P, and T.J. Morén. Heat and mass transfer during sapwood drying above the fibre saturation point. *Drying Technology*, 18:1647–1664, 2000. (pages 5 and 61).

[8] O.A. Plumb, G.A. Spolek, and B.A. Olmstead. Heat and mass transfer in wood during drying. *International Journal of Heat and Mass Transfer*, 28:1669–1678, 1985. (page 5).

[9] B. Time. Studies on hygroscopic moisture transport in Norway spruce (picea abies). Part 1: Sorption measurements of spruce exposed to cyclic step changes in relative humidity. *Holz als Roh- und Werkstoff*, 60:271–276, 2002. (pages 5 and 41).

[10] B. Time. Studies on hygroscopic moisture transport in Norway spruce (picea abies). Part 2: modelling of transient moisture transport and hysteresis in wood. *Holz als Roh- und Werkstoff*, 60:405–410, 2002. (page 5).

[11] M. de Meijer and H. Militz. Moisture transport in coated wood. Part 1: Analysis of sorption rates and moisture content profiles in spruce during liquid water uptake. *Holz als Roh- und Werkstoff*, 58:354–362, 2000. (pages 5, 53 and 64).

[12] M. de Meijer and H. Militz. Moisture transport in coated wood. Part 2: Influence of coating type, film thickness, wood species, temperature and moisture gradient on kinetics of sorption and dimensional change. *Holz als Roh- und Werkstoff*, 58:467–475, 2001. (pages 5, 41, 42 and 64).

[13] R.J. Gummerson, C. Hall, and W.D. Hoft. Unsaturated water flow within porous materials observed by NMR imaging. *Nature*, 281:56–57, 1979. (page 5).

[14] A. Rosenkilde, J. Gorce, and A. Barry. Measurement of moisture content profiles during drying of scots pine using magnetic resonance imaging. *Holzforschung*, 58:138–142, 2004. (pages 5 and 61).

[15] A. Rosenkilde and P. Glover. High resolution measurement of the surface layer moisture content during drying of wood using a novel magnetic resonance imaging technique. *Holzforschung*, 56:312–317, 2002. (page 5).

[16] J. Ekstedt, A. Rosenkilde, S. Hameury, M. Sterley, and H. Berglind. Measurement of moisture content profiles in coated and uncoated scots pine using magnetic resonance imaging. In *COST E 53 Conference - Quality Control for Wood and Wood Products*, pages 27–32, 2007. (pages 5 and 61).

[17] R. Valkenborg. *NMR on technological porous materials*. PhD thesis, Technical University of Eindhoven, 2001. (pages 5 and 29).

[18] R.S. Menon, A.L. MacKay, J.R.T. Hailey, M. Bloom, A.E. Burgess, and J.S. Swanson. An NMR determination of the physiological water distribution in wood during drying. *Journal of Applied Polymer Science*, 33:1141–1155, 1987. (pages 5 and 36).

[19] R.S. Menon, A.L. MacKay, S. Flibotte, and J.R.T. Hailey. Quantitative separation of NMR images of water in wood on the basis of $T_2$. *Journal of Magnetic Resonance*, 82:205–210, 1989. (page 5).

[20] C.D. Araujo, A.L. MacKay, J.R. Hailey, K.P. Whittall, and H. Le. Proton magnetic resonance techniques for characterization of water in wood: application to white spruce. *Wood Science and Technology*, 26:101–113, 1992. (pages 5 and 12).

[21] C.D. Araujo, A.L. MacKay, K.P. Whittall, and J.R. Hailey. A diffusion model for spin-spin relaxation of compartmentalized water in wood. *Journal of Magnetic Resonance Series B*, 101:248–261, 1993. (page 5).

[22] Y. Xu, C.D. Araujo, A.L. MacKay, and K.P. Whittall. Proton spin-lattice relaxation in wood - $T_1$ related to local specific gravity using a fast-exchange model. *Journal of Magnetic Resonance Series B*, 64: 55–64, 1996. (page 5).

[23] G. Almeida, S. Gagné, and R.E. Hernández. A NMR study of water distribution in hardwoods at several equilibrium moisture contents. *Wood Science and Technology*, 41:293–307, 2007. (pages 5 and 12).

[24] K. Kopinga and L. Pel. One-dimensional scanning of moisture in porous materials with NMR. *Review of Scientific Instruments*, 85:3673–3681, 1994. (page 6).

[25] Leo Pel, Henk Huinink, and Klaas Kopinga. Ion transport and crystallization in inorganic building materials as studied by nuclear magnetic resonance. *Applied Physics Letters*, 81:2893–2895, 2002. (page 6).

[26] S.J.F. Erich, J. Laven, L. Pel, H.P. Huinink, and K. Kopinga. Dynamics of cross linking fronts in alkyd coatings. *Applied Physics Letters*, 86: 134105, 2005. (page 6).

[27] S.J.F. Erich, H.P. Huinink, O.C.G. Adan, J. Laven, and A.C. Esteves. The influence of the pigment volume concentration on the curing of alkyd coatings: A 1D mri depth profiling study. *Progress in Organic Coatings*, 63:399–404, 2008. (pages 6 and 77).

[28] J.F. Siau. *Transport Processes in Wood*. Springer-Verlag, 1st edition, 1984. (pages 8, 10, 11, 12, 13 and 43).

[29] G.L. Comstock and W.A. Côté. Factors affecting permeability and pit aspiration in coniferous sapwood. *Wood Science and Technology*, 2:279–291, 1968. (page 9).

[30] C.A.S. Hill. Acetylated wood - the science behind the material. `www.westgatejoinery.co.uk/Accoya-Sciencebehindacetylatedwood.pdf`. (page 10).

[31] C.A.S. Hill. *Wood modification: chemical, thermal and other processes*. John Wiley & Sons, 2006. (pages 10 and 86).

[32] E. Obataya. Reversible volumetric changes of acetylated wood with after-treatments. *Wood Science and Technology*, 39:472–483, 2005. (page 10).

[33] R.A.T.M. van Benthem, J. Laven, and M. Ming. Coatings technology. College syllabus 6KM23, TU/e, 2007. (page 13).

[34] M. de Meijer. Comparative study on penetration characteristics of modern wood coatings. *Wood Science and Technology*, 32:347–365, 1998. (pages 15, 16 and 53).

[35] F. Bloch. Nuclear induction. *Physical Review*, 70:460–474, 1946. (pages 17 and 20).

[36] F. Bloch, W.W. Hansen, and M. Packard. The nuclear induction experiment. *Physical Review*, 70:474–485, 1946. (page 17).

[37] E.M. Purcell, H.C. Torrey, and R.V. Pound. Resonance absorption by nuclear magnetic moments in a solid. *Physical Review*, 69:37–38, 1946. (page 17).

[38] E.L. Hahn. Spin echoes. *Physical Review*, 80:580–594, 1950. (pages 17 and 23).

[39] C.P. Slichter. *Principles of Magnetic Resonance*. Springer, 3rd edition, 1990. (page 18).

[40] N. Bloembergen, E.M. Purcell, and R.V. Pound. Relaxation effects in nuclear magnetic resonance absorption. *Physical Review*, 73:679–712, 1948. (pages 20 and 21).

[41] H.Y. Carr and E.M. Purcell. Effects of diffusion on free precession in nuclear magnetic resonance experiments. *Physical Review*, 94:630–638, 1954. (page 25).

[42] S. Meiboom and D. Gill. Modified spin-echo method for measuring nuclear relaxation times. *Review of Scientific Instruments*, 29:688–691, 1958. (page 25).

[43] R. Freeman and H.D. Hill. High-resolution study on NMR spin echoes: "J-spectra". *Journal of Physical Chemistry*, 54:301–313, 1971. (page 25).

[44] S.W. Provencher. Contin: a general purpose constrained regularization program for inverting noisy linear algebraic and integral equations. *Computer Physics Communications*, 27:229–242, 1982. (pages 26 and 35).

[45] M.T. Vlaardingerbroek and J.A. den Boer. *Magnetic Resonance Imaging*. Springer-Verlag, 2nd edition, 1996. (page 26).

[46] K.R. Brownstein and C.E. Tarr. Importance of classical diffusion in NMR studies of water in biological cells. *Physical Review A*, 19:2446–2452, 1979. (page 27).

[47] K.R. Brownstein. Diffusion as an explanation of observed NMR behavior of water absorbed on wood. *Journal of Magnetic Resonance*, 40:505–510, 1980. (page 27).

[48] L.G. Thygesen. Moisture in untreated, acetylated, and furfurylated Norway spruce studied during drying using time domain NMR. *Wood and Fiber Science*, 40:309–320, 2008. (page 37).

[49] T.B. Laming, J.F. Rijsdijk, and J.C. Verwijs. *Houtsoorten - informatie voor de praktijk*. Houtinstituut TNO, 1978. (pages 37 and 86).

[50] J. Bear and Y. Bachmat. *Introduction to Modeling of Transport Phenomena in Porous Media*. Kluwer, Dordrecht, The Netherlands, 4 edition, 1990. (page 42).

[51] L. Pel, H. Brocken, and K. Kopinga. Determination of moisture diffusivity in porous media using moisture concentration profiles. *International Journal of Heat and Mass Transfer*, 39:1273–1280, 1996. (page 42).

[52] J. Danvind and M. Ekevad. Local water vapor diffusion coefficient when drying Norway spruce sapwood. *Journal of Wood Science*, 2006. doi: 10.1007/s10086-005-0753-4. (page 42).

[53] L. Boltzmann. *Wiedemanns Annalen der Physik und Chemie*, 53:959, 1894. (page 43).

[54] C. Matano. On the relation between the diffusion coefficient and concentration of solids metals. *Journal of the Physical Society of Japan*, 8: 109–115, 1933. (page 43).

[55] T. Ulvcrona, H. Lindberg, and U. Bergsten. Impregnation of norway spruce (picea abies l. karst.) wood by hydrophobic oil and dispersion patterns in different tissues. *Forestry,*, 79:123–134, 2006. (page 53).

[56] T. Olsson, M. Megnis, J. Varna, and H. Lindberg. Study of the transverse liquid flow paths in pine and spruce using scanning electron microscopy. *Journal of Wood Science*, 47:282–288, 2001. (page 53).

[57] J.G. Salin. Theoretical analysis of mass transfer from wooden surfaces. In *Proceedings of the 13th International Drying Symposium*, volume C, page 1826, 2002. (page 61).

[58] S.J.F. Erich, O.C.G. Adan, L. Pel, H.P. Huinink, and K. Kopinga. NMR imaging of coatings on porous substrates. *Chemistry of Materials*, 18: 4500–4504, 2006. (page 77).

Appendix A

# Sorption isotherms

Figure A.1 shows the sorption isotherms of meranti, spruce and pine. Figure A.2 shows the sorption isotherms for Accoya; $EMC_R$ indicates the EMC corrected for the mass change due to acetylation.

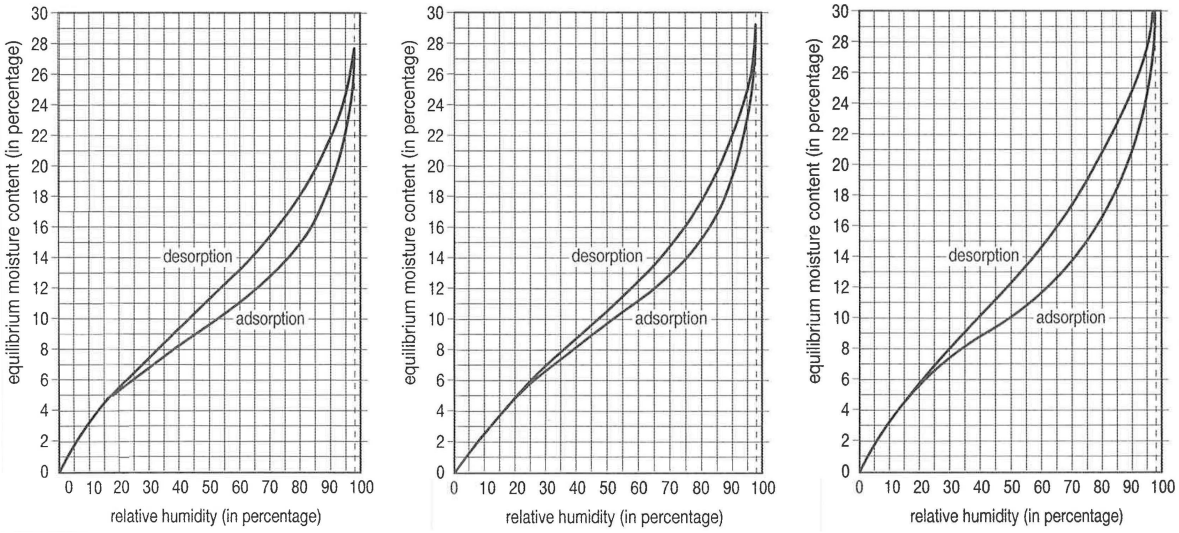


*(a) dark red meranti* *(b) Norway spruce* *(c) pine*

**Figure A.1** *Hygroscopic curves of dark red meranti, Norway spruce and pine, modified from [49].*

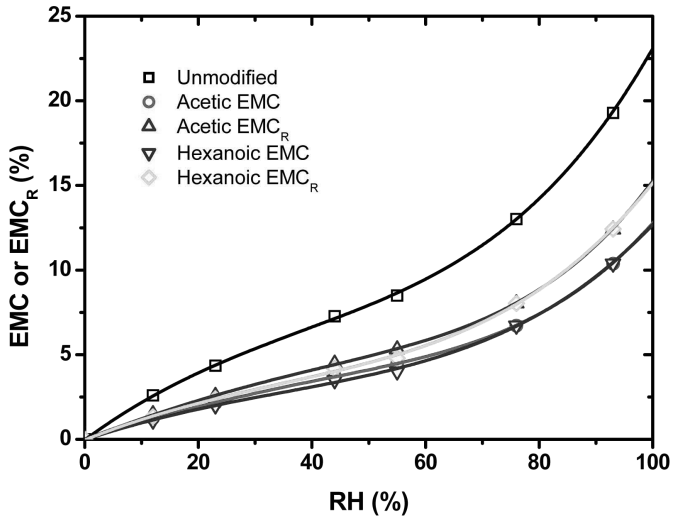


**Figure A.2** *Hygroscopic curve of Accoya, taken from [31]*

Appendix B

# FID calibration curves

The average FID SI of the equilibrated and saturated samples are plotted against the EMC in figure B.1. The data points have been connected for clarity. The change in slope at the FSP is significantly smaller for the FID SI plotted against MC than for the HSE SI because the FID signal is recorded only 100 $\mu$s after excitation, as opposed to 1700 $\mu$s for the HSE as explained in section 4.6.

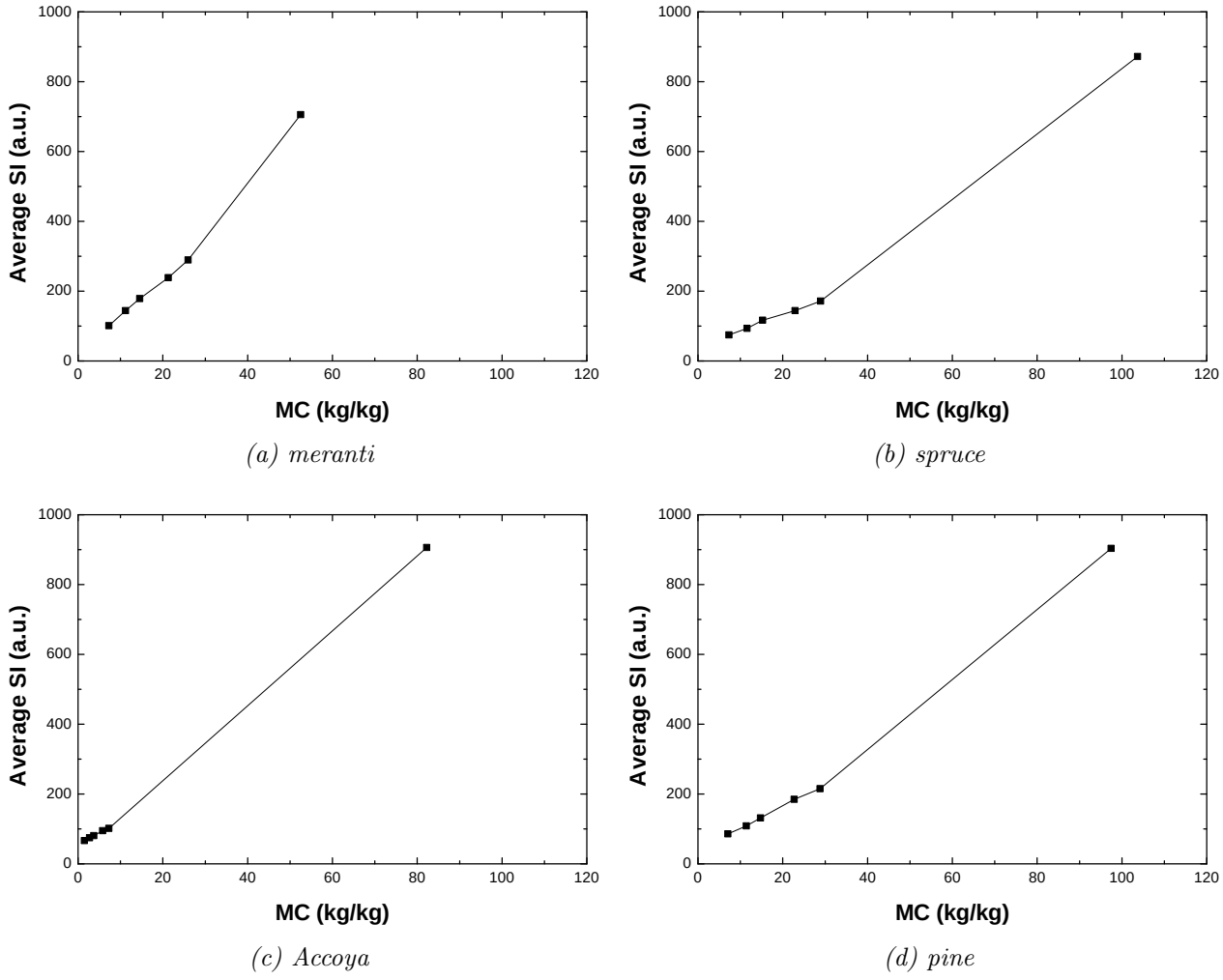


*(a) meranti* *(b) spruce*

*(c) Accoya* *(d) pine*

**Figure B.1** *The FID signal intensity of each wood type for samples equilibrated at 22%, 53%, 75%, 93% and 100% RH and at saturation.*

Appendix C

# Relaxation time distributions of uncoated pine and Accoya

For the calibration given in section 4.6, pine and Accoya samples were equilibrated over saturated salt solutions. Relaxation time distributions of these samples are shown in figure C.1. The distributions show that the relaxation time of the bound contribution of pine is equal for all samples equilibrated at different RHs. On the other hand, the relaxation time of the bound contribution of Accoya increases with increasing MC. This could be a result of acetylation which lowers moisture-wall interactions within the cell wall because of which the relaxation time of bound water increases with increasing MC. This explained in more detail in section 5.2.1.

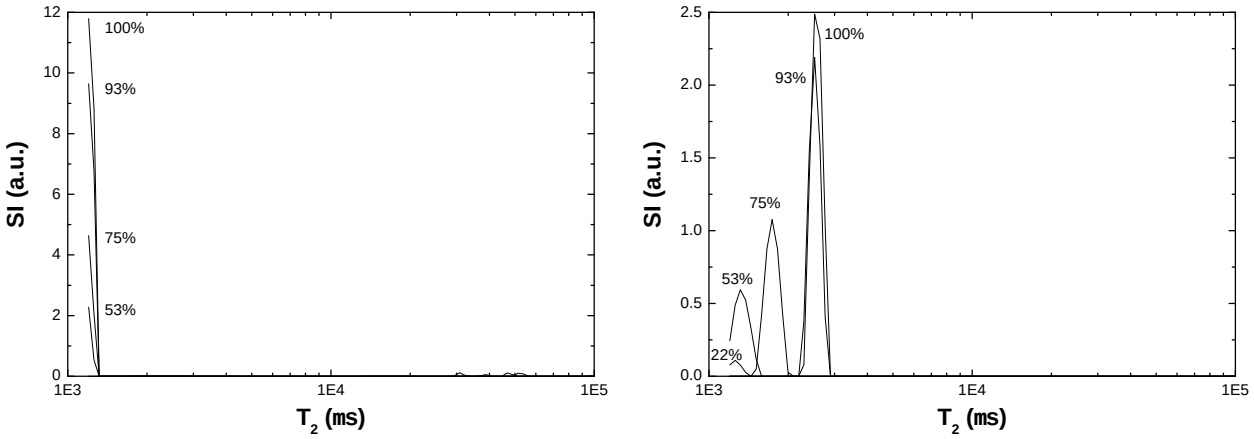


*(a) uncoated pine.* *(b) uncoated Accoya.*

**Figure C.1** *Relaxation time distributions for uncoated pine and Accoya equilibrated at 22%, 53%, 75%, 93% and 100% RH.*

Appendix D

# NMR03 tips & tricks

This appendix discusses some practical issues of the 4.7 T NMR scanner called NMR03. Table D.1 shows its main characteristics. The main magnetic field of the scanner has a strength of 4.7 T which gives a Larmor frequency of approximately 200 MHz according to equation (3.2.4). The $B_0$ field is generated by a super conducting coil immersed in liquid helium which is contained in a thermostat filled with liquid nitrogen. The current in the coil is approximately 105 A. A constant drift of the current results in a frequency drift of - 55.30 Hz/h which is corrected for by the measurement software. The scanner uses dynamic $x, y$ and $z$-gradients with a maximum field strength of 752 mT/m for the latter (this is limited by the software and insured by slow burning 20 A fuses in the output cables of the gradient amplifiers). The scanner comprises a single RF coil to emit the pulses and to pick up the NMR signal. Since these differ quite a few orders of magnitude a duplexer is used to separate them and to block the receiver during transmission. The scanner is operated by a two CPU system running dedicated C++ software.

**Table D.1** *Main properties of the NMR scanner*

| | |
|---|---|
| $B_0$ field strength | 4.7 T |
| $I_0$ | 105 A |
| $f_L$ | 200 MHz |
| frequency drift | - 55.30 Hz/h |
| $G_{z,max}$ HSE ($t_e = 1700\mu$s) | 752 mT/m |
| $G_{z,max}$ CPMG ($t_e = 1200\mu$s) | 300 mT/m |
| max RF output power | 50 dBm |

Tips and tricks:

- HSE profiles are best measured using the CPMG (raw, no hanning filter) script, by recording one echo. This script stores data in the *.fourier file format. Fourier files can be processed by the data-processor and smooth v2 subsequently.
- The gradient monitor cables should not be moved as high frequency cross talk influences the gradient strength via the monitor cables of the gradient amplifiers.
- Chose a center frequency and set the date and given drift in the client software. Thereafter, only the coil has to be tuned approximately once a month.

- Smooth v2 allows transformation of frequency to position (set gradient to 0 before loading to preserve frequency on the $x$-axis), alignment of profiles (help included in smooth v2), conversion from SI to MC for different wood types, smoothing, regridding (interpolating and averaging profiles in time, better known as "Klazen"), calculation of the integral and average between cursors of each profile and Boltzmann transformation of the profiles.

The NMR signal induced in the RF coil is typically not larger than a few $\mu V$ and at high frequency. Therefore the signal has to be amplified, filtered and demodulated to a lower frequency before recording. Figure D.1 shows a schematic overview of the analog electronics allowing digitization using an ADC present in the analog signal recorder (ASR).

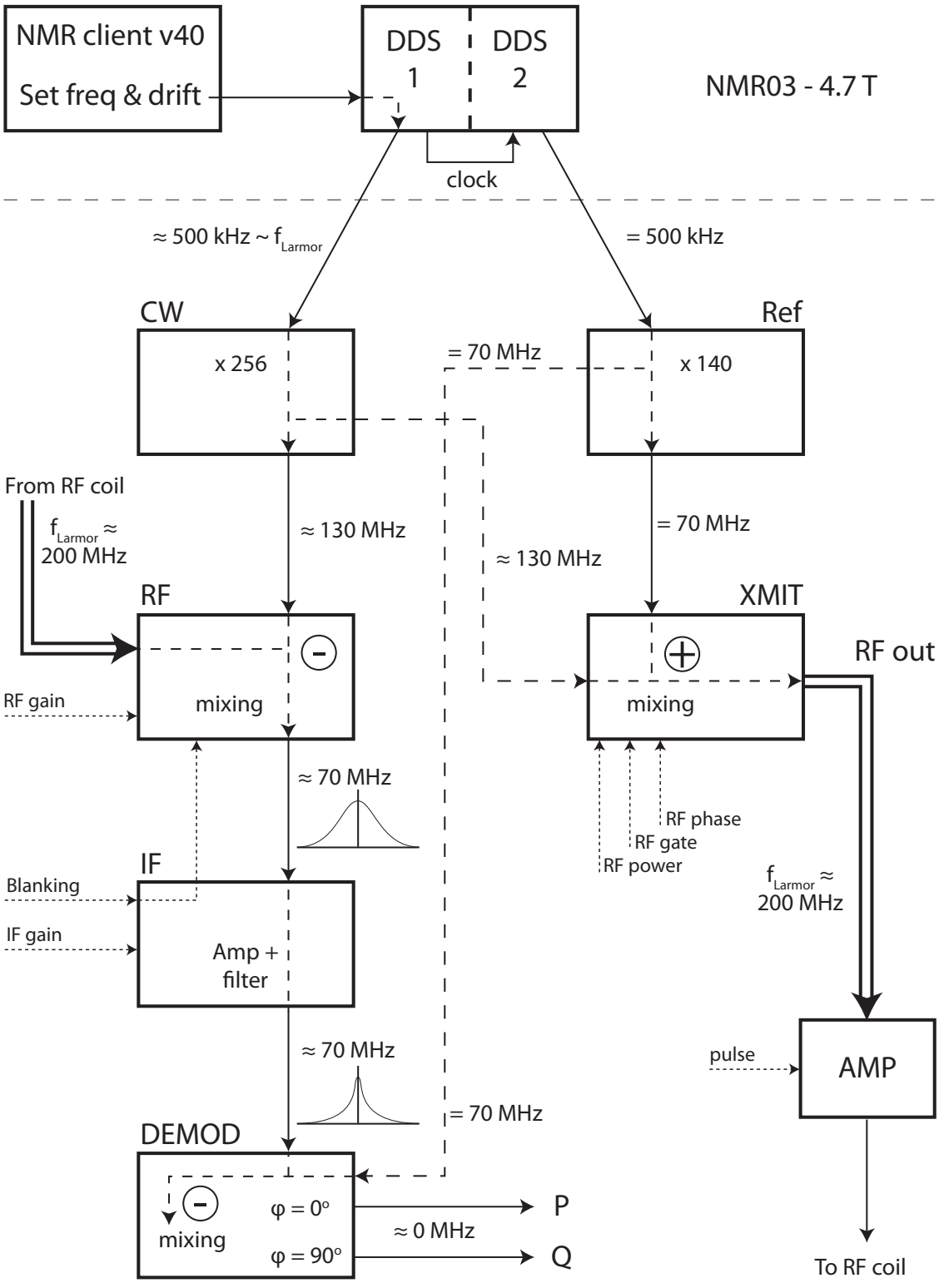


**Figure D.1** *Schematic overview of the high frequency front end. Two digital components are shown above the dashed line. All below are analog parts.*